Oxy-Fuel Combustion of Coal

Brix, Jacob; Jensen, Anker Degn; Jensen, Peter Arendt

Publication date:
2011

Document Version
Publisher's PDF, also known as Version of record

Oxy-Fuel Combustion of Coal

PhD-Thesis

Jacob Brix

Supervisors:

Professor Anker Degn Jensen

Associate Professor Peter Arendt Jensen

CHEC Research Centre

Department of Chemical and Biochemical Engineering

Technical University of Denmark

Abstract

This Ph.D. thesis describes an experimental and modeling investigation of the thermal conversion of coal and an experimental investigation of the emission of NO from char combustion in O_2/N_2 and O_2/CO_2 atmospheres. The motivation for the work has been the prospective use of the technology "Oxy-Fuel Combustion" as a mean of CO_2 abatement in large scale energy conversion.

Entrained Flow Reactor (EFR) experiments have been conducted in O_2/N_2 and O_2/CO_2 mixtures in the temperature interval 1173 K – 1673 K using inlet O_2 concentrations between 5 – 28 vol. %. Bituminous coal has been used as fuel in all the experiments. Devolatilization experiments showed that the volatile weight loss was not affected by the change from N_2 to CO_2. Analysis by Scanning Electron Microscopy (SEM) and Brunauer-Emmett-Teller (BET) surface area of sampled char did not reveal differences between the two atmospheres either. Char conversion profiles, obtained from sampled char did not show differences in conversion rate between O_2/N_2 and O_2/CO_2 atmospheres across the span of O_2 concentrations in the interval of reactor temperatures 1173 K – 1373 K. At the reactor temperatures 1573 K and 1673 K and an inlet O_2 concentration of 5 vol. % it was found that char conversion rate was lowered in O_2/CO_2 compared to O_2/N_2. This is caused by the lower diffusion coefficient of O_2 in CO_2 (~ 22 %) that limits the reaction rate in zone III compared to combustion in O_2/N_2. Using char sampled in the EFR experiments ThermoGravimetric Analyzer (TGA) reactivity profiles for combustion and CO_2 gasification has been found at 5 vol. % O_2 or 80 vol. % CO_2 and a heating rate of 5 K/min to a peak temperature of 1273 K or 1373 K. These experiments did not reveal differences in reactivity between EFR-chars formed in O_2/N_2 and O_2/CO_2. Reactivity profiles for TGA combustion of partly converted EFR-char, sampled at 1173 K and 28 vol. % O_2, showed the presence of two phases of distinctively different reactivity. The least reactive of these phases are believed to be formed from interactions between mineral matter and secondary volatiles evolved during the fierce heating upon particle ignition at the high O_2 concentrations. From TGA reactivity profiles of EFR-chars devolatilized at 1173 K – 1673 K intrinsic kinetic parameters has been found for combustion. The rate constant includes both a deactivation and an activation term.

Intrinsic kinetics was also found for CO_2 gasification though using only EFR-char devolatilized at 1273 K, 1473 K and 1573 K due to a lack of samples. Interestingly, it was found that devolatilization temperature did not affect the gasification rate constant. A detailed COal COmbustion MOdel (COCOMO) encompassing among others the three char morphologies; cenospheres, network- and dense chars, each distributed between six discrete particle sizes has been developed. The model showed a reasonable ability to predict the conversion profiles obtained in the EFR experiments using the intrinsic TGA kinetics for combustion and gasification. At the reactor temperature 1173 K COCOMO over predicts char conversion at O_2 inlet concentrations of 5 and 28 vol. %. At the reactor temperature 1273 K COCOMO also over predicts char conversion at an inlet O_2 concentration of 5 vol. %. Over prediction at the high O_2 concentration is caused by the formation of char with a low reactivity as discussed above. Simulation under these conditions show that particle excess temperatures of 500 – 600 K is reached upon ignition at heating rates as high as 20000 K/s, which can indeed cause a significant release of secondary volatiles. At the low O_2 concentration deviation between model and experiments is caused by an experimental delay in ignition that is not captured by the model. Though this causes a deviation in total conversion COCOMO still predicts conversion rates accurately after ignition. A laboratory scale Fixed Bed Reactor (FBR), operated isothermally at 1073 K, has been used for combustion of millimeter-sized lignite- and bituminous char particles in 5 – 80 vol. % O_2 in N_2 or CO_2 atmospheres. Particle temperatures have been recorded by a Charged Coupled Device (CCD) camera and experiments have been carried out with single and multiple particles of different sizes. NO emission from lignite char were not affected by the change of N_2 with CO_2. Emissions from bituminous char were lower in O_2/CO_2. Emissions for both char types decreased as the O_2 concentration or the particle size increased. An intermediate particle size was found where emissions peaked for the bituminous char. The CCD camera measured in situ temperatures accurately during experiments and the ability of film recording proved a valuable tool for data interpretation. The results suggest that transport phenomena and kinetics alone can not account for changes in NO emissions between O_2/N_2 and O_2/CO_2. The effect of mineral catalysis and the presence of other N-containing species, such as HCN and NH_3, may also play a role.

Resumé

Denne Ph.d. afhandling beskriver en eksperimentel- og modelundersøgelse af kulomsætning ved suspensionsfyrede forhold samt en eksperimentel undersøgelse af NO emission fra koksforbrænding udført i O_2/N_2 og O_2/CO_2 atmosfærer. Motivationen til dette arbejde har været muligheden for at bruge "Oxy-Fuel Forbrænding" som en metode til at reducere CO_2 emissionen fra energikonvertering i industriel skala.

Forsøg er udført i en FastBrændselsReaktor (FBR) i O_2/N_2 og O_2/CO_2 atmosfærer i temperaturintervallet 1173 K – 1673 K og ved O_2 indgangskoncentrationer mellem 5 og 28 vol. %. Bituminøst kul har været benyttet som brændsel under alle forsøgene. Pyrolyseeksperimenter viser, at vægttabet af flygtige bestanddele ikke bliver påvirket ved skiftet fra N_2 til CO_2. Analyse med ElektronMikroskopi (EM) og Brunauer-Emmett-Teller (BET) måling på opsamlet pyrolysekoks viser heller ikke nogen indflydelse af gasatmosfære. Koksomsætningsprofiler, fundet fra opsamlet koks, viser ikke forskel i omsætningshastighed mellem O_2/N_2 og O_2/CO_2 ved de anvendte O_2 koncentrationer i temperaturintervallet 1173 K – 1373 K. Ved reaktortemperaturer på 1573 K og 1673 K og ved en indgangskoncentration af O_2 på 5 vol. % er omsætningshastigheden i O_2/CO_2 langsommere end i O_2/N_2. Dette skyldes en lavere diffusionskoefficient af O_2 i CO_2 (~ 22 %), hvilket begrænser omsætningshastigheden af koks i zone III.

Reaktivitetsprofiler for FBR-koks er målt i en TermoGravimetrisk Analysator (TGA) for forbrænding og forgasning ved enten 5 vol. % O_2 eller 80 vol. % CO_2 under en opvarmningshastighed på 5 K/min til enten 1273 K eller 1373 K. Disse profiler viser ingen forskel i reaktivitet mellem FBR-koks skabt i O_2/N_2 og O_2/CO_2 atmosfærer. Reaktivitetsprofiler for TGA forbrænding af delvist omsat FBR-koks, opsamlet ved 1173 K i 28 vol. % O_2, viser tilstedeværelsen af to faser med forskellig reaktivitet. Den mindst reaktive fase tænkes dannet fra interaktioner mellem koksens mineralindhold og flygtige bestanddele fra en sekundær pyrolyse igangsat af den intense partikelopvarmning, der finder sted under antændingen ved den høje O_2 koncentration. Ud fra reaktivitetsprofiler for FBR-koks, dannet ved pyrolyse ved temperaturer mellem 1173 K og 1673 K, er der fundet kinetiske parametre for forbrænding. Hastighedskonstanten indeholder både et aktiverings- og deaktiveringsled. Kinetiske parametre er også fundet for CO_2 forgasning,

dog kun med FBR-koks dannet ved 1273 K, 1473 K og 1573 K, da der var begrænsede mængder af koks til rådighed. Forbavsende viser hastighedskonstanten for CO_2 forgasning ikke tegn på termisk deaktivering.

Detaljeret modellering med en "COal COmbustion MOdel (COCOMO)", udviklet i projektet, viser en rimelig evne til at beskrive koksomsætningsprofilerne, fundet under FBR-forsøgene, ved brug af TGA-kinetikken. COCOMO udfører beregninger på de tre koksmorfologier; cenosfærer, netværkskoks og kompakt koks, hver fordelt mellem seks diskrete partikelstørrelser. Ved en reaktortemperatur på 1173 K overestimerer COCOMO koksomsætningsgraden ved indgangskoncentrationer af O_2 på 5 og 28 vol. %. Ved en reaktortemperatur på 1273 K overestimerer COCOMO også koksomsætningsgraden ved 5 vol. % O_2. Overestimeringen ved den høje iltkoncentration skyldes tilstedeværelsen af koks med forskellig reaktivitet, som det er beskrevet ovenfor. Simuleringer under disse betingelser viser, at partikelovertemperaturer på 500 – 600 K nås under antændingen med opvarmingshastigheder op til 20000 K/s, hvilket bestemt vil medføre en frigivelse af flygtige bestanddele. Ved den lave O_2 koncentration skyldes afvigelsen mellem COCOMO og de eksperimentelle data, at der sker en forsinkelse i koksantændelsen under forsøgene. Selv om COCOMO ikke fanger forsinkelsen, beskrives koksomsætningshastigheden stadig præcist.

I en laboratorieskala Pakket Reaktor (PR), kørt isotermt ved 1073 K, er der udført forbrændingsforsøg med brunkuls- og bituminøse kokspartikler i millimeterstørrelse med henblik på måling af NO emission. Forsøgene er udført med O_2 koncentrationer mellem 5 og 80 vol. % i N_2 eller CO_2. Der er blevet målt partikeltemperaturer med et digitalkamera under forsøgene. NO emissionen fra brunkulskoks er ikke påvirket af skiftet fra N_2 til CO_2, mens emissionen fra bituminøst koks er lavest i O_2/CO_2. Emissionen fra begge typer koks falder med en stigning i enten O_2 koncentrationen eller partikelstørrelsen. En intermediær partikelstørrelse, hvor NO emissionen toppede, blev fundet for bituminøst koks. Digitalkameraet gav præcise temperaturmålinger under forsøgene. Resultaterne tyder på, at transportfænomener og kinetik alene, ikke er i stand til at redegøre for forskellene i NO emission mellem O_2/N_2 og O_2/CO_2. Effekten af mineralsk katalyse samt eksistensen of N-holdige gasser som HCN og NH_3 kan også spille en rolle.

Preface

This dissertation constitutes the partial fulfillment of a Ph.D.-thesis. It was carried out at the Department of Chemical and Biochemical Engineering at the Technical University of Denmark as part of the CHEC (Combustion and Harmful Emission Control) research centre with Professor Anker Degn Jensen and Associate Professor Peter Arendt Jensen as supervisors.

I would like to give my sincere thanks to Anker Degn Jensen, Peter Arendt Jensen and Peter Glarborg for excellent supervision and for increasing the quality of the work through fruitful discussions and careful reading of my manuscripts.

I thank the members of CHEC and the department for the creation a collegial work environment with a high degree of knowledge exchange. I especially want to address this thank to Carsten Nørby and Thomas Wolfe for their help during the experiments.

I thank Henning Engelbrecht Larsen and Sønnik Clausen at Risø DTU for their help with the CCD camera experiments and for their patience during subsequent data treatment.

I sincerely thank the students Peter Løvengreen Bonnek, Joachim Bachmann Nielsen, Leyre Gómez Navascués, Jesper Banke Grosmann and Morten Storgaard Petersen for their contributions to the experimental results of this thesis.

I thank the members of the EU project “Friendly Coal” for the discussions during project meetings and for bringing a broad perspective to my understanding of oxy-fuel combustion.

For financial support I acknowledge the Technical University of Denmark, the European Community’s Research Fund for Coal and Steel (RFCS), the Danish Agency for Science Technology and Innovation, Energinet.dk, Vattenfall Research and Development AB and

ALSTOM Power Systems Gmbh. The support and funding from these entities are greatly valued.

I thank my family, family-in-law and friends for their sincere interest in my project and for the help and support when it demanded most of my time. I especially want to thank my mother for a supportive upbringing.

At last I will like to thank my beautiful wife Helene for her continued support in the sometimes laborious efforts of finishing this work and my daughter Isabella for bringing sunshine into our family. I therefore dedicate this thesis, and the thousands of hours put into it, to them.

Kgs. Lyngby, January 2011

Jacob Brix

List of Articles

Article I: Coal Devolatilization and Char Conversion under Suspension Fired Conditions in O_2/N_2 and O_2/CO_2 Atmospheres.

Article II: Coal Char Reactivity: A Thermogravimetric Study on Chars Obtained in O_2/N_2 and O_2/CO_2 in an Entrained Flow Reactor Under Suspension Fired Conditions and in a TGA.

Article III: Modeling Char Conversion under Suspension Fired Conditions in O_2/N_2 and O_2/CO_2 Atmospheres.

Article IV: Oxy-Fuel Combustion of Coal Char: Particle Temperature and NO Formation.

Table of Content

1 Introduction to Carbon, Capture and Storage

In the recent years there has been an ever increasing awareness of the supposed role of anthropogenic CO_2 emission on the climate. This focus has resulted in stricter environmental regulations both globally and within the European Union [1,2].

Today fossil fuels, coal in particular, accounts for approximately 85 % of the energy production world wide [3,4]. To overcome present and future environmental regulations and to solve the potential problems related to CO_2 emissions the energy industry relaying on fossil fuels is under strain to find technological alternatives that will utilize the fuels more environmental friendly, if they are to be kept as feedstocks. This technological development is necessary since the dependence on fossil fuels as an energy source will be present for years to come despite the research in alternative energy sources [1,3,5]. The abundance of coal can be seen in figure 1 where the 10 countries with the largest known coal reserves (2006) are shown. These countries account for 91 wt. % of the worlds total known coal reserves, which are not expected to be depleted for hundreds of years.

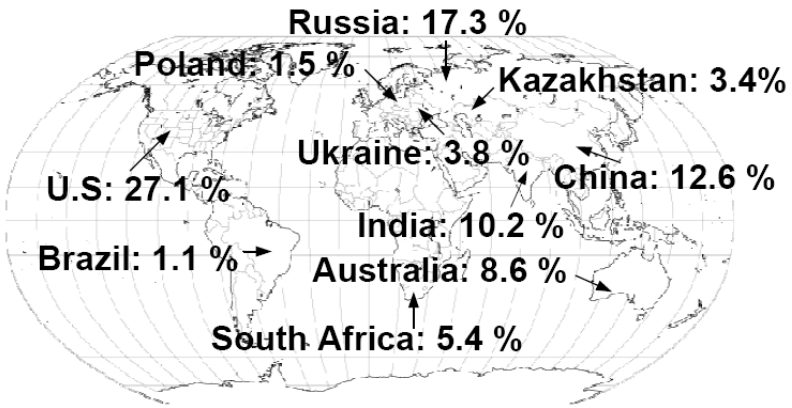

Figure 1 The 10 countries with the largest known coal reserves in the world [6,7]. The world total reserve is estimated to be 909064 million tonnes. The percentage in the figure is of this number.

There are different approaches to accomplish a reduction in CO_2 emission from fossil fuel based energy generation. One is to enhance the efficiency of conventional power plants and thereby reduce the need for fuel. This is however not considered as sufficient to overcome the climate challenge since the likelihood of a steep enhancement of plant efficiencies is small. Another approach is Carbon Capture and Storage (CCS) where the

CO_2 produced in the combustion process is captured and stored in suitable geological formations such as depleted oil and gas fields, saline formations and unmineable coal seems [4]. In the possible sequestration locations known today it is estimated that 1120 – 3400 billion tonnes of CO_2 can be stored [4]. In 2001 the world's total emission of CO_2 was app. 24 billion tonnes of which energy generation accounted for 44 % [3]. Major contributors to the global CO_2 emission can be seen and compared in figure 2.

If the before mentioned storage capacity is utilized to store CO_2 based on the 2001 total emissions CCS can be applied for 47 – 144 years, and if the application time is based only on the emissions from energy generation the time frame is 107 – 326 years. Before this capacity is used up, even with a projected increase in emissions, new alternative power generation technologies now in development will most likely have been implemented at an industrial scale.

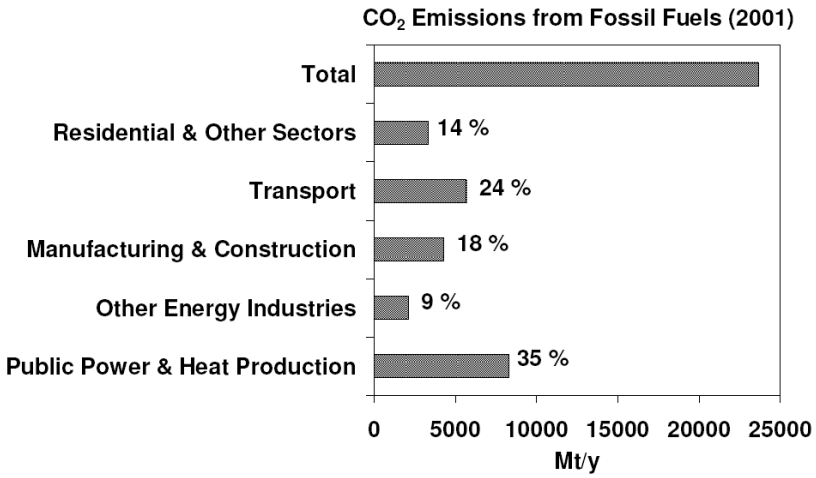

Figure 2 Major contributors to the global CO_2 emission [3].

1.1 Concepts for Carbon Capture and Storage

There are three general concepts when CCS is to be used in power generation [3,4]. These concepts are illustrated in the general schemes below (auxiliary equipment has been omitted from the figures).

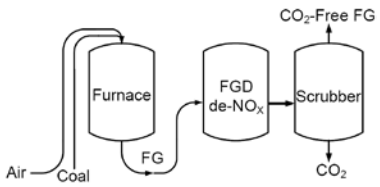

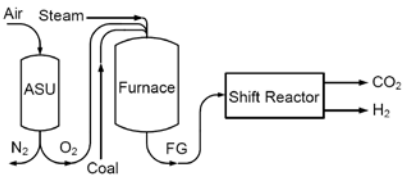

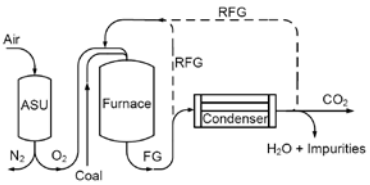

1. Post-combustion capture 2. Pre-combustion capture (IGCC) 3. Oxy-fuel combustion

The CCS concepts shown above have both advantages and disadvantages connected to their operation. At the moment research projects all over the world are undertaken to analyze and improve CCS-processes covering all of the three concepts. In the next three subsections the governing technologies in each concept are presented and discussed.

1.1.1 Post-Combustion Capture

In post-combustion capture CO_2 is recovered from the plant flue gas [3,4]. One way of extracting the CO_2 from the flue gas is by amine absorption in which amines reacts with CO_2 to form water soluble compounds [4]. Typical amines used for absorption is MonoEthanolAmine (MEA) and MethylDiEthanolAmine (MDEA) [8] but different amine solvents with a variety of additives are commercially available [4].

The absorption process is costly mainly because of two factors. The first is the low concentration of CO_2 found in the flue gas, normally below 15 vol. %, which gives a low driving force for mass transfer [4] and hence large and costly equipment and absorbent volumes. The other factor is the energy requirement for solvent regeneration [3]. Intensive research is being carried out by several market participants in order to improve the mass transfer, heat integration and solvent properties as ways to reduce expenses [4].

Other methods of CO_2 removal from plant flue gases are also being pursued. Among these methods the reaction of soluble carbonate with CO_2 to form bicarbonate, the use of NH_3 instead of amine and the application of membranes can be pointed out but others are also in play [4]. Common for all of them is that they are aiming at reducing the energy requirement compared to amine regeneration but none of them are yet functional at a scale required for industrial implementation.

1.1.2 Pre-Combustion Capture

The most dominant process in this category of CCS is Integrated Gasification Combined Cycles (IGCC's) with carbon capture and storage. In this process the fuel is gasified thereby producing a stream rich in CO, H_2, CO_2 and H_2O. This stream is mixed with steam and sent to a shift reactor where the steam reacts with the remaining CO to form additional H_2 and CO_2 [3,4]. The shift reactor is operated at elevated pressures up to 84 bars [9] but normally pressures between 20 – 30 bars are used for the process[1] [10]. After separating CO_2 from H_2, the H_2 is mixed with steam or N_2, from the Air Separation Unit (ASU) producing O_2 for the gasification, and burned in a turbine [4,8]. The fact that the exit stream from the shift reactor contains a high concentration of CO_2 at elevated pressure eases its separation from H_2 and the following sequestration [4].

The possible methods of separation when CO_2 is to be extracted from the shift reactor effluent includes absorption using amines or other chemical solvents, identical to post-combustion capture, but because of the high concentration of CO_2 physical solvents can also be used [3,4]. Important aspects in the choice of solvent, chemical or physical are the price of regeneration before the solvent is recycled back to the process and its lifetime measured as possible numbers of recycles. In general regeneration of a physical solvent is less energy intensive than regeneration of a chemical solvent as no chemical bonds needs to be broken [3]. The high concentration of CO_2 in the shift reactor effluent therefore makes use of a physical solvent possible and attractive [3]. Some physical solvents are methanol, propylene carbonate, N-methyl-pyrrolidone, dimethylether, polyethylene or glycol [11].

The use of membranes for the capture of CO_2 is also being investigated either as a stand-alone method or in combination with e.g. amine absorption. A crucial property of a suitable membrane, besides its selectivity, is its maximum operating temperature since the gas stream to be treated is at high temperature [4]. Also, if the retentate stream from a membrane separator needs further treatment, i.e. absorption due to low membrane efficiency, the advantage of a high CO_2 concentration to facilitate mass transfer is lost. It will therefore be difficult to optimize the process economically.

[1] Reactor pressures of 70 – 80 bars have been proposed for IGCC-CCS [4] and it is therefore possible that the shift reactor will have to operate at similar pressures.

Another process for pre-combustion CCS, gaining a lot of interest, is chemical looping where air oxidizes a solid intermediate that is then sent to oxidize the fuel [4]. In this way the diluting effect of N_2 on the CO_2 from the combustion is avoided and the capture costs are reduced. Chemical looping can also be applied as part of a gasification unit. There are two different approaches to this kind of gasification, namely direct mixing of the solid fuel particles and the oxidized intermediate [12] or a separate gasification of the solid fuel [13,14]. In both cases the exothermic oxidation of the solid intermediate provides energy for the process and the volatiles and gaseous gasification products are combusted by the oxidized intermediate. For the first scheme to be feasible for CO_2 emission reduction an efficient separation of the reduced solid intermediate and the unconverted fuel particles is essential.

1.1.3 Oxy-Fuel Combustion

What separates oxy-fuel combustion as a concept from post-combustion and pre-combustion capture is that no actual capture is necessary. In oxy-fuel combustion the fuel is burned in a mixture of O_2 and recycled flue gas (~30 % O_2 for retrofit plants [8,15]) thereby producing a high purity CO_2 stream ready for sequestration [3-5]. The recycled flue gas serves two purposes, namely to dampen the combustion temperature and to act as a carrier of the combustion heat and the recycle ratio can be manipulated to achieve heat transfer characteristics similar to air-blown combustion making retrofits possible [8].

In oxy-fuel combustion an ASU is supplying a near pure O_2 stream (95% – 99.5 % [5,20-22])[2], which is then mixed with recycled flue gas prior to the boiler entrance. After the boiler the flue gas is sent through a condenser (recycling can take place before or after the condenser depending on whether wet or dry recycle is desired) where water vapor produced in the combustion process is removed along with many of the inorganic impurities originating from the combustion [3-5,23]. The removal of water vapor must be effective because the presence of H_2O in the high pressure transport of CO_2 to storage could cause gashydrates to form [24] and also give problems with corrosion. At the end of the process a CO_2 stream of 90 % purity or higher will be ready for compression and

[2] The exact value depends on process conditions and if adsorption-based or cryogenic air separation is used. The economical impact vs. purity necessity of oxygen is also still debated.

sequestration [3,5]. Flue gas compositions obtained in different oxy-fuel pilot plant experiments can be seen in table 1.

Table 1 CO_2 percentages in the flue gas obtained for oxy-fuel combustion of pulverized coal. In the case of no flue gas recycle gaseous atmospheres have been created from bottled gases.

O_2/CO_2 % in Flue Gas	**O_2/CO_2 % Feed Gas**	**Flue Gas Recycle**	**Reference**
4.5 % O_2/ 81 % CO_2[3]	30 % O_2/ 70 % CO_2	No	[16]
2.1 % O_2/ 97 % CO_2	35 % O_2/ 65 % CO_2	Yes	[17]
2.2 % O_2/ 98 % CO_2	35 % O_2/ 65 % CO_2	Yes	[17]
2.7 % O_2/ 92 % CO_2[4]	35 % O_2/ 65 % CO_2	Yes	[17]
4.2 – 3.7 % O_2/ 94 % CO_2	25-29 % O_2/ 71-69 % CO_2	Yes	[18]
5.0 – 3.7 % O_2/ 95 % CO_2	21-29 % O_2/ 79-71 % CO_2	No	[19]

In the plant description above flue gas cleaning has been omitted because the extent to which it is needed has not been clarified. A discussion of this will be taken in section 1.2. Further it can prove necessary to treat the CO_2 stream after potential flue gas cleaning and condensation if it is to be used for e.g. Enhanced Oil Recovery (EOR). To what level further CO_2 purification is needed is hardly foreseen and depends on the level of boiler leakage and O_2 purity [25].

A different scheme for enhanced NO_x reduction in the oxy-fuel combustion process have been proposed [26] where a fraction of the heat is recovered from the flue gas prior to particulate removal and recirculated to the boiler entrance by the recycle stream. The scheme performance is based entirely on modeling, and show that the same coal combustion intensity as in air combustion can be achieved in 15 vol. % O_2 using this technique, which would make the near burner environment less oxidizing and hence reduce NO_x emission. Experiments by Toporov et al. [27,28] have yielded stable oxy-fuel flames at O_2 concentrations lower than 21 vol. % by burner optimization aiming at

[3] 10 % of the total gas flow into the furnace was air used for coal entrainment.
[4] A leakage was discovered by the authors.

internal heat recirculation and stabilization of CO production. In the scheme of Toporov et al. [27,28] an Ion Transport Membrane (ITM's) is used for O_2 production with recirculated flue gas as sweep gas on the permeate side of the membrane. It should be noted, though, that lower O_2 concentrations at constant stoichiometry means that a larger volume of flue gas must be recycled.

1.2 Cost-Effectiveness of Carbon Capture and Storage

Before proceeding further into the technical and engineering aspects of CCS-technology it must be recognized that the cost-effectiveness of a plant with carbon capture always will be reduced compared to a plant without. The reason for this is the various additional equipment and associated work that are needed for the capture, compression, transport and storage, solvents, ASU etc. which is not required for a conventional plant. When this is said it must be added that much of the technology such as air separation is subjected to intensive research and that the effectiveness penalties arising from CCS therefore are likely to decrease [3]. The discussion taken in this section will focus on a cost-effectiveness comparison between the three CCS approaches listed in section 1.1.

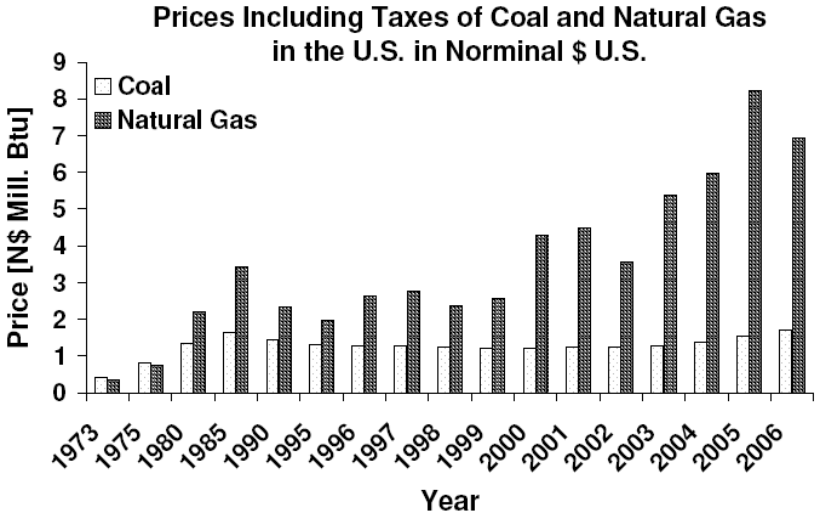

Figure 3 Nominal prices of coal and gas on the U.S. market from 1973 – 2006. "Nominal" means that prices include taxes on the fuels [29].

When comparing the price of a kWh plants must be separated into gas fired and coal fired plants. The reason for this is mainly the higher price of gas compared to coal, which

makes energy penalties associated with CCS more expensive to cover in a gas fired plant [3]. A comparison of the evolution of prices of coal and gas on the U.S. market is shown in figure 3.

Cost projections of both coal fired and natural gas fired CCS-plants were made by Davison [3] based on the IEA Greenhouse Gas R & D Program where engineering contractors and developers have made design packages for post-combustion capture, IGCC-CCS and oxy-fuel combustion. The results of this study show that the cost of electricity production is highest for oxy-fuel combustion (532 MW) and smallest for IGCC-CCS (730 MW) when coal is used as fuel. It must however be taken into account, and is so by Davison, that the dimensioning of the plants are made based on fixed equipments sizes, e.g. turbines. This results in a capacity of the oxy-fuel plant which is 27 % lower than for the IGCC. It is usually the case that the cost of a kWh decreases with increasing plant capacity and the 21 % higher cost of a kWh in the oxy-fuel plant compared to the IGCC can therefore not be taken as final.

Wall [8] estimated process efficiencies around 35 % LHV for all the 3 types of CCS concepts corresponding to efficiency penalties of 7 – 8 % LHV compared to conventional power plants. In this paper oxy-fuel combustion was presented as the CCS-technology with the lowest Cost Of Electricity (COE) having a difference compared to conventional air-blown combustion corresponding to a CO_2 tax of $ 15 per ton of CO_2. This value can be compared with $ 25 per ton for post – combustion capture and $ 20 per ton for pre-combustion capture [8].

The conclusions of Davison [3] and Wall [8] shows that many uncertainties needs to be clarified in order to make a detailed unambiguous cost estimate of the CCS-technologies, which is suitable for comparison. An important aspect of the cost-effectiveness is for example the purity of the captured CO_2. If the intended use of the captured CO_2 is EOR then the requirement for purity is > 95 % CO_2 and < 10 ppm O_2 [8]. This high level of purity sets high demands for the equipment and post treatment of the CO_2. Before actual test scale plants have been built and optimized the uncertainties regarding the level of air tightness in the oxy-fuel boiler and the actual level of CO_2 purity in IGCC-CCS are difficult to evaluate, which gives a larger overall uncertainty in economic evaluations such as those presented above. Instead comparison of the different technologies should be

made focusing on the prospect of development and the evaluation of possible step change reductions in operating costs due to the research that are currently going on.

Two flue gas pollutants that can prove to be conclusive when deciding on CCS-technology are SO_x and NO_x. NO_2 and SO_2 forms heat stable salts with the amine solvent MEA and a very intensive Flue Gas Desulphurization (FGD) is therefore necessary [8]. NO_2 only account for a few percent of the NO_x and the SO_2 is therefore the crucial component of the two. In contrast to this there is a possibility that FGD [3,23,24,30] and Selective Catalytic Reduction (SCR) of NO_x [3,30] may not be required for oxy-fuel combustion. Because the NO_x is recycled along with the flue gas into the boiler a significant reduction of these components is taking place in the flame, and the development of low-NO_x burners specifically for oxy-fuel combustion therefore have a great potential [8]. The possibility of omitting FGD depends on the level of sulphur in the fuel and the tolerance level of the equipment [3,8]. If large amounts of SO_2 are contained in the recycled flue gas it may cause corrosion once further oxidized and reacted with H_2O to form H_2SO_4. Once the flue gas is captured it is expected that the SO_2 [3,23,24] and the NO_x [3] can be stored together with CO_2. There are however possible technical impacts that can affect the co-storage of the three gases. If calcium sulphates are produced, i.e. in saline formations, the porosity and therefore the storage capacity will be reduced [24]. The prospect of omitting the SCR-unit and the FGD-unit is something that needs to be investigated further before conclusions can drawn but it provides an important decrease in energy penalty for oxy-fuel combustion if possible. If these units can not be omitted the prospect of a high primary reduction of NO_x still proves promising for the cost of the SCR.

1.2.1 Cost-Effectiveness of Air Separation

Air separation is a very costly part of IGCC-CCS and oxy-fuel combustion in particular and this technology therefore deserves a section dedicated to its use and development prospects. This section will not go into technical details for the variety of plant configurations found in the literature but focus on general features that can be subjected to economic optimizations.

The three ASU – technologies that have either a dominant role now or holds the greatest promises for improvements are [31]:

- Cryogenic separation.
- Pressure Swing Adsorption (PSA).
- Membrane separation.

Cryogenic separation is the most used of the technologies today because it is capable of producing high purity O_2 in large amounts (> 3000 tons a day) and argon as a sellable by-product [31]. Because cryogenic separation has been developing over the last four decades a step increase in the process efficiency is not likely to take place even though technical improvements, i.e. of compressors for inlet air compression and structured packing for distillation, also in the future will reduce the cost of near pure O_2 production [32]. As an example of the efficiency improvement of cryogenic ASU's the cost of low pressure gaseous O_2 measured as kWh/Nm^3 went down 43 % from 0.67 in 1970 to 0.38 in 1985 but only 21 % over the next 15 years to 0.3 in 2000 [31]. In the same time periods as mentioned before the capacity of the largest cryogenic separation plants went up 127 % and 44 % respectively too a capacity of 3400 tonnes O_2/day in 2000 [31]. This shows that less decrease in production cost for each percent of increase in capacity were gained in the period 1985 – 2000 compared to the period 1970 - 1985.

In PSA separation plants compressed air is passed through a vessel containing a selective adsorbent. This adsorbent is usually zeolite molecular sieves when the desired product is O_2 [33]. When the zeolite becomes saturated with N_2 the compressed air stream is switched to another vessel with fresh adsorbent [31,33]. Because practical and financial limitations exist when sizing the adsorption vessels an increase in plant capacity is made by adding more vessels and therefore more zeolite. The only major target for economic optimization in these plants is therefore the effectiveness of the adsorbent [31]. In this field research has reduced the production cost of O_2 by 50 % since the early 1990'ties with the prospect of considerable economic improvements still to come [31]. It is therefore possible that PSA can become attractive to use in CCS plants based on

gasification and oxy-fuel combustion though with the batch wise operation being a possible concern.

The concept of polymeric membrane separation of gas mixtures is well known. As it is normally the case the financial prospects in air separation using membranes depends on the obtainable flux and selectivity of the membranes. Most of the polymeric membranes for air separation are permeable to O_2 with selectivity such that they can be used for production of O_2 enriched air [33]. It must however be mentioned that the use of polymeric membranes in ASU's is a concept newer than PSA and cryogenic separation [33]. The simplicity of the process therefore makes it potentially attractable if improvements in membrane performance can be achieved.

A type of membrane that holds promise is ITM's. An ITM is a solid inorganic ceramic membrane operating at high temperatures (1073 K – 1173 K) [32-34]. In this membrane O_2 is carried through as oxygen ions by a partial pressure difference [33]. To keep a high O_2 partial pressure difference across the membrane a sweep gas, e.g. recycled flue gas, can be passed on the permeate side and the retentate side can be pressurized. This separation concept is still developing but it is projected to reduce production costs by more than 33 % when compared to cryogenic separation and reach compatible production capacities within few years [32].

The purity of O_2 in CCS is of great importance since any impurities will reduce the CO_2 concentration in the plant flue gas thereby necessitating further treatment. The obtainable purities for the technologies presented in this section can be seen in table 2.

Table 2 Obtainable purity of O_2 for different methods of separation [33]. The purity shown in this table is not necessarily the most cost-effective and the price of O_2 production between technologies is not the same.

Process	**Purity of O_2 Vol. %**
Pressure Swing Adsorption	~ 95
Cryogenic Separation	99 <
Membrane (Polymeric)	~ 40
Membrane (ITM)	99 <

2 An Overview of Coal Combustion in an Oxy-Fuel Environment

This chapter will focus on three key aspects of oxy-fuel combustion namely, flame stability and combustion temperature, devolatilization and char conversion. These aspects, though interrelated, are crucial factors, the understanding of which, will determine the success of oxy-fuel combustion as an industrial CO_2 abatement technology. Also treated in this chapter is NO_x emission as this holds great promises of future savings in oxy-fuel combustion especially if co-storage of NO_x and CO_2 is not possible. A detailed discussion of literature findings should however not be expected as this chapter only provides the reader with a technical overview covering some of the aspects of oxy-fuel combustion that are currently subjects of research. Detailed discussions on specific issues are taken in each of the articles included in this thesis in connection with the data treatment they relate to.

2.1 Flame Stability and Combustion Temperature

When flue gas is recycled to act as diluting gas in the combustion process the physical properties of the gas phase change significantly compared to air blown combustion. This is illustrated in table 3 that shows relevant physical properties of N_2 and CO_2.

Table 3 Physical properties of N_2 and CO_2 at 1123 K and atmospheric pressure [124].

Species	**Density [kg/m^3]**	**Heat Capacity [J/mol K]**	**Mass Diffusion Coefficient of O_2 in X [m^2/s]**
N_2	0.244	34.18	$1.7 \cdot 10^4$
CO_2	0.383	57.83	$1.3 \cdot 10^4$
Ratio N_2/CO_2	0.64	0.59	1.31

Liu et al. [16] carried out combustion experiments in a 20 kW down-fired combustor using pulverized bituminous coal in air and O_2/CO_2 mixtures at O_2 concentrations ranging from 21 - 35 vol. %. Results of Liu et al. [16] are presented in figure 4 and show the development from instable to stable flame as the O_2 concentration in the O_2/CO_2 mixtures increases from low to high (21 vol. % - 30 vol. %).

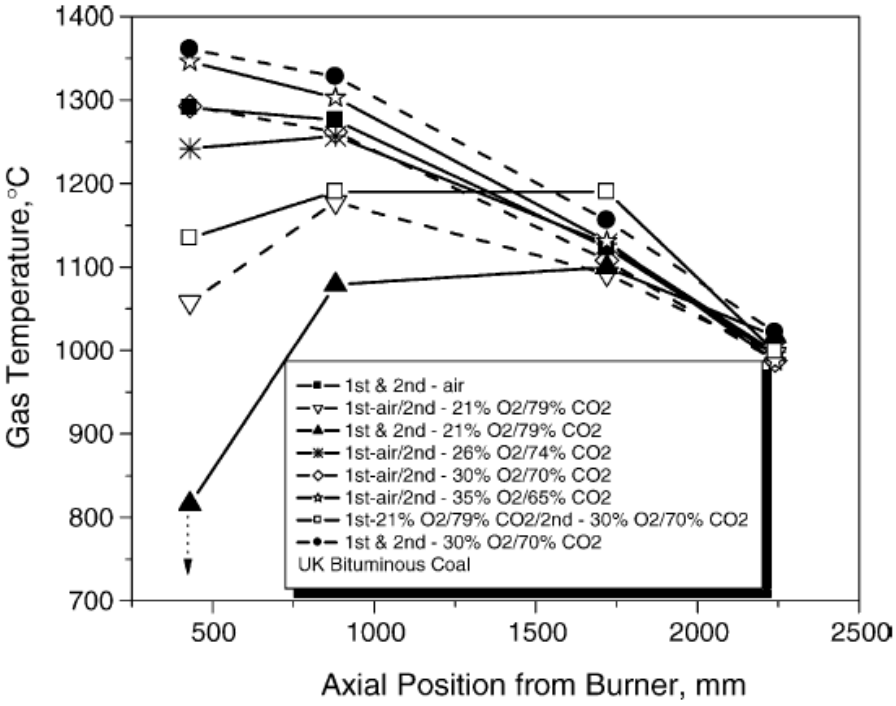

Figure 4 Temperature profiles measured by Liu et al. [16]. 1st and 2nd refers to non-swirling primary gas used for coal transport and swirling secondary gas. Total stoichiometry is 1.2.

With a mixture composed of 30 vol. % O_2 and 70 vol. % CO_2 Liu et al. [16] obtain both a stable flame and a reactor temperature profile similar to combustion in air. Their results also shows that the instability experienced at 21 vol. % O_2 in CO_2 is not present when air is used as primary gas (and N_2 thereby reduces the over all heat capacity near the ignition point in the flame), witnessing of the flame retarding effect of CO_2 when it is present in and near the flame at high concentrations.

Tan et al. [17] performed air blown and oxy-fuel combustion experiments in a vertical flow combustor using pulverized coals of different rank. They observed a less bright and more compact flame during oxy-fuel combustion than during air blown combustion. As observed by Liu et al. [16] Tan et al. [17] observed flame instability at an O_2 concentration of 21 vol. % and obtained flame stability, furnace temperatures and heat fluxes only deviating slightly from air blown combustion at an O_2 concentration between 28 - 35 vol. %. Similar results have been obtained by several authors [18,19,35,36]. Operating an oxy-fuel furnace at these conditions will however change burner aerodynamics due to changes in momentum flux of the primary and secondary gases and

cause a more detached flame [36]. A stable turbulent flame has however been achieved at 21 vol. % O_2 by Toporov et al. [28] using a strongly swirled secondary stream that facilitates a strong internal recirculation of hot combustion products back into the flame zone.

The instability experienced at the lower O_2 concentrations can be explained by the lower flame propagation speed with which pulverized coal clouds are ignited in CO_2 compared to N_2. This is illustrated well in figure 5 where measurements of flame propagation speed has been conducted using N_2, CO_2 or Ar as balance gas at different O_2 concentrations under microgravity. Figure 5 show that at approximately 30 vol. % O_2 in CO_2 a flame speed is obtained that match that in air. This has been reproduced by Suda et al. [37] who concluded that the difference in flame speed is caused mainly by the higher heat capacity of CO_2.

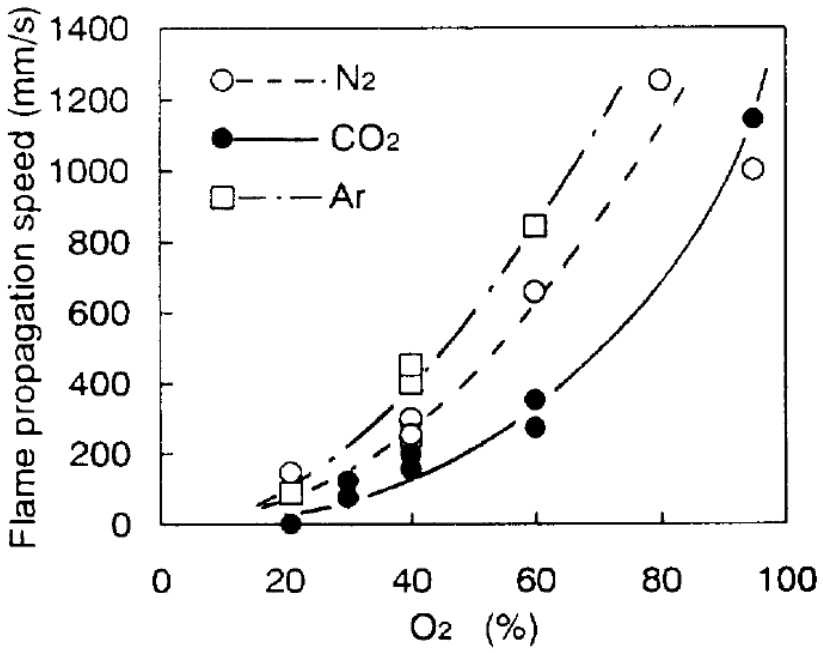

Figure 5 Flame propagation speeds measured by Kiga et al. [38] in a microgravity combustion chamber using a high volatile bituminous coal. Particle sizes are less than 74 μm.

From wire mesh reactor studies in air and O_2/CO_2 using brown coal and bituminous coal as fuels Qiao et al. [39] found that the ignition temperature of char were approximately 1.5 - 5 % higher in O_2/CO_2 compared to O_2/N_2. Even lower increases in ignition

temperature of 0.5 - 2.5 % under suspension fired conditions were reported by Arias et al. [40]. The ignition temperature in O_2/CO_2 decreased rapidly as the O_2 concentration was increased. Qiao et al. [39] included O_2/Ar and O_2/He mixtures, as well as air and O_2/CO_2, and found that the increase in ignition temperature correlated well with an increase in thermal conductivity. Conductivity could however not be the explanation for the differences between air and O_2/CO_2 (CO_2 and N_2 have almost identical thermal conductivities). The difference in ignition temperature between these gases was explained by the authors using endothermic CO_2-gasification.

Molina and Shaddix [35] found a delay in homogenous volatile ignition of a bituminous coal between O_2/N_2 and O_2/CO_2 atmospheres. They used an Entrained Flow Reactor (EFR) and explained their findings by an increased thermal sink in CO_2, due to its higher heat capacity and density, and by reduced mixing of the volatiles and gas caused by lower diffusivities in CO_2. The lower diffusivity of volatiles in CO_2 is also expressed through a more compact coal flame in oxy-fuel combustion [17,41] as discussed above.

From oxy-fuel and air blown combustion experiments in a 1.2 MW furnace using bituminous coal Nozaki et al. [42] showed that directing a part of the O_2 stream directly through the burner via an injection lance, without increasing overall O_2 concentration in the furnace, had a stabilizing effect on the flame and resulted in a higher combustion temperature. Their experiments also showed that a dry recycle increased the burner temperature with 150 K. At a first glance this seems strange since the heat capacity of H_2O is significantly lower than that of CO_2. Their findings therefore suggest that factors such as radiation/absorption and endothermic radical formation, involving the O/H/OH pool, dominate the temperature effect of H_2O in the recycle.

When the gaseous environment changes from N_2 based to CO_2 based the radiation from the gas phase changes as well towards higher emissivity and higher heat absorption. Andersson et al. [43] did, however, conduct radiation intensity measurements in lignite fired air and oxy-fuel flames and found that the replacement of N_2 with CO_2 only resulted in slightly higher total radiation intensity at identical temperatures due to the large contribution from particle radiation that reduced the effect of gaseous media. They found though that wet recycle of the flue gas increases radiation intensity more than the increase in CO_2 partial pressure. This observation is in line with that of Nozaki et al. [42] since

higher radiation intensity will cause a higher heat loss. In an earlier study Andersson and Johnsson [44] conducted measurements of radiation intensity in propane fired air and oxy-fuel combustion. Here they found a much larger difference (~30 %) in total radiation intensity between air and 27 vol. % O_2 in CO_2 at identical temperatures. Though partly due to an increased soot particulate formation in the oxy-fuel case their findings show the damping effect the presence of coal/char particles have on potential differences in overall radiation when retrofitting from air-blown to oxy-fuel combustion.

2.2 Devolatilization, Volatile Combustion and Char Morphology

The process of devolatilization starts at temperatures around 473 K to 673 K where hydrogen bonds are disrupted, water is evaporated and non-chemically bound molecules, encapsulated in the coal structure, are transported to the particle surface. For coals with high oxygen content crosslinking in the coal structure will also take place. After this initial phase of devolatilization, primary devolatilization, where weak bonds in the coal structure are thermally broken, starts. This results in the release of large organic fragments that condenses, thereby forming char, or leaves the coal particle as tar [45-47]. During primary devolatilization functional groups in the coal such as alkyl groups, hydroxyl groups and carboxy groups decomposes and release gaseous volatiles [45-47]. Also released during primary devolatilization are free radical groups such as CH_2 and O [47]. These radical groups have a major influence on the chemistry in the volatile flame and are therefore important for e.g. NO_x formation and destruction. After primary devolatilization ends secondary devolatilization begins where more stable chemical bonds such as those found in ether linkage, carbonyl groups and hetero-atoms are broken [45,46]. Primary devolatilization is normally considered completed when the H_2 evolution from depolymerization stops and ring rupture starts to produce HCN. The distribution of volatile gaseous species is highly dependent on coal composition and therefore rank and origin wherefore the description above is only qualitative. In general the amount of gaseous volatiles decreases as the coal rank increases and the amount of tar is highest for the intermediate coal ranks such as bituminous coals and low for both low and high rank coals [47].

Table 4 Mechanisms and functional coal groups taking part in the formation of the most important volatiles produced by primary devolatilization [45-48].

Volatile	**Mechanism**	**Functional Coal Group**
Tars	Distillation and decomposition	Weakly bonded ring clusters
CO_2	Decarboxylation	Carboxy groups
C_xH_y	Dealkylation	Alkyl groups
H_2O	Condensation and ether linkage formation	Hydroxyl groups and carboxy groups
H_2	Depolymerization	Weakly bonded ring clusters

Table 5 Mechanisms and functional coal groups taking part in the formation of the most important volatiles produced by secondary devolatilization [45,46,48].

Volatile	**Mechanism**	**Functional Coal Group**
CO	Decarboxylation and ring rupture	Ether linkage, carbonyl groups and hetero-oxygen
HCN	Ring rupture	Hetero-nitrogen
H_2	Ring condensation	Aromatics
C_xH_y	Dealkylation	Alkyl groups

The most important volatiles formed during primary and secondary devolatilization along with their formation mechanisms can be seen in table 4 and table 5, respectively. In practical applications of coal the devolatilization chemistry discussed above unfolds under the influence of operational parameters that are dependent of equipment, making data interpretation complicated. Under suspension fired conditions, using pulverized coal, the influence of heating rate on the resulting char properties is significant. Especially for medium rank coals, such as bituminous coal, the dualistic effects of volatile release and softening/resolidification of the char matrix are influenced by the heating rate of the particles. There has only been conducted a limited number of studies concerning devolatilization in oxy-fuel combustion and these has dealt mostly with devolatilization time, volatile ignition, flame temperature and the potential effect of CO_2 gasification.

These first three subjects were treated in section 2.1 and the following will therefore mostly focus on the influence of CO_2 gasification.

In a single particle reactor Bejarano and Levendis [49] found, using a three-color pyrometer, that the duration of the volatile flame from bituminous coal particles is significantly longer in O_2/CO_2 mixtures than in O_2/N_2 mixtures at similar O_2 concentrations and that the flame temperature is approximately 200 K lower ($T_{furnace}$=1400 K, $d_{particle}$ = 45 – 63 um). The duration of the volatile flame becomes similar when comparing an O_2 concentration in N_2 of 20 vol. % with one of 30 vol. % in CO_2. At these conditions the temperature of the volatile flames also becomes similar. This observation is consistent with the observations on flame characteristics discussed in section 2.1. Results by Molina and Shaddix [35], also obtained under single particle conditions ($T_{furnace}$=800 - 1250 K (non-isothermal reactor), $d_{particle}$ = 106 – 125 um) using bituminous coal, are somewhat contradictory in that they find no difference in the duration of volatile combustion once initiated, only a delay in volatile ignition. A similar delay in volatile ignition is found by Zhang et al. [50]. The disagreement could be due to differences in particle size, though Bejarano and Levendis [49] obtained similar results for a 75 – 90 um particle size fraction. It is not likely that the disagreement is due to a difference in volatile content since the proximate analysis gives 33.5 wt. % and 34.9 wt. % for the coals used by Bejarano and Molina, respectively. Probably it is due to differences in heating rate and chemical composition of the volatile pool. As the mixing of volatiles and O_2 contribute significantly to the ignition delay in O_2/CO_2 due to lower diffusion coefficients, differences in volatile species, and therefore mixing properties, would be expected to influence ignition considerably.

Jamil et al. [51] used a wire-mesh reactor to pyrolyse a brown coal, both as raw coal, demineralized coal and Na or Ca doped coal, in CO_2 or He, using heating rates of 1 or 1000 K s^{-1}, to peak temperatures up to 1173 K. They found that the tar yield was not affected by the gaseous atmosphere but that significant gasification took place in CO_2 causing an additional weight loss of up to 10 wt. %. Once a peak temperature of 1173 K was reached the weight loss caused by gasification was however not significantly affected by holding time at this temperature for raw- and demineralized coal. In the case of alkali doped coals the gasification reaction did however primarily contribute during the

holding time. This could suggest that the catalytic properties of ash towards gasification in the raw coal are reduced during pyrolysis, possibly by alkali evaporation or thermal deactivation of catalytic sites.

The effect of CO_2 gasification during devolatilization/pyrolysis is often discussed in the literature. Several authors reports that gasification contributes to char consumption [50,52-56] but several factors make it difficult to draw unambiguous conclusions. Firstly, a number of the studies have been conducted using low rank coals [50,51,55,56], which is known to be significantly more reactive than the medium rank coals used by other authors [52,54,56]. Secondly, some of the studies are carried out using ThermoGravimetric Analyzers (TGA) [52,54], which means that residence times are long (minutes to hours) and heating rates are low making it difficult to extrapolate the findings to industrial boiler operation. The studies carried out in flow reactors [50,53,55,56] use residence times between 0.4 and 1 second, somewhat longer than the devolatilization time of approximately 0.2 s in a boiler, and reports additional weight losses up to 25 wt. %, presumably caused by CO_2 gasification. This is a very significant contribution to over all fuel conversion and it some what contradicts the effect of gasification observed during char consumption with respect to reaction rate. The influence of gasification will be further discussed in section 2.3 in the context of char consumption.

2.2.1 Development of Char Morphology during Devolatilization

Char development during devolatilization is important for the combustion process. It is the morphology of the char, through its influence on pore structure, that determines its combustion behavior comprising among others reaction rate and thereby particle temperature as well as pore transport of reactant and product molecules such as O_2, CO_2 and NO. It is therefore imperative to examine the influence of devolatilization conditions on the development of char morphology. In general the development of char morphology is dependent on coal rank. This section will mainly focus on bituminous coal since this rank is widely used in industrial power generation.

Bituminous coals being representative of medium rank coals exhibit fluidity and softening when heated [47,57,58]. This fluidity is realized as a competition between bond

breaking reactions such as breakage of weakly bonded clusters and cross linking of condensing molecular fractions. The low temperature cross linking found for low rank, high oxygen containing coals, keep these coals from softening and the high aromatics, low hydrogen containing, high rank coals does not contain sufficient amounts of e.g. weakly bonded clusters to exhibit a softening behavior.

The fraction of coal components not connected to the coal matrix, thereby promoting the softening and fluidity in bituminous coals is called metaplast [58] and its behavior strongly influences the morphology of the resulting char. The volatiles formed in the interior of a softening particle will have difficulties escaping to the gaseous surroundings due to the breakdown of the internal pore structure following the fluidization/softening of the particle. This means that bubbles will form and merge inside the particle causing it to swell and it is to a large extent these bubbles that will determine the final char structure [47]. If internal bubble pressure becomes large enough to overcome the surface tension of the fluid particle the bubbles will burst and release the volatiles, thereby leaving large craters at the particle surface extending to its interior [59]. These craters will act as important transport ducts of products and reactants during the combustion process due to a low influence of Knudsen's diffusion.

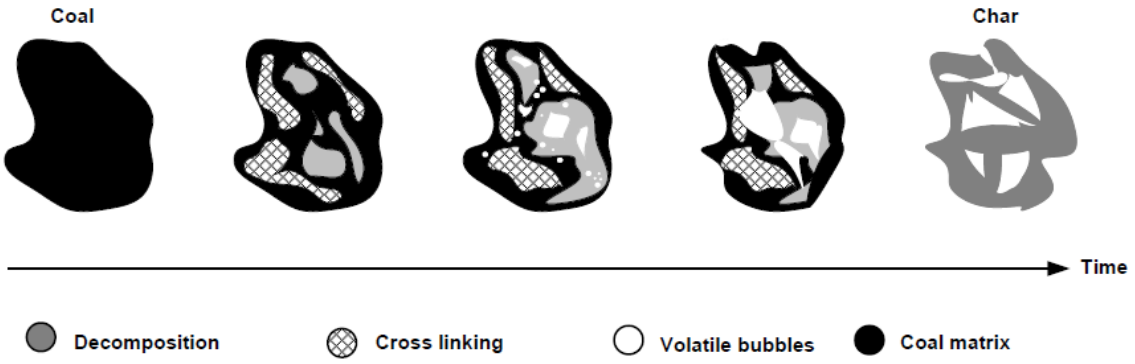

Figure 6 Softening and bubble formation of a medium rank coal particle during the formation of char.

The maceral composition of coal will directly affect its swelling behavior with the observed tendency that vitrinite and liptinite induces softening and swelling, while inertinite reduce them [47]. This behavior is related to a decrease in volatile release for coals of similar carbon content as the maceral constituents goes from liptinite over

vitrinite to inertinite [60]. The heating process for medium rank coals, responsible for char creation, is illustrated in figure 6.

Several authors [47,61,62] have described detailed classification systems that aim at standardizing the char after morphology for a more predictive evaluation of the chars combustion behavior. These classification systems contain several groups and subgroups and can therefore be difficult to apply in practice. In general three morphologies comprising cenospheres, network- and dense chars are reported to be present and these three morphologies are often used in practical applications such as modeling [47,63-65]. Schematic representations of the three morphologies, used by Ma and Mitchell [65] can be seen in figure 7.

Figure 7 Char configurations used for modeling by Ma and Mitchell [65]. Colors are; White = Cavity, Grey = Porous Char Matrix, Black = Inorganic Constituents.

The effect of CO_2 replacing N_2 on the resulting char morphology is not evident as only limited data on this is available in the literature. For some coals the swelling of the char does not seem to be affected by gaseous atmosphere [56] while other coals show sensitivity towards CO_2 with the tendency of slightly increased swelling [53]. It has been suggested that cross linking, facilitated by CO_2, could have a resolidifying effect on the char matrix for some coals, thereby limiting its structural break down and reduce its swelling, though it has never been validated experimentally [66]. No unambiguous conclusions can be drawn on CO_2's influence on char surface area and reactivity either. Rathnam et al. [53] and Al-Makhadmeh et al. [56] reports N_2-BET surface areas of chars obtained from pyrolysis in CO_2 at 1673 K and 1423 K, respectively, that deviates

between -88 % to 48 % from the surface areas of chars obtained from pyrolysis in N_2 at the same conditions. The coals used by Rathnam et al. [53] and Al-Makhadmeh et al. [56] range from low to medium rank. For some chars visual differences, seen by Scanning Electron Microscopy (SEM), have been reported [53,55] and for others no differences have been seen [56]. Some authors contribute these visual differences to partial gasification of the char surface [53,55].

The effect of heating rate on swelling and char structure is significant and not linear and the different thermal properties of N_2 and CO_2 therefore present a potential cause of differences in char structure at non-isothermal conditions. At heating rates below approximately 10^3 K s^{-1}, depending on the maceral composition of the coal, the swelling is reported to increase [67]. When heating rate increases to above 10^4 K s^{-1} the swelling declines from its maximum level and so does particle porosity [67].

2.3 Char Conversion

The heart of the combustion process in both air blown and oxy-fuel combustion is the fuel conversion. The conversion takes place through volatile and char combustion and the implications of an O_2/CO_2 environment on these reaction pathways are therefore crucial. Devolatilization and volatile combustion was discussed in sections 2.1 and 2.2 wherefore this section will focus on the thermal conversion of char.

Alterations in the rate of char consumption will change the heat release from heterogeneous combustion and therefore the heat transfer in the boiler. In addition to changes in heat transfer there is also a risk of poorer fuel utilization. As an important feature of oxy-fuel combustion is the possibility of retrofitting existing air blown plants it is therefore important not only to elucidate differences between O_2/N_2 and O_2/CO_2 char conversion but also to match the burnout and conversion profile of air blown plants.

Várhegyi et al. [68] conducted TGA experiment on bituminous- and lignite chars in O_2/CO_2 and O_2/Ar environments. The chars were prepared by heating to 1223 K at a heating rate of 10 K min^{-1}. A size fraction of 120 – 200 μm were then used for experiments carried out with O_2 concentrations between 5 and 100 vol. % using heating rates of 10, 20, 25 and 50 K min^{-1} to a peak temperature of 1173 K. Várhegyi et al. [68]

concluded that the presence of high concentrations of CO_2 did not affect the char conversion rate due the low gasification rate compared to the char-O_2 reaction rate. This conclusion is supported by other authors working under similar conditions [53,69,70]. Authors that report differences in TGA conversion rate between O_2/N_2 and O_2/CO_2 often operate under the influence of diffusion control making conclusions on intrinsic kinetics difficult [52,55].

From Drop Tube Furnace (DTF) experiments at 1673 K Rathnam et al. [53] found increased burnouts of up to 5 percentage points for four different coals in O_2/CO_2 compared to O_2/N_2. As the O_2 concentration was increased from 5 to 15 vol. % this difference did however vanish. As discussed in section 2.2 Rathnam et al. [53] also carried out DTF pyrolysis at the same conditions with the same coals and here they saw an increase in volatile yield between 1.3 and 12.7 percentage points when CO_2 was used instead of N_2. There is no obvious connection between a high additional weight loss during pyrolysis and combustion in the experiments of Rathnam et al. [53]. This makes it difficult to conclude on the effect of CO_2 gasification as other factors may play a role in the weightloss during pyrolysis (see section 2.2) and transport phenomena likely influence the char conversion rate during combustion. Opposite to the findings of Rathnam et al. [53] Arias et al. [40] saw a 2 – 5 percentage point decrease in char conversion when bituminous coal was burned in an EFR at 21 vol. % O_2 in CO_2 compared to combustion in N_2, which was also found by Liu et al. [16,71], Li et al. [55] and Wang et al. [19] under similar conditions.

Al-Makhadmeh et al. [56] conducted experiments under suspension fired conditions at 1573 K at 5 and 15 vol. % O_2 in N_2 or CO_2 using a lignite- and a bituminous char. At 5 vol. % O_2 they found no differences in char conversion rate between O_2/CO_2 and O_2/N_2 whereas conversion was faster in O_2/N_2 at 15 vol. % O_2. This could be due to the high fuel load used by the authors, which causes high gas temperatures. At 15 vol. % O_2, where combustion is fierce, the difference in heat capacity between N_2 and CO_2 could lower the gas temperature in CO_2 (see section 2.1) and cause a lower conversion rate. Zhang et al. [50] found that the conversion rate of brown coal in a DTF was nearly the same at 21 vol. % O_2 in N_2 or CO_2 at 1273 K but that the initial conversion rate was lowered in O_2/CO_2 compared to O_2/N_2 when combustion took place at 1073 K. They

attributed this to an enhanced effect of CO_2 gasification at the higher temperature. Zhang et al. [50] came to a similar conclusion on bituminous coal combustion, though the effect of gasification was found to be less pronounced [72]. Measurements of dynamic conversion profiles in O_2/N_2 and O_2/CO_2, such as those of Al-Makhadmeh et al. [56] and Zhang et al. [50], are rare and more is needed for a thorough evaluation of conversion rate at industrially relevant conditions.

Observations of particle combustion temperature in O_2/CO_2 mixtures compared to O_2/N_2 mixtures were made by Bejarano and Levendis [49] who measured the burning temperature of bituminous- and lignite char particles in the two different gaseous environments using a three-color pyrometer under single particle conditions. At equivalent O_2 concentrations the burning temperature was always lower for chars burning in the O_2/CO_2 environment by around 200 – 120 K depending on the fuel. As discussed in section 2.2 the authors found that longer time was needed for volatile combustion in the CO_2 environment but they also found longer char burn out times exceeding the time delay arising from the devolatilization. This suggests a delayed heterogeneous ignition, which is supported by data from Molina and Shaddix [35].

2.3.1 Modeling Char Conversion

When heterogeneous char conversion is to be modeled several aspects must be taken into consideration. A structural model, describing the evolution of density and size of the particles during reaction, must be established. Transport of reactants and products, both in the stagnant gas film layer surrounding a particle and in the particles interior, must be adequately described. It is also important for a trustworthy model that the char conversion rate is accurately determined. Heat transfer between the particle and its surroundings must also be accounted for as both char conversion rate and transport phenomena are highly dependent on temperature.

The construction of a structural model for the particles during the combustion process stems from the discussion on morphology in section 2.2.1. As char is not homogeneous detailed models therefore considers the char to consist of different morphologies [63-65]. A variety of equations, describing particle mass balances, can be encountered in the

literature all arising from the assumptions made by the modeler. These equations will not be treated here but they can be found many places in the literature e.g. [73-75]. Here a discussion will instead be taken on universal aspects of char combustion that must be accounted for by the modeler and how these are often accommodated.

To account for transport of reactants and products till and from a particle an often used approach is the single film model expressed by eq. 1 [76], which ignores the effect of counter diffusion. The mass transfer coefficient, k_A, is depending on the diffusion coefficient of component A in the film layer, the thickness of the film layer and the logarithmic mean concentration of A in the film layer. In eq. 1 N_A is the flux of A and ΔC_A is the absolute difference in concentration of A across the film layer. The mass transfer coefficient is often found by eq. 2, which is valid for a sphere experiencing forced convective flow [77]. The Reynolds number is that of the particle and Schmidt's number is found for the film layer. Similar to eq. 1 and eq. 2, convective heat flux and heat transfer coefficient for the particle can be found [77].

$$N_A = k_A \cdot \Delta C_A \qquad \text{Eq. 1}$$

$$\frac{k_A \cdot d}{D_A} = 2 + 0.6 \cdot \left(\mathrm{Re}^{\frac{1}{2}} \cdot Sc^{\frac{1}{3}} \right) \qquad \text{Eq. 2}$$

When combustion progresses the reaction rate will reach a level where the diffusion of reactant, usually O_2, is too slow to maintain a uniform concentration profile throughout the particle and may even reach a situation where the O_2 concentration at the particle surface approaches zero. On this basis three different combustion zones are used when discussing char conversion. In zone I the concentration of reactant is that of the bulk gas throughout the particle and its conversion rate are therefore determined solely by chemical kinetics. In zone II diffusion limitations cause a concentration profile to form inside the particle. Depending on the transport properties of the surrounding gas film the surface concentration of reactant may also start to decrease. During zone III combustion particle conversion is taking place under external mass transfer control. Here the reaction rate is so fast that the surface concentration of the reactant that is effectively zero.

Examples of the concentration profiles belonging to each of the three combustion zones can be seen in figure 8.

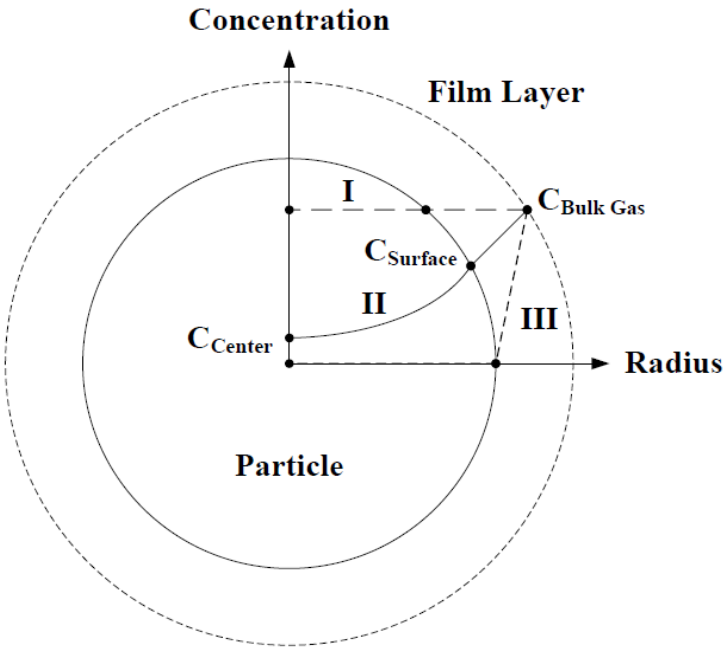

Figure 8 Concentration profiles indicating combustion zone I: No diffusion resistance, II: Internal and external diffusion resistance and III: External diffusion resistance.

When combustion is taking place under the influence of diffusion resistance the development of a concentration profile inside the particle means that the reaction rate will decrease towards its center. To account for this a generalized Thiele modulus, as expressed by eq. 3 [78], is often used to calculate an effectiveness factor from eq. 4, which applies for spheres. Eq. 3 is applicable for an irreversible reaction of reaction order $n > -1$ taking place in an isothermal particle. When n = 1 eq. 3 is exact, otherwise the accuracy is within 10 – 15 %. In eq. 3 V and S are the volume and the surface area of the particle, k is the reaction rate constant, C_s the surface concentration of reactant, ρ_s the apparent density of the particle and D_{eA} the effective diffusion coefficient of the reactant. The effectiveness factor in eq. 4 can be multiplied onto the reaction rate to account for the fractional decrease in particle conversion rate.

$$\phi = \frac{V}{S} \cdot \sqrt{\frac{n+1}{2} \cdot \frac{k \cdot C_s^{n-1} \cdot \rho_s}{D_{eA}}} \qquad \text{Eq. 3}$$

$$\eta = \frac{3 \cdot \phi \cdot \coth(3 \cdot \phi) - 1}{3 \cdot \phi^2} \qquad \text{Eq. 4}$$

The above is a short introduction into the considerations of a modeler. Depending on the structural description of the particles, assumptions relating to transport phenomena and the choice of kinetic expression for char conversion the resulting mass balance can take a variety of forms.

2.4 NO_x Emission in Oxy-Fuel Combustion

It has been found by several researchers [16-18,26,71,79-81] that oxy-fuel combustion changes the NO_x production/destruction characteristics towards a decreased emission compared to air blown combustion. Even though this effect is scientifically proven it is still highly disputed what causes the decreased emission. As both gas phase chemistry and physical parameters change between O_2/N_2 and O_2/CO_2 combustion it is imperative to examine both homogeneous and heterogeneous NO_x chemistry in search of an explanation.

2.4.1 Homogeneous Formation and Reduction of NO_x

The vast majority of the homogeneous NO_x chemistry is taking place during devolatilization and near the flame zone of the boiler. The implications oxy-fuel combustion will have on the homogeneous NO_x formation/destruction are therefore likely to be alterations in equilibriums and reaction pathways caused by higher concentrations of CO_2 and NO_x in this part of the furnace. If flue gas recirculation is taking place as wet recycle a higher concentration of H_2O also interfere through its influence on radical formation/destruction, especially in the O/H/OH pool. Increased amounts of CO_2 and H_2O in the near burner region will also interact in the gas phase chemistry through their role as collision partners.

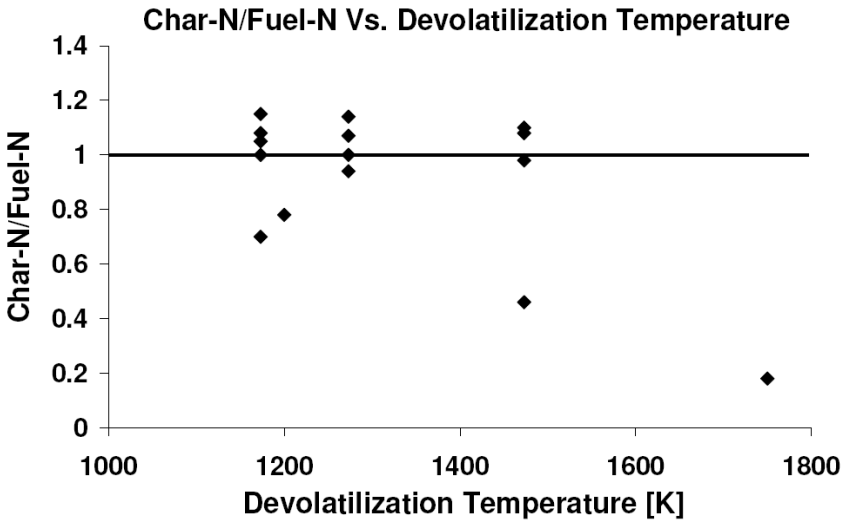

Figure 9 The relation between nitrogen content in fuel and char for different pyrolysis temperatures. Particle sizes are below 250 μm with the vast majority being in the range 44 – 63 μm. Heating rates are high, characterizing heating rates normally found in pulverized coal combustion [82-86].

The importance of homogeneous NO_x formation versus heterogeneous NO_x formation in the production of fuel-NO_x is strongly dependent on the fuel-N partition during devolatilization. This partition is a complicated function of temperature, heating rate and the distribution of N-functional groups in the fuel. It is therefore not always immediate what behavior to expect for a certain fuel. In general it can be expected that more fuel-N escapes by devolatilization at higher temperatures and heating rates [87], which is illustrated in figure 9 for temperature.

It can be seen from figure 9 that at temperatures prevailing in the devolatilization zone of a boiler more nitrogen tends to be lost as volatiles than is retained in the char. Besides temperature the composition of the coal with respect to elemental carbon also has an effect, showing a tendency of increased N-retention as the content of elemental carbon (coal rank) [58] increases.

Andersson et al. [18] conducted air and oxy-fuel combustion experiments with pulverized lignite using a 100 kW test unit with flue gas recycling. They found that NO emissions decreased 70 – 75 % when air was replaced with O_2/CO_2 at an O_2 concentration between 25 and 29 vol. %. In the interval 1.18 – 1.41, stoichiometry was not found to have a strong influence. From modeling Andersson et al. [18] concluded that the cause of the lower NO emissions in oxy-fuel combustion was an increased NO destruction as NO

formation was found to be slightly higher than in air. It was found that the inverse Zeldovich mechanism, R 1 - R 3, contributes significantly to NO reduction at high temperatures.

$$O + N_2 \rightleftharpoons NO + N \qquad \text{R 1}$$

$$N + O_2 \rightleftharpoons NO + O \qquad \text{R 2}$$

$$N + OH \rightleftharpoons NO + H \qquad \text{R 3}$$

Glarborg and Bentzen [88] performed experiments in O_2/N_2 and O_2/CO_2 using CH_4 as fuel. The temperature interval investigated was 1200 – 1800 K. Peak CO concentrations were found to increase in O_2/CO_2 by a factor 4 - 19 compared to O_2/N_2 across the temperature interval [88]. This increase was found, primarily, to be due to reaction R 4 though reaction between CH_4 and methylene radicals (CH_2) contributed to some extent.

$$CO_2 + H \rightleftharpoons CO + OH \qquad \text{R 4}$$

The implications of reaction R 4 do not only concern the formation of CO. Mendiara and Glarborg [91] found that a high CO_2 concentration enhanced NO formation from NH_3 under reducing conditions while it inhibited NO formation at stoichiometric and lean conditions. Giménez-López et al. [92] found that an oxy-fuel atmosphere inhibited the oxidation of HCN under reducing, stoichiometric and oxidizing atmospheres at temperatures prevailing in an industrial boiler. Mendiara and Glarborg [91] and Giménez-López et al. [92] explained the effect of CO_2 with an alteration of the O/H/OH radical pool caused by reaction R 4 where CO_2 competes with molecules such as O_2 for atomic hydrogen. That a change in O/H/OH radical pool indeed does alter the NO formation chemistry is seen in figure 10 that shows the main reaction pathways for HCN and NH_3 oxidation reported in the literature [93-95].

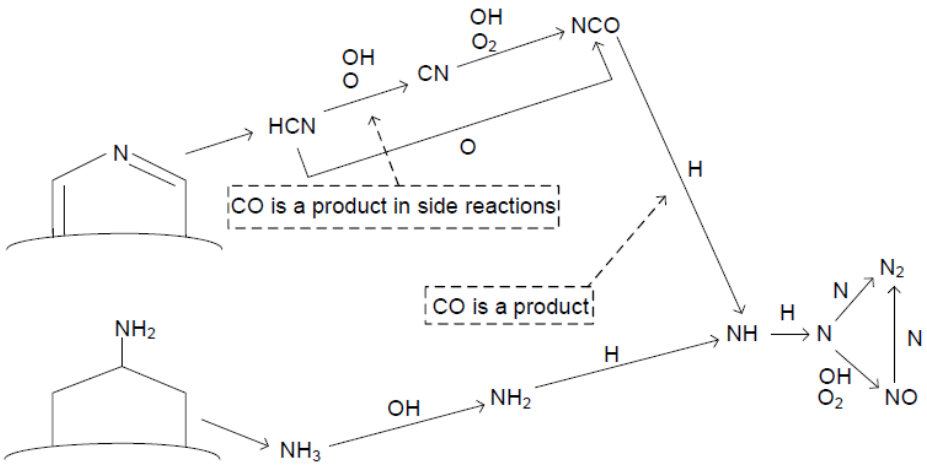

Figure 10 Main reaction pathways for the homogeneous production/destruction of fuel-NO where an alteration in O/H/OH radical pool will affect equilibrium [93-95].

2.4.2 Heterogeneous Formation and Reduction of NO_x

The heterogeneous formation and reduction of NO_x, mainly NO, is a subject of continued debate, in particular the mechanism for NO formation/destruction on the surface of char. There is in general agreement on a formation mechanism as given by reactions R 5 and R 6 [96].

$$O_2 + C + C(N) \rightarrow C(O) + C(NO) \qquad \text{R 5}$$

$$C(NO) \rightarrow C + NO \qquad \text{R 6}$$

A subject of debate related to NO release from char during oxidation is whether HCN could be acting as an intermediate in the NO formation similar to that known in volatile oxidation. Investigations by Thomas and coworkers [97-99] show that small amounts of HCN, produced during oxidation of devolatilized char, are in fact found. Other investigators [100-104] support the findings of Thomas and coworkers [97-99] though the primary release of char-N as HCN can not be taken as unambiguous [105]. The existence of HCN as a primary product will however affect the NO release in oxy-fuel combustion through the homogeneous mechanism discussed in section 2.4.1.

The switch from N_2 to CO_2 itself changes the primary release products to the extent CO_2 gasification is taking place (see sections 2.2 and 2.3). Park et al. [106] investigated nitrogen release from pulverized bituminous coal char during the reaction with O_2, CO_2 and H_2O using Ar as carrier gas. Their experiments showed that an increased concentration of CO_2 moved the selectivity towards lower release ratios of char-N to NO. In contrast to gasification with H_2O no HCN or NH_3 were measured when CO_2 was used as reactant. These findings are of interest for the case of oxy-fuel combustion because they prove that increasing concentrations of CO_2 actively interferes with the NO formation through the suppression of it and its precursors. It will however be the char-O_2 reaction that determines how the majority of char-N is released.

Even though most researchers agree on the direct oxidation of char nitrogen through a path equivalent or similar to reactions R 5 - R 6 there are still a wide dispute as to how the heterogeneous NO reduction over the char is taking place. With respect to determination of reaction kinetics, comparison between different chars are made complicated by the proven catalytic effect that especially alkali metals have on the NO-char reaction [107-111], the different experimental conditions employed by the researchers and the distribution of nitrogen functionalities found in different chars. Therefore an actual kinetic comparison of the different expressions found in the literature is not made here and focus is kept on mechanistic features of surface reactions.

Since most of the mechanistic studies on the heterogeneous formation and destruction of NO have been conducted under N_2, Ar or He atmospheres this section will mostly present the findings from these studies. The potential effects of high concentrations of CO_2 will be evaluated through comparison with oxy-fuel studies reported in the literature.

Levy et al. [112] suggested the heterogeneous reduction mechanism for NO on char shown in reactions R 7 - R 10. The authors based this mechanism on experiments performed in a laminar flow furnace at 1250 K and 1750 K with He as the main gas. Reaction R 10 suggests an enhancing effect of CO, which was indeed found by the authors [112]. The enhancing effect of CO has been confirmed by other authors under different conditions [113-115] although not all of these authors contribute the enhancement to reaction R 10. The effect of CO has been found to decrease with increasing temperature [112,115].

The first step of the reaction sequence in R 7 - R 10 is the adsorption and following dissociation of NO on the char surface. This reaction step is generally accepted and it therefore forms the basis for almost all mechanisms found in the literature [116-120].

$$NO + 2C \rightarrow C(N) + C(O) \quad \text{R 7}$$

$$C(N) + C(N) \rightarrow N_2 + 2C \quad \text{R 8}$$

$$C(O) \rightarrow CO \quad \text{R 9}$$

$$C(O) + CO \rightarrow CO_2 + C \quad \text{R 10}$$

The reaction between NO and char have been found to exhibit clear two regime behavior where initially desorption of surface oxides is believed to control the reduction up until approximately 873 - 1073 K after which the reaction becomes chemisorption controlled [113,121]. Figure 11 shows the reactivity of NO over three different carbon samples. From the figure it can be seen that the two regime behavior is only present for experiments without CO and that the reactivity of NO without CO present approaches that with CO present as the temperature increases. It is therefore surprising that Levy et al. [112] observed the enhancing effect of CO, though small, at temperatures as high as 1750 K. This observation can be due to the relatively high CO concentration of 1.4 % used by Levy et al. [112] compared to values between 100 and 4000 ppm used in many of the literature studies. In oxy-fuel combustion CO concentrations are higher than in air blown combustion by a factor of 2-3 [16,79,122], exceeding the 1.4 vol. % of Levy et al. [112], depending on stoichiometry and reactor position, and CO could therefore have a positive effect on NO reduction in oxy-fuel combustion even at high temperatures.

Aarna and Suuberg [114] found that the addition of CO to the NO-char reaction in a fixed bed reactor at 1073 K enhanced the reaction rate instantaneously to a level exceeding that of a clean char surface (i.e. without oxide complexes) and suggested that a parallel surface catalyzed reaction, R 11, is taking place and that the stripping of oxide complexes may not be the governing enhancing effect of CO. R 11 is suggested several places in the literature [113,118-120,123].

$$2NO + 2CO \rightarrow N_2 + 2CO_2$$ R 11

Above it can be seen that the effect of CO is the most likely mechanistic enhancement on heterogeneous NO reduction that can be expected when N_2 is replaced with CO_2 in the combustion process.

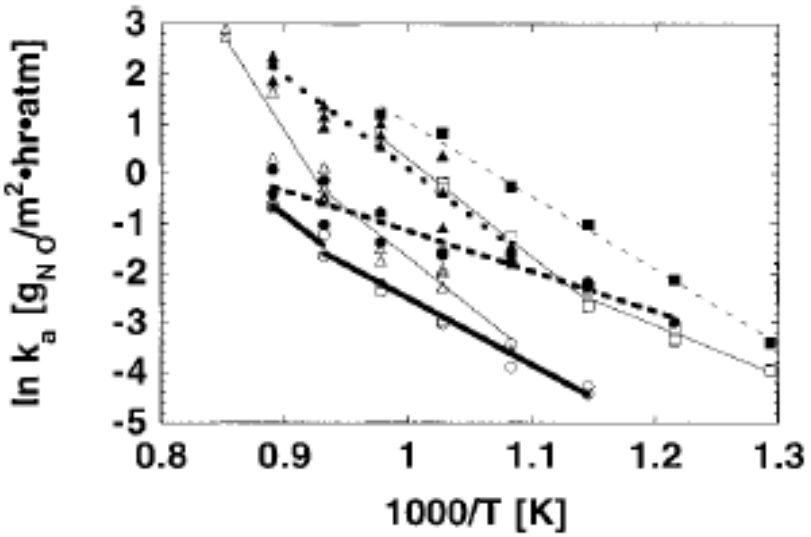

Figure 11 Reactivity of NO measured in a fixed bed reactor. Open symbols and solid lines indicate experiments with NO. Solid symbols and dashed lines indicate experiments with NO and CO. Triangles: Graphite (65 ppm NO, 276 ppm CO). Squares: Wyodak coal char (70 ppm NO, 400 ppm CO). Circles: Resin char (65 ppm NO, 270 ppm CO). From Aarna and Suuberg [114].

Another important aspect of heterogeneous NO reduction in O_2/CO_2 vs. O_2/N_2 is the changed transport properties of NO and O_2 illustrated by the diffusion coefficients in table 3 (O_2 and NO exhibits similar diffusion properties). The lower diffusion coefficient of O_2 in CO_2 means that zone II and III char combustion is reached at lower particle temperatures. This facilitates that the particles interior becomes reducing as the O_2 does not penetrate it effectively. Further increases in particle temperature will therefore increase NO reduction rate faster than NO production rate as the later is proportional to combustion rate. This effect is reported in the literature for O_2/N_2 combustion [94] and it can potentially affect O_2/CO_2 combustion strongly as NO could have a longer residence

time in the particle. It is however a task for detailed modeling to quantify this effect during oxy-fuel combustion.

3 Conclusions on the Literature

If coal is to be kept as a feedstock for energy generation in a carbon constrained world CCS technology will have to be utilized. Among the CCS-technologies, closest to industrialization, oxy-fuel combustion is a promising candidate for use in areas with available storage sites. The price of CO_2 capture in oxy-fuel combustion is still uncertain as technical aspects such as possible plant size, O_2 purity requirement, degree of N_2-leakage into the boiler, CO_2 purity requirements for transport and storage and the price and feasibility of O_2 production in very large scale have not been elucidated. The prospect of co-storage of NO_x, SO_x and CO_2 offer savings in plant construction and operation but for oxy-fuel combustion to stand out markedly compared to e.g. post-combustion capture and IGCC's a step reduction in O_2 production cost must be made. This is likely to take place through technological improvements of the unit operations in cryogenic plants, the introduction of upcoming technologies, such as membrane separation, at an industrial scale or the lowering of O_2 purity requirements.

From several literature investigations it was found that boiler temperature profiles similar to air-blown combustion can be obtained in oxy-fuel combustion using inlet O_2 concentrations of 28 – 35 vol. %. During normal burner operation at O_2 concentrations close to that in air, oxy-fuel combustion will produce an unstable flame not suited for continues boiler operation. Experiments does however show that by changing burner configuration and inducing a strong internal recirculation in the boiler it is possible to achieve stable flames at O_2 concentrations similar to that in air. During stable combustion at similar O_2 concentrations O_2/CO_2 environments will give lower gas and particle temperatures, slower ignition and volatile combustion and possibly slightly longer burnout times than combustion in O_2/N_2. The effect of CO_2 gasification is not clear from literature experiments. While some authors find a strong contribution from CO_2 gasification to fuel conversion results of others question this. There does not seem to be a strong correlation between observed CO_2 gasification during devolatilization and

subsequent char conversion. There exists a strong need for dynamic char conversion profiles, obtained under industrial condition in O_2/CO_2 and O_2/N_2, for the evaluation of fuel conversion in oxy-fuel combustion.

The NO emission from coal combustion is significantly affected by the change from N_2 to CO_2 based combustion. The NO gas phase chemistry is especially affected by the competition with CO_2 for atomic hydrogen, which affects the O/H/OH radical pool and inhibits the oxidation of HCN and NH_3. The inverse Zeldovich mechanism may also play a role through NO reduction at high gas phase temperature.

Heterogeneous reduction of NO over char is mostly affected by the higher concentration of CO in O_2/CO_2 compared to O_2/N_2 combustion, possibly by the removal of oxygen surface complexes or by direct surface catalyzed reduction. The lower diffusion coefficient of O_2 in CO_2 compared to N_2 may cause an enhanced NO reduction due to longer residence times of NO in the particles.

4 Abbreviations

ASU	Air Separation Unit
CCS	Carbon, Capture and Storage
COE	Cost Of Electricity
DTF	Drop Tube Furnace
EFR	Entrained Flow Reactor
EOR	Enhanced Oil Recovery
FGD	Flue Gas Desulphurization
IEA	International Energy Agency
IGCC	Integrated Gasification Combined Cycle
ITM	Ion Transport Membrane
MDEA	MethylDiEthanolAmine
MEA	MonoEthanolAmine
PSA	Pressure Swing Adsorption
SCR	Selective Catalytic Reduction
SEM	Scanning Electron Microscopy
TGA	ThermoGravimetric Analyzer

5 References

[1] Tan R, Corragio G, Santos S. Oxy-coal combustion with flue gas recycle for the power generation industry, IFRF, 2005

[2] www.ipcc.ch, 19-06-08

[3] Davison J. Performance and costs of power plants with capture and storage of CO_2. Energy 2007;32:1163-6

[4] Figueroa DJ, Fout T, Plasynski S, McIlvried H. Advances in CO_2 capture technology-The U.S. department of energy's carbon sequestration program. Int J Greenhouse Gas Control 2008;2:9-0

[5] Buhre BJP, Elliot LK, Sheng CD, Gupta RP, Wall TF. Oxy-fuel combustion technology for coal-fired power generation, Prog Energy Combust Sci 2005;31: 283-7

[6]http://www.bp.com/liveassets/bp_internet/globalbp/globalbp_uk_english/reports_and_publications/statistical_energy_review_2007/STAGING/local_assets/downloads/pdf/coal_section_2007.pdf, 17-12-09

[7] www.oplevnaturvidenskaben.dk, 30-05-07

[8] Wall TF. Combustion processes for carbon capture. Proc Combust. Inst 2007;31:31-7

[9] Newsome SD. The water-gas shift reaction. Catal Rev-Sci Eng 1980;21:275-8

[10] Chorkendorff J, Niemantsverdriet JW. Concepts of modern catalysis and kinetics. 1st edition. WILEY-VCH; 2005

[11] Kanniche M, Bouallou C. CO_2 capture study in advanced integrated gasification combined cycle. Appl Therm Eng 2007;27:2693-2

[12] Berguerand N, Lyngfelt A. Design and operation of a 10 kW_{th} chemical-looping combustor for solid fuels – Testing with South African coal. Fuel 2008;87:2713 – 6

[13] Xiang W, Wang S. Investigation of gasification chemical looping combustion combined cycle performance. Energy Fuels 2008;22:961-6

[14] Wang J, Anthony EJ. Clean combustion of solid fuels. Appl Energy 2008;85:73 – 9

[15] Murphy JJ, Shaddix CR. Combustion kinetics of coal chars in oxygen-enriched environments. Combust Flame 2006;144:710-9

[16] Liu H, Zailani R, Gibbs BM. Comparisons of pulverized coal combustion in air and in mixtures of O_2/CO_2. Fuel 2005;84: 833-0

[17] Tan Y, Croiset E, Douglas MA, Thambimuthu KV. Combustion characteristics of coal in a mixture of oxygen and recycled flue gas. Fuel 2006;85:507-2

[18] Andersson K, Normann F, Johnsson F, Leckner B. NO emission during oxy-fuel combustion of lignite. Ind Eng Chem Res 2008;47:1835-5

[19] Wang CS, Berry GF, Chang KC, Wolsky AM. Combustion of pulverized coal using waste carbon dioxide and oxygen. Combust Flame 1988;72:301-0

[20] Singh D, Croiset E, Douglas PL, Douglas MA. Techno-economic study of CO_2 capture from an existing coal-fired power plant: MEA scrubbing vs. O_2/CO_2 recycle combustion. Energy Convers Manage 2003;44:3073 –1

[21] Acharya D, Krishnamurthy KR, Leison M, MacAdam S, Sethi VK, Anheden M, Jordal K, Yan J. Development of a high temperature oxygen generation process and its application to oxycombustion power plants with carbon dioxide capture. http://www.engr.pitt.edu/pcc/Past%20Conferences/2005/294.pdf, 30-09-08

[22] Okawa M, Kimura N, Kiga T, Takano S, Arai K, Kato M. Trial design for CO_2 recovery plant by burning pulverized coal in O_2/CO_2. Energy Convers Manage 1997;38:123 –7

[23] Strömberg L. Combustion in a CO_2/O_2 mixture for a CO_2 emission free process. Second Nordic Minisymposion on Carbon Dioxide Capture and Storage

[24] Andersson K, Johnsson F. Process evaluation of an 865 MW_e lignite fired O_2/CO_2 power plant. Energy Convers Manage 2006;47: 3487-8

[25] Li H, Yan J, Yan J, Anheden M. Impurity impacts on the purification process in oxy-fuel combustion based CO_2 capture and storage. Appl Energy 2009;86:202-3

[26] Liu H, Okazaki K. Simultaneous easy CO_2 recovery and drastic reduction of SO_x and NO_x in O_2/CO_2 coal combustion with heat recirculation. Fuel 2003;82:1427-6

[27] Toporov D, Förster M, Kneer R. How to burn pulverized coal in CO_2 atmosphere at low oxygen concentrations. VDI-BERICHTE 2007;1988:55 – 0

[28] Toporov D, Bocian P, Heil P, Kellermann A, Stadler H, Tschunko S, Förster M, Kneer R. Detailed investigation of a pulverized fuel swirl flame in CO_2/O_2 atmosphere. Combust Flame 2008;155:605-8

[29] www.doe.gov, 17-03-08

[30] Kimura N, Omata K, Kiga T, Takano S, Shikisima S. The characteristics of pulverized coal combustion in O_2/CO_2 mixtures for CO_2 recovery. Energy Convers Manage 1995;36:805-8

[31] Castle WF. Air separation and liquefaction: Recent developments and prospects for the beginning of the new millennium. Int J Refrig 2002;25:158-2

[32] Armstrong PA, Foster EP, Gunardson HH. ITM oxygen for gasification. SPE/PS-CIM/CHOA 97801

[33] Smith AR, Klosek J. A review of air separation technologies and their integration with energy conversion processes. Fuel Process Technol 2001;70:115-4

[34] Yantovski E, Gorski J, Smyth B, Elshof Jt. Zero-emission fuel-fired power plants with ion transport membrane. Energy 2004;29:2077-8

[35] Molina A, Shaddix CR. Ignition and devolatilization of pulverized bituminous coal particles during oxygen/carbon dioxide coal combustion. Proc Combust Inst 2007;31:1905-2

[36] Khare SP, Wall TF, Farida AZ, Liu Y, Moghtaderi B, Gupta RP. Factors influencing the ignition of flames from air-fired swirl pf burners retrofitted to oxy-fuel. Fuel 2008;87:1042-9

[37] Suda T, Masuko K, Sato J, Yamamoto A, Okazaki K. Effect of carbon dioxide on flame propagation of pulverized coal clouds in CO_2/O_2 combustion. Fuel 2007;86:2008-5

[38] Kiga T, Takano S, Kimura N, Omata K, Okawa M, Mori T, Kato M. Characteristics of pulverized-coal combustion in the system of oxygen/recycled flue gas combustion. Energy Convers Manage 1997;38:129-4

[39] Qiao Y, Zhang L, Binner E, Xu M, Li, C-Z. An investigation of the causes of the differences in coal particle ignition temperature between combustion in air and in O_2/CO_2. Fuel 2010;89: 3381-7

[40] Arias B, Pevida C, Rubiera F, Pis JJ. Effect of biomass blending on coal ignition and burnout during oxy-fuel combustion. Fuel 2008;87:2753-9

[41] Smart J, Lu G, Yan Y, Riley G. Characterisation of an oxy-fuel flame through digital imaging. Combust Flame 2010;157:1132-9

[42] Nozaki T, Takano S, Kiga T, Omata K, Kimura N. Analysis of the flame formed during oxidation of pulverized coal by an O_2-CO_2 mixture. Energy 1997;22:199-5

[43] Andersson K, Johansson R, Hjärtstam S, Johnsson F, Leckner B. Radiation intensity of lignite-fired oxy-fuel flames. Exp Therm Fluid Sci 2008;33:67-6

[44] Andersson K, Johnsson F. Flame and radiation characteristics of gas-fired O_2/CO_2 combustion. Fuel 2007;86:656-8

[45] Solomon PR, Serio MA, Suuberg EM. Coal pyrolysis: Experiments, kinetic rates and mechanisms. Prog Energy Combust Sci 1992;18:133-0

[46] Mill CJ. Pyrolysis of fine coal particles at high heating rate and pressure. Ph.d Thesis. University of New South Wales, Australia, 2000

[47] Yu J, Lucas JA, Wall TF. Formation of the structure of chars during devolatilization of pulverized coal and its thermoproperties: A review. Prog Energy Combust Sci 2007;33:135-0

[48] Loudon GM. Organic Chemistry. 4th edition. Oxford; 2002

[49] Bejarano PA, Levendis YA. Single-coal-particle combustion in O_2/N_2 and O_2/CO_2 environments. Combust Flame 2008;153:270 – 7

[50] Zhang L, Binner E, Qiao Y, Li C-Z. In situ diagnostics of Victorian brown coal combustion in O_2/N_2 and O_2/CO_2 mixtures in drop-tube furnace. Fuel 2010;89:2703-2

[51] Jamil K, Hayashi J-i, Li C-Z. Pyrolysis of a Victorian brown coal and gasification of nascent char in CO_2 atmosphere in a wire-mesh reactor. Fuel 2004;83:833-3

[52] Li Q, Zhao C, Chen X, Wu W, Li Y. Comparison of pulverized coal combustion in air and in O_2/CO_2 mixtures by thermo-gravimetric analysis. J Anal Appl Pyrolysis 2009;85:521-8

[53] Rathnam RK, Elliott LK, Wall TF, Liu Y, Moghtaderi B. Differences in reactivity of pulverised coal in air (O_2/N_2) and oxy-fuel (O_2/CO_2) conditions. Fuel Process Technol 2009;90:797-2

[54] Duan L, Zhao C, Zhou W, Qu C, Chen X. Investigation on coal pyrolysis in CO_2 atmosphere. Energy Fuels 2009;23:3826-0

[55] Li X, Rathnam RK, Yu J, Wang Q, Wall T, Meesri C. Pyrolysis and combustion characteristics of an Indonesian low-rank coal under O_2/N_2 and O_2/CO_2 conditions. Energy Fuels 2010;24:160-4

[56] Al-Makhadmeh L, Maier J, Scheffknecht G. Coal pyrolysis and char combustion under oxy-fuel conditions. The 34'Th International Technical Conference on Coal Utilization & Fuel Systems, Clearwater Florida

[57] Fong WS, Khalil YF, Peters WA, Howard JB. Plastic behaviour of coal under rapid-heating high-temperature conditions. Fuel 1986;65:195-1

[58] Cai H-Y, Megaritis A, Messenböck R, Dix M, Dugwell DR, Kandiyoti R. Pyrolysis of coal maceral concentrates under pf-combustion conditions (II): Changes in heteroatom partitioning as a function of rank. Fuel 1998;77:1283-9

[59] Oh MS, Peters WA, Howard JB. An experimental and modeling study of softening coal pyrolysis. AIChE Journal 1989;35:775-2

[60] Cai H-Y, Megaritis A, Messenböck R, Dix M, Dugwell DR, Kandiyoti R. Pyrolysis of coal maceral concentrates under pf-combustion conditions (I): Changes in volatile release and char combustibility as a function of rank. Fuel 1998;77:1273-2

[61] Bailey JG, Tate A, Diessel CFK, Wall TF. A char morphology system with applications to coal combustion. Fuel 1990;69:225-9

[62] Shu X, Xu X. Study on morphology of chars from coal pyrolysis. Energy Fuels 2001;15:1347-3

[63] Cloke M, Wu T, Barranco R, Lester E. Char characterisation and its application in a coal burnout model. Fuel 2003;82:1989-0

[64] Wu T, Lester E, Cloke M. A burnout prediction model based around char morphology. Energy Fuels 2006;20:1175-3

[65] Ma L, Mitchell R. Modeling char oxidation behavior under zone II burning conditions at elevated pressures. Combust Flame 2009;156:37-0

[66] Borrega AG, Alvarez D. Comparison of chars obtained under oxy-fuel and conventional pulverized coal combustion atmospheres. Energy Fuels 2007;21:3171-9

[67] Gale TK, Bartholomew CH, Fletcher TH. Decreases in the swelling and porosity of bituminous coals during devolatilization at high heating rates. Combust Flame 1995;100:94-0

[68] Várhegyi G, Szabó P, Jakab E, Till F. Mathematical modeling of char reactivity in Ar-O_2 and CO_2-O_2. Energy Fuels 1996;10:1208-4

[69] Niu S-l, Han K-h, Lu C-m. Characteristic of coal combustion in oxygen/carbon dioxide atmosphere and nitric oxide release during this process. Energ Convers Manage 2011;52:532-7

[70] Liu H. Combustion of coal chars in O_2/CO_2 and O_2/N_2 mixtures: A comparative study with non-isothermal thermogravimetric analyzer (TGA) tests. Energy Fuels 2009;23:4278-5

[71] Liu H, Zailani R, Gibbs BM. Pulverized coal combustion in air and in O_2/CO_2 mixtures with NO_x recycle. Fuel 2005;84:2109-5

[72] Zhang L, Binner E, Chen L, Qiao Y, Li C-Z, Bhattacharya S, Ninoiya Y. Experimental investigation of the combustion of bituminous coal in air and O_2/CO_2 mixtures: 1. Particle Imaging of the combustion of coal and char. Energy Fuels 2010;24:4803-1

[73] Wen CY, Noncatalytic heterogeneous solid fluid reaction models. Industrial and Engineering Chemistry 1968;60:34-4

[74] Hurt R, Sun J-K, Lunden M. A kinetic model of carbon burnout in pulverized coal combustion. Combust Flame 1998;113:181-7

[75] Mitchell RE, Ma L, Kim B. On the burning behavior of pulverized coal chars. Combust Flame 2007;151:426-6

[76] Hansen LA. Enhedsoperationer i den kemiske industri 2002. 4th edition. Polyteknisk forlag;2002

[77] Bird RB, Stewart WE, Lightfoot EN. Transport phenomena. 2nd edition. John Wiley & Sons, Inc.;2002

[78] Froment GF, Bischoff KB. Chemical reactor analysis and design. 2nd edition. John Wiley & Sons, Inc.;1990

[79] Hu Y, Naito S, Kobayashi N, Hasatani M. CO_2, NO_x and SO_2 emissions from the combustion of coal with high oxygen concentration gases. Fuel 2000;79:1925-2

[80] Hu YQ, Kobayashi N, Hasatani M. Effects of coal properties on recycled-NO_x reduction in coal combustion with O_2/recycled flue gas. Energy Convers Manage 2003;44:2331-0

[81] Okazaki K, Ando T. NO_x reduction mechanism in coal combustion with recycled CO_2. Energy 1997;22:207-5

[82] Nelson PF, Nancarrow PC, Bus J, Prokopiuk A. Fractional conversion of char N to NO in an entrained flow reactor. Proc Combust Inst 2002;29:2267-4

[83] Valix MG, Harris DJ, Smith IW, Trimm LD. The intrinsic combustion reactivity of pulverized coal chars: The use of experimental pore diffusion coefficients. Twenty-Fourth Symposium (International) on Combustion 1992:1217-3

[84] Molina A, Eddings EG, Pershing DW, Sarofim AF. Nitric oxide destruction during coal and char oxidation under pulverized-coal combustion conditions. Combust Flame 2006;136:303-2

[85] Moors JH.J, Banin VE, Haas JHP, Weber R, Veefkind A. Prediction and validation of burnout curves for Göttelborn char using reaction kinetics determined in shock tube experiments. Fuel 1999;78:25-9

[86] Liu H, Kojima T, Feng B, Liu D, Lu J. Effect of heterogeneous reactions of coal char on nitrous oxide formation and reduction in a circulating fluidized bed. Energy Fuels 2001;15:696-1

[87] Solomon PR, Fletcher TH. Impact of coal pyrolysis on combustion. Twenty-Fifth Symposium (International) on Combustion 1994:463-4

[88] Glarborg P, Bentzen LLB. Chemical effects of high CO_2 concentration in oxy-fuel combustion of methane. Energy Fuels 2008;22:291-6

[89] Liu F, Guo H, Smallwood G.J. The chemical effect of CO_2 replacement of N_2 in air on the burning velocity of CH_4 and H_2 premixed flames. Combust Flame 2003;133:495-7

[90] Masri AR, Dibble RW, Barlow RS. Chemical kinetic effects in nonpremixed flames of H_2/CO_2 fuel. Combust Flame 1992;91:285-9

[91] Mendiara T, Glarborg P. Ammonia chemistry in oxy-fuel combustion of methane. Combust Flame 2009;156:1937-9

[92] Gimeénez-López J, Millera A, Bilbao R, Alzueta MU. HCN oxidation in an O_2/CO_2 atmosphere: An experimental and kinetic modeling study. Combust Flame 2010;157:267-6

[93] Miller JA, Bowman CT. Mechanism and modeling of nitrogen chemistry in combustion. Prog Energy Combust. Sci 1989;15:287-8

[94] Glarborg P, Jensen AD, Johnsson JE. Fuel nitrogen conversion in solid fuel fired systems. Prog Energy Combust Sci 2003;29:89-3

[95] Gardiner WC Jr. Gas-phase combustion chemistry. 1st edition. Springer;2000

[96] Molina A, Eddings EG, Pershing DW, Sarofim AF. Char nitrogen conversion: Implications to emissions from coal-fired utility boilers. Prog Energy Combust Sci 2000;26:507-1

[97] Wang W, Brown SD, Hindmarsh CJ, Thomas KM. NO_x release and reactivity of chars from a wide range of coals during combustion. Fuel 1994;73:1381-8

[98] Jones JM, Harding AW, Brown SD, Thomas KM. Detection of reactive intermediate nitrogen and sulfur species in the combustion of carbons that are models for coal chars. Carbon;33:833-3

[99] Brown SD, Thomas KM. A comparison of NO release from coals and entrained-flow reactor chars during temperature-programmed combustion. Fuel 1993;72:359-5

[100] Molina A, Murphy JJ, Winter F, Haynes BS, Blevins LG, Shaddix CR. Pathways for conversion of char nitrogen to nitric oxide during pulverized coal combustion. Combust Flame 2009;156:574-7

[101] Orikasa H, Tomita A. A study of the HCN formation mechanism during the coal char gasification by O_2. Energy Fuels 2003;17:1536-0

[102] Winter F, Wartha C, Löffler G, Hofbauer H. The NO and N_2O formation mechanism during devolatilization and char combustion under fluidized-bed conditions. 26’th Symposium (International) on Combustion 1996:3325-4

[103] Winter F, Wartha C, Löffler G, Hofbauer H. The NO and N_2O formation mechanism during devolatilization and char combustion under fluidized-bed conditions. 26'th Symposium (International) on Combustion 1996:3325-4

[104] Visona SP, Stanmore BR. Modeling NO_x release from a single coal particle II. Formation of NO from char-nitrogen. Combust Flame 1996;106:207-8

[105] Goel S, Zhang B, Sarofim AF. NO and N_2O formation during char combustion: Is it HCN or surface attached nitrogen. Combust Flame 1996;104:213-7

[106] Park D-C, Day SJ, Nelson PF. Nitrogen release during reaction of coal char with O_2, CO_2 and H_2O. Proc Combust Inst 2005;30:2169-5

[107] Wu SL, Iilsa K. Kinetics of NO reduction by black liquor char. Energy Fuels 1998;12:457-3

[108] Bueno-López A, Soriano-Mora JM, García-García A. Study of the temperature window for the selective reduction of NO_x in O_2-rich gas mixtures by metal-loaded carbon. Catal Commun 2006;7:678-4

[109] Zhao Z, Li W, Qiu J, Wang X, Li B. Influence of Na and Ca on the emission of NO_x during coal combustion. Fuel 2006;85:601-6

[110] Zhu ZH, Lu GQ, Yang RT. New insights into alkali-catalyzed gasification reactions of carbon: Comparison of N_2O reduction with carbon over Na and K catalysts. J Catal 2000;192:77-7

[111] Wang Z, Zhou J, Wen Z, Liu J, Cen K. Effect of mineral matter on NO reduction in coal reburning process. Energy Fuels 2007;21:2038-3

[112] Levy JM, Chan LK, Sarofim AF, Beér JM. NO/char reactions at pulverized coal flame conditions. Eighteenth Symposium (International) on Combustion 1981:111-0

[113] López D, Calo J. The NO-carbon reaction: The influence of potassium and CO on reactivity and populations of oxygen surface complexes. Energy Fuels 2007;21:1872-7

[114] Aarna, I.; Suuberg, E. R.: "The Role of Carbon-Monoxide in the NO-Carbon Reaction", Energy Fuels, 13, 1999, 1145-1153

[115] Aarna I, Suuberg EM. A review of the kinetics of the nitric oxide-carbon reaction. Fuel 1997;76:475-1

[116] Chambrion P, Kyotani T, Tomita A. C-NO reaction in the presence of O_2. Twenty-Seventh Symposium (International) on Combustion 1998:3053-9

[117] Kyotani T, Tomita A. Analysis of the reaction of carbon with NO/N_2O using Ab Initio molecular orbital theory. J Phys Chem B 1999;103:3434-1

[118] Pevida C, Arenillas A, Rubiera F, Pis JJ. Synthetic coal char for the elucidation of NO heterogeneous reduction mechanisms. Fuel 2007;86:41-9

[119] Jones JJ, Patterson PM, Pourkashanian M, Williams A. Approaches to modelling heterogeneous char NO formation/destruction during pulverized coal combustion. Carbon 1999;37:1545-2

[120] Chambrion P, Kyotani T, Tomita A. Role of N-containing surface species on NO reduction by carbon. Energy Fuels 1998;12:416-1

[121] Aarna I, Suuberg EM. A study of the reaction order of the NO-carbon gasification reaction. Twenty-Seventh Symposium (International) on Combustion 1998:3061-8

[122] Andersson K, Normann F, Johnsson F, Leckner B. NO emission during oxy-fuel combustion of lignite. Ind Eng Chem Res 2008;47:1835-5

[123] Chan LK, Sarofim AF, Beér JM. Kinetics of the NO-carbon reaction at fluidized bed combustor conditions. Combust Flame 1983;52:37-5

[124] Toftegård MB, Brix J, Jensen PA, Glarborg P, Jensen AD. Oxy-fuel combustion of solid fuels. Prog Energy Combust Sci 2010;36:581-5

Article I

Coal Devolatilization and Char Conversion under Suspension Fired Conditions in O_2/N_2 and O_2/CO_2 Atmospheres

Coal Devolatilization and Char Conversion under Suspension Fired Conditions in O_2/N_2 and O_2/CO_2 Atmospheres

Jacob Brix, Peter Arendt Jensen, Anker Degn Jensen*

Department of Chemical and Biochemical Engineering, Building 229 Søltofts Plads, 2800 Kgs. Lyngby, Denmark
**Corresponding Author: e-mail: aj@kt.dtu.dk, Fax: +45 45 88 22 58, Phone: +45 45 25 28 41*

Abstract

The aim of the present investigation is to examine differences between O_2/N_2 and O_2/CO_2 combustion during devolatilization and char conversion of a bituminous coal at conditions covering temperatures between 1173 K – 1673 K and inlet oxygen concentrations between 5 – 28 vol. %. The experiments have been carried out in an electrically heated entrained flow reactor that is designed to simulate the conditions in a suspension fired boiler. Coal devolatilized in N_2 and CO_2 atmospheres provided similar results regarding char morphology, char N_2-BET surface area and volatile yield. This strongly indicates that a shift from air to oxy-fuel combustion does not influence the devolatilization process significantly. Char combustion experiments yielded similar char conversion profiles when N_2 was replaced with CO_2 under conditions where combustion was primarily controlled by chemical kinetics. When char was burned at 1573 K and 1673 K a faster conversion was found in N_2 suggesting that the lower molecular diffusion coefficient of O_2 in CO_2 lowers the char conversion rate when external mass transfer influences combustion. The reaction of char with CO_2 was not observed to have an influence on char conversion rates at the applied experimental conditions.

Keywords: Oxy-fuel, Devolatilization, Combustion, Char

1. Introduction

It is a growing concern that anthropogenic CO_2 emission to the atmosphere causes the planets temperature to raise. This concern has initiated extensive research programs to pursue alternative energy sources that can meet the increasing demands in both industrialized and developing countries without emitting CO_2 as fossil fuel based power plants are large emission sources. Today fossil fuels accounts for approximately 85 % [1,2] of the energy production world wide and it is therefore not likely that new technologies, which is not presently mature, can substitute fossil fuels, such as coal, in the short to midterm future [3]. To overcome the challenges the power industry, which is today relaying on conventional coal combustion, must find alternative technologies that allow for the continued use of coal, a fuel which is abundant, relatively cheap and steady in supply.

An interesting alternative to traditional air-blown combustion is the oxy-fuel combustion process. In oxy-fuel combustion, oxygen is separated from air before it enters the boiler and mixed with recycled flue gas to obtain a plant exit stream of almost pure CO_2 [3]. This CO_2 stream can subsequently be stored in suitable geological formations such as depleted oil and gas reservoirs or saline aquifers [2].

Many technical aspects still need to be clarified for oxy-fuel combustion to be industrialized. Fundamental knowledge of the oxy-fuel combustion process is therefore of importance. This knowledge must include an understanding of coal devolatilization and char conversion in a CO_2 rich gas since these processes influence heat release characteristics, fuel burn out and the need for oxygen, all of which have important economic implications for the process.

Rathnam *et al.* [4] examined the reactivity of four pulverized coals in the size range 69-90 μm. They conducted experiments in a drop tube furnace (DTF) at 1673 K under single particle conditions using oxygen concentrations between 3 and 21 % in N_2 and 5 and 30 % in CO_2. From their experiments they found 4 - 24 % higher apparent volatile yields in CO_2 compared to N_2 although the standard deviations of the data indicated possible overlaps between N_2 and CO_2 yields for three of the four coals studied. The authors attributed the higher volatile yield in CO_2 to gasification. That the presence of CO_2 increases the volatile yield compared to N_2 was also found by Al-Makhadmeh *et al.* [5]

from entrained flow reactor (EFR) pyrolysis tests. Using a bituminous coal they found an increase in volatile yield of approximately 16 % when N_2 was replaced with CO_2 at 1423 K. This contradicts the findings of Borrego and Alvarez [6] that devolatilized high and low volatile bituminous coal particles in the size range 36-75 μm using a DTF operated at 1573 K. They found a decrease in volatile yield of 62 % and 32 % for the low volatile and high volatile coal, respectively, when N_2 was replaced with CO_2. These decreases in volatile yield are surprisingly high and could be caused by the high amount of cold gas (1/3 of the total gas volume) used for particle transport during their experiments. Since CO_2 has a higher thermal capacity than N_2 the large amount of cold gas could lower the particle heating rate in CO_2 causing the lower volatile yields.

To examine the difference in volatile yield closer Rathnam *et al.* [4] conducted thermogravimetric analysis (TGA) pyrolysis on one of their coals in pure N_2 and CO_2, using a heating rate of 25 K/min. They found very similar weight loss curves at temperatures below 1030 K. At this temperature the weight loss in CO_2 started to accelerate significantly compared to N_2 indicating an effect of char gasification by CO_2. This effect of CO_2 was also found by Li *et al.* [7] in their TGA pyrolysis experiment using pulverized bituminous coal at similar temperatures and heating rates of 10, 20 and 30 K/min. That CO_2 gasification can take place during pyrolysis have also been found by other investigators [8,9]. Due to the long residence time and low heating rate of the coal in a TGA direct comparison with DTF and EFR experiments, where devolatilization is completed in a time scale of less than a second, should however be made with caution, especially if these experiments are carried out in an oxidizing atmosphere. Rathnam *et al.* [4] also compared coal burnout in O_2/N_2 and O_2/CO_2 at varying oxygen concentrations using their DTF. Here a tendency of higher overall coal conversions (1-3 Wt. %) in O_2/CO_2 was found for two of the four coals with most pronounced differences at low oxygen concentrations. Chars produced in their DTF and combusted in a TGA, using a heating rate of 25 K/min, showed an increased reactivity in CO_2 compared to N_2 at temperatures above 1100 K and an oxygen concentration of 2 %. At oxygen concentrations above 2 % the TGA experiments showed no difference in reactivity as char burnout was accomplished at lower temperatures where the effect of CO_2 gasification does not impact on char consumption. In the TGA experiments of Várhegyi

et al. [10], which were carried out by burning bituminous coal in oxygen concentrations ranging between 5-100 vol. % in Ar or CO_2, the effect of CO_2 gasification was also found to be negligible due to the low gasification rate compared to the char oxidation rate.

Bejarano and Levendis [11] conducted single particle combustion experiments in both O_2/N_2 and O_2/CO_2 using a bituminous coal, a lignite coal and a synthetic char in a laminar DTF with fixed temperatures of 1400 K and 1600 K. Using a three-color pyrometer they were able to measure the temperature of the burning particles. The particle size fractions of the coal used in their experiments were 45-53 μm, 75-90 μm and 150-180 μm whereas the synthetic char had a diameter of 43 μm. When burning 45-53 μm bituminous coal particles at a reactor temperature of 1400 K a particle temperature drop at 50 % burnout, of approximately 150-200 K, was observed for oxygen concentrations in the range 20-80 vol. % when N_2 was replaced with CO_2. In this range of oxygen concentrations the particle temperature increased approximately from 1800 K to 2620 K in O_2/CO_2 and from 2000 K to 2800 K in O_2/N_2. Burnout times at identical oxygen concentrations were found to be 44-80 % longer in O_2/CO_2 compared to O_2/N_2 depending on the oxygen concentration. The authors argued that the combustion was taking place in Zone II by comparing calculated diffusion-limited burnout times with experimental data. Their conclusion is however sensitive to factors such as particle swelling, development of char morphology during devolatilization and choice of combustion model. If a shrinking sphere model is applied to calculate burnout times in Zone III the relative difference in burnout times is a measure of the relative difference in oxygen diffusivity in the particle boundary layer. For the experiments just mentioned the burnout times in 20 % O_2/ 80 % CO_2 and 40 % O_2/ 60 % CO_2 is approximately 44 % and 46 % higher than in the corresponding N_2 based atmospheres. The diffusion coefficient of O_2 in N_2, as calculated by Chapman-Enskog's equation [12], using average temperatures between the particles and the bulk gas, is however 42 % and 40 % higher than in CO_2. This could imply that the experimental data of Bejarano and Levendis [11] is obtained closer to Zone III than anticipated by the authors, which is most clearly seen at the lower oxygen concentrations where the largest differences in conversion rates exist. When experiments were carried out using lignite lower differences in particle temperatures were found between N_2 and CO_2 based atmospheres (~ 100 K) compared to combustion of

bituminous coal. Burnout times for lignite were found to be lower than for bituminous coal with smaller differences (~ 3 ms) between O_2/N_2 and O_2/CO_2 environments. Bejarano and Levendis [11] attributed this behavior to a higher reactivity and a lower fixed carbon content of lignite. In addition, low rank coals tend to form network chars whereas medium rank coals have a tendency to form cenospheric chars [13]. It is therefore likely that a more pronounced effect from CO_2 gasification on char conversion will be present during combustion of a low rank coal where CO_2 can react on the pore surface of the char when the reaction with oxygen is controlled partly or completely by external mass transfer.

Molina and Shaddix [14] carried out experiments in a laminar EFR under single particle conditions using bituminous coal particles in the size range 106-125 μm. Using a Charged-Coupled Device (CCD) camera they obtained luminous profiles of particles burning in both O_2/N_2 and O_2/CO_2 mixtures from which the time where devolatilization begins and the time where volatile ignition takes place could be deduced based on a large number of repeated experiments. Ignition time in 21 % O_2/ 79 % CO_2 was approximately 11 % (~ 3 ms) longer than in the equivalent N_2 mixture at the same gas temperature. For 30 % O_2 the increase in ignition time was reduced to approximately 8 % (~ 2 ms). The authors explained these observations with the increased thermal capacity ($\rho_p \cdot C_p$) and lower diffusivity of gaseous components in CO_2 compared to N_2. These factors cause a delayed ignition and a slower consumption of volatiles through an increased heat uptake by the gas and a lower reactant mixing rate during devolatilization. No visual differences were found in devolatilization time neither between carrier gases or oxygen concentrations, which the authors explained with similar particle heating curves.

The short review above presents data from several researchers. Conclusions based on the comparison of their data are however difficult as differences in particle temperature histories, coal composition, and equipment limitations such as gas mixing etc. strongly influences the results. It is therefore apparent that there is a continued need for broad consistent data sets that can promote the understanding of coal conversion in oxy-fuel combustion.

The present investigation aims at clarifying differences in consumption rates when bituminous coal is devolatilized and burned in O_2/N_2 and O_2/CO_2 mixtures. To base

discussions on data obtained from combustion in both Zone I, Zone II and Zone III experiments have been carried out covering a wide range of both temperatures and oxygen concentrations. As the aim of this study has been char conversion rate at constant oxygen concentrations no focus has been on stoichiometries other than to ensure sufficient amounts of oxygen in the reactor.

2. Experimental

2.1 Equipment

The experiments were carried out using an entrained flow reactor shown in figure 1. The reaction zone is cylindrical with a length of 2 m and a diameter of 0.08 m and it is heated by 7 electrical heating elements. The maximum temperature of these heating elements is 1773 K. On top of the reactor a 0.8 m long gas preheater, consisting of 2 electrical heating elements, preheats the secondary gas stream to a prescribed temperature. Coal particles are fed to the reactor from a dosing system consisting of a silo and a screw feeder connected to a vibration transporter. This transporter is connected to a water cooled feeding probe going through the center of the gas preheater. The actual feed rate is controlled by the weight of the silo and screw feeder. The feeding equipment is contained in an airtight chamber so that the primary gas used for pneumatic particle transport to the reactor can be controlled accurately. This primary gas was either N_2 or CO_2 except when experiments were carried out in air.

Sampling of particles at different residence times is done using a water cooled sampling probe that can be used over the entire reaction zone. The top of the probe is shaped like a funnel and has a diameter of 0.034 m. At the bottom of the probe a filter separates gas and particles. The gas suction through the probe is performed alternately depending on whether the purpose of suction is particle collection or gas analysis. Both gas analysis and char sampling were performed at each sampling position. The oxygen concentration measured at the sampling position is the local concentration after volatile consumption and initial char oxidation. CO and CO_2 concentrations were detected by an IR-analyzer and a paramagnetic analyzer were used for analysis of O_2. All streams leaving the setup are sent to a central flue gas ventilation system.

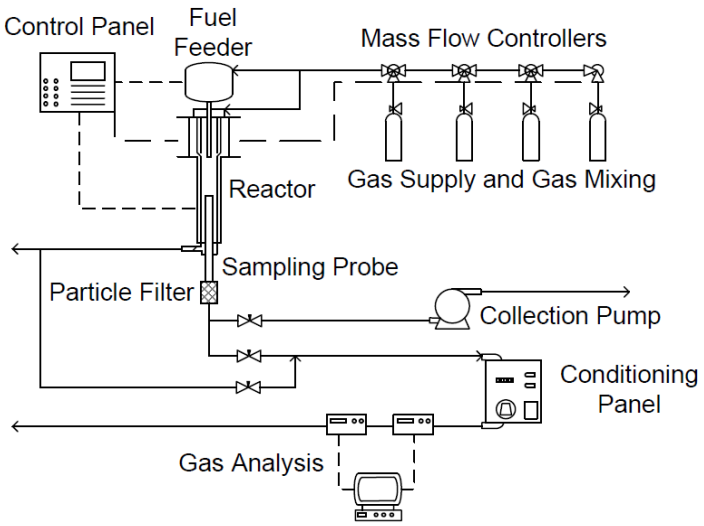

Figure 1 Experimental setup. Solid lines indicate tubes and dashed lines indicate wires for control and data logging. All streams leaving the setup is sent to a central ventilation system.

The analysis gas is sent through a conditioning panel where it is cleaned for remaining dust and particles and any water vapor is removed. Very small amounts of water vapor were present in the gas due to a low fuel feed rate. All mass flow controllers, heating elements and the fuel feeder can be controlled from a central panel and all measurements from the gas analyzers are stored by a computer using LabVIEW software. When experiments were carried out in 21 vol. % O_2 in N_2, air was used directly from a compressor. All other gaseous environments were created by mixing bottled gases.

2.2 Devolatilization

Devolatilization experiments were carried out at the temperatures shown in table 1. Table 1 also show residence times and the carrier gas used at each temperature. The residence times, τ_{dev}, are found by extrapolation of char conversion profiles at each temperature to a residence time where the char conversion is zero indicating that particle heating and devolatilization is completed. When treating char conversion profiles this residence time is subtracted from the particle sampling time in order to get a time scale where only heterogeneous char conversion is taking place. The residence times at the sampling positions, $\tau_{sampling}$, are calculated assuming a laminar flow profile, which is integrated with the radius of the sampling probe as the upper radial boundary condition. The result

is shown in equation (1). The mean gas velocity in the reactor, v_{mean}, has been close to 1 m s^{-1} in all experiments, both during devolatilization and char combustion. $L_{sampling}$, $D_{reactor}$, $R_{reactor}$ and R_{probe} are the traversed reactor length, reactor diameter, reactor radius and sampling probe radius, respectively.

$$\tau_{sampling} = \frac{D_{reactor}^2 \cdot L_{sampling}}{4 \cdot v_{mean} \cdot \left(2 \cdot R_{reactor}^2 - R_{probe}^2\right)} \quad (1)$$

Because tar was clogging the sampling probe and central flue gas ventilation systems it was necessary to add oxygen to the secondary gas stream to crack/partially burn the tar molecules released during devolatilization. A stoichiometric ratio of three (corresponding to 5-6 vol. % O_2) was found to remove the tar without promoting heterogeneous char consumption. That the degree of heterogeneous char consumption was negligible, due to low residence times and mixing limitations at the reactor entrance, was confirmed by sampling also at a position slightly further downstream in the reaction zone for selected experiments, which showed similar weight losses. The position in the reactor, $L_{sampling}$, used as sampling point was a few centimeters below the location with the highest measured CO concentration.

Table 1 Devolatilization temperatures used in the experiments. CO_2/N_2 indicates that devolatilization have been carried out separately in both gases. $\tau_{sampling}$ is the reactor residence time where char sampling took place as defined by equation (1). τ_{dev} is the residence time where particle heating and devolatilization is completed.

T [K]	1173	1273	1373	1473	1573	1673
Gas	CO_2	CO_2	CO_2	CO_2	CO_2/N_2	CO_2/N_2
$\tau_{sampling}$ **[s]**	0.47	0.39	0.25	0.22	0.16	0.15
τ_{dev} **[s]**	0.297	0.221	0.209	0.196	0.182	0.15

Devolatilization was mainly carried out using CO_2 as carrier gas. At 1573 K and 1673 K experiments were also carried out in N_2 to see any effects of carrier gas. The amount of remaining char combustibles was found using ash tracing in a muffle furnace at 1088 K

for 2.5 hr in air. The volatile content was subsequently found by the mass balance shown in (2), which assumes that no ash leaves the particles during devolatilization.

$$\alpha_v = 1 - m_{so}\frac{\alpha_A}{m_A} - \alpha_m \tag{2}$$

In (2) α_A, α_m and α_v are the weight fractions of coal ash, coal moisture and coal volatiles , respectively. m_{so} and m_A are the masses of sampled char and of ash measured after burn-off in the muffle furnace.

2.3 Combustion

Combustion studies were carried out at the same temperatures as shown in table 1. Both N_2 and CO_2 were used as carrier gas with inlet oxygen concentrations between 5 and 28 vol. %. These concentrations correspond to stoichiometric ratios between 2 and 15 at a coal feed rate of 50 g hr^{-1}, which was used in all experiments. A total of 31 char conversion profiles were obtained from the experiments of which only representative samples are shown in this paper. Char was sampled at reactor residence times from about 0 to 1 s. Reynolds numbers for the gas were between 400 and 1100 depending on reactor conditions meaning that the gas flow profile was laminar. A laminar flow profile along with a carefully controlled sampling volume flow allow for a precise determination of particle residence times using equation (1). To calculate char conversion at each sampling point equations (3) and (4) are constructed from mass balances using the same assumption as for equation (2).

$$\alpha_A^* = \frac{\alpha_A}{1 - \alpha_v - \alpha_m} \tag{3}$$

$$X = \frac{m_A\left(1 - \alpha_A^*\right) - \alpha_A^* m_c}{m_A\left(1 - \alpha_A^*\right)} \tag{4}$$

α_A^*, m_c and X are the initial weight fraction of ash in the char after devolatilization, the mass of remaining combustibles in a char sample and dimensionless char conversion, respectively. The definition in equation (4) allows for accurate comparison of char conversion rates across a wide temperature interval as the increase in volatile yield when the temperature increases is accounted for.

2.4 Fuel

The coal is a South American bituminous coal (El Cerrejón) sieved to the size range 90-106 μm. The composition of the unsieved coal is given in table 2 in the column "Original". Ash tracing was used on the sieved coal and the ash content of the applied size fraction was 5.9 Wt. %.

Table 2 Proximate and ultimate analysis of the coal used for experiments. In the column "Corrected" the original data has been corrected for ash content of the particle size fraction 90 – 106 μm.

Proximate Analysis		**Original**	**Corrected**
Upper heating value	MJ/kg ar	28.19	28.19
Effective heating value	MJ/kg ar	27.09	27.09
Moisture	Wt. % ar	5.0	5.2
Ash	Wt. % ar	9.6	5.9
Volatiles	Wt. % ar	34.9	34.9
Ultimate Analysis			
Carbon	Wt. % ar	68.9	71.73
Hydrogen	Wt. % ar	4.61	4.8
Oxygen (diff.)	Wt. % ar	9.82	10.23
Nitrogen	Wt. % ar	1.44	1.5
Sulfur	Wt. % ar	0.62	0.64

Ash tracing was also done on a smaller particle size fraction and this confirmed that the ash was concentrated in the small particles. In all calculations the original values in table 2 have therefore been corrected for ash content assuming that the same fractional

correction applies to all coal constituents. The actual composition of the size range 90-106 µm can be seen in the column "Corrected". Correction of the volatile yield has not been attempted as this is determined by experiments at each experimental temperature. The heating values has not been corrected either as this information is not used here.

Even though sieving was used to obtain a narrow particle size fraction of 90-106 µm laser diffraction measurements using a Malvern Mastersizer with ethanol as solvent revealed the particle size distribution (PSD) shown in figure 2.

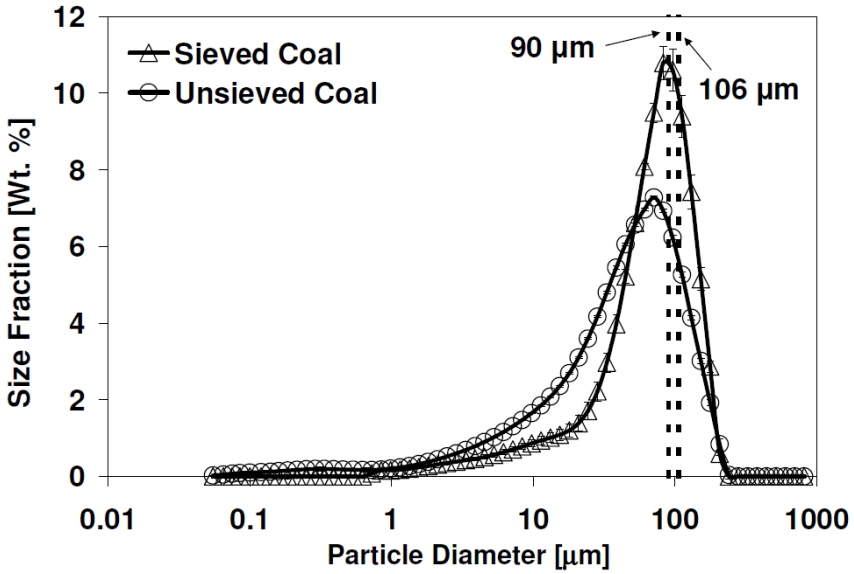

Figure 2 Particle size distributions of sieved and unsieved coal.

That the PSD has a long tail towards small particle sizes is most likely caused by small particles adhering to each other or to the larger particles when placed in the sieves, a problem which has also been reported by Ballester and Jiménez [15]. The mass based mean diameters of the PSD's for unsieved and sieved coal particles are 56.8 µm and 75.8 µm, respectively.

3. Results

3.1 Repeatability

To test the repeatability of the char conversions several experiments have been carried out twice. These experiments show a pooled standard deviation of 3.3 % though individual sets of experiments showed uncertainty up to 12 %.

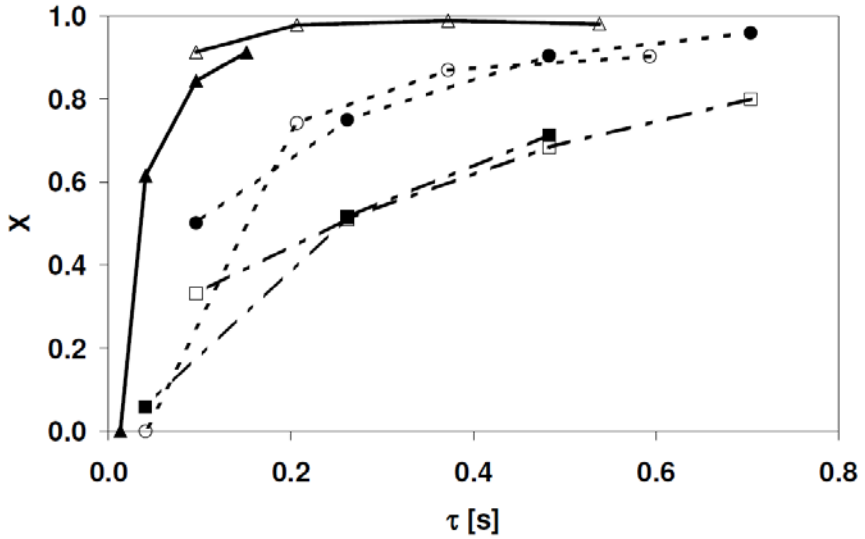

Figure 3 Char conversion profiles obtained in CO_2 at 1373 K. (● 6.1 vol. % O_2)(o 5.9 vol. % O_2)(▲ 19.0 vol. % O_2)(Δ 18.2 vol. % O_2)(□ 3.6 vol. % O_2)(■ 4.6 vol. % O_2). Oxygen concentrations are the averages of the local concentrations measured in each experiment. $\lambda \sim 2.4 - 10.2$.

Figure 3 shows three sets of repeated experiments performed at 1373 K in CO_2. Both char and gas sampling were done at each residence time so all char conversions has a corresponding measured oxygen concentration. The oxygen concentrations given in the captions in this paper are the average oxygen concentration of each experiment.

3.2 Devolatilization

The results obtained from devolatilization experiments are shown in figure 4. It may seem suspicious that the volatile content drops at the temperatures 1573 K and 1673 K compared to at 1473 K. That it does so for both temperatures in N_2 and CO_2 suggest that the drop is not due to experimental inaccuracy. The explanation for this drop is found in two factors, namely the low residence time used for sampling and that equation (2) is

sensitive towards inaccuracies in ash content determination. Sampling at low residence time at the high temperatures was done to avoid heterogeneous char conversion caused by the presence of oxygen. The sensitivity of equation (2) towards inaccuracies in ash content means that ash evaporation could affect the calculated volatile content. Because of the lower volatile content found at 1573 K and 1673 K the value found at 1473 K will be used in (3) and (4) for all three temperatures.

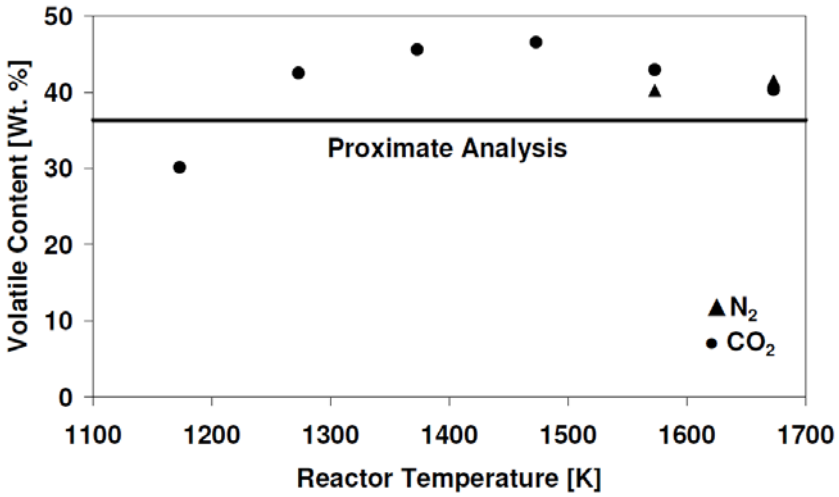

Figure 4 Volatile content found at the experimental temperatures.

Figure 4 shows that at 1173 K the volatile yield found using the EFR is slightly lower than that found by proximate analysis. This is expected as the residence time in the EFR is much lower than that used in proximate analysis, which limits the influence of secondary pyrolysis. The fact that char has been sampled under identical conditions at 1573 K and 1673 K in N_2 and CO_2 suggest that no pronounced effect of CO_2 on volatile yield exists at these conditions. This is not in agreement with neither Rathnam *et al.* [4] and Al-Makhadmeh *et al.* [5] nor Borrego and Alvarez [6]. Al-Makhadmeh *et al.* [5] and Rathnam *et al.* [4] used sampling residence times of 1 s (1423 K) and 0.62 s (1673 K) and found the volatile yield in CO_2 to increase 16 % and 4-24 %, depending on the coal type. The reactor used by Al-Makhadmeh *et al.* [5] was electrically heated with a cold entrainment gas that only made up 4 % of the total gas volume. The heat source and ratio of cold to hot gas is not stated explicitly by Rathnam *et al.* [4]. Borrego and Alvarez [6] used a residence time of 0.3 s (1573 K) and found a decrease in volatile yield of 62 % and

32 % in CO_2, depending on the coal type. As discussed earlier the large differences could be influences by the high amount of cold entrainment gas used by the authors. Authors that find an increased volatile yield in CO_2 often contribute this to gasification of the fuel. Though this appears to be a natural conclusion and a likely cause, the low residence times needed for devolatilization at high temperatures (> 1500 K) and the fact that a volatile cloud is expected to form around the particles [14], thereby limiting the access of the CO_2 to the particle surface, makes it prudent to examine other possibilities. The conditions used during experiments will inevitably affect the results wherefore factors such as mixing between cold and hot gas streams, particle heating rate and total particle residence times must be included when data is compared. The cold fuel carrier gases used in the present investigation made up app. 18 vol. % of the total gas volume at 1573 K and 1673 K and the sampling residence times are much lower than in any of the referred investigations. Under these conditions no difference was found between devolatilization in N_2 and CO_2. In suspension fired boiler operation, where heating and devolatilization is completed in a time scale of 150 – 200 ms it is therefore questionable if CO_2 gasification will make a significant contribution to fuel conversion during devolatilization of low to medium reactive coals.

3.2.1 Char Morphology

Figure 5 shows scanning electron microscopy (SEM) images of chars obtained from devolatilization at 1673 K in N_2 and CO_2 and reveal no visual differences.

N_2-BET analysis of the chars in figure 5 showed surface areas of 270 and 280 $m^2\ g^{-1}$ for char devolatilized in N_2 and CO_2, respectively, further suggesting that no significant differences exists. This is not in agreement with the N_2-BET results of Borrego and Alvarez [6] who found an increased surface area of as much as several hundred percent, depending on the coal, when chars were prepared in CO_2 compared to N_2. Al-Makhadmeh *et al.* [5] finds both a decreased and an increased surface area also of as much as several hundred percent, depending on the coal, when CO_2 is used to prepare the char compared to N_2. Care should however be taken when comparing measured surface areas of different chars prepared in different reactors from different coals. Factors such as heating rate, coal composition, residence time and temperature are known to cause

variations [13] and the residence time and temperature are especially important factors if CO_2 gasification shall contribute to a higher specific surface. As a further example of this Borrego and Alvarez [6] finds no significant differences in CO_2-BET surface areas between char prepared in N_2 and CO_2 whereas Rathnam *et al.* [4] reports increases of 10 – 43 % when chars are prepared in CO_2 compared to N_2.

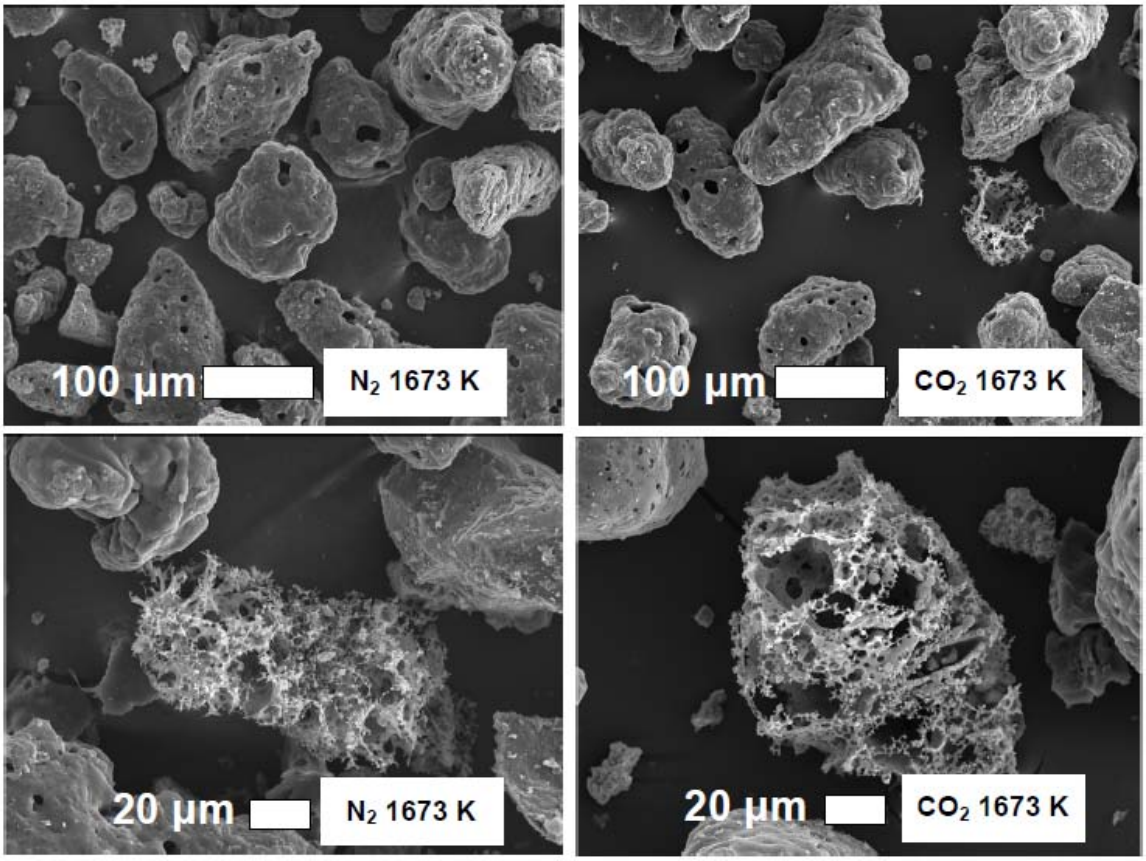

Figure 5 SEM images of chars obtained at 1673 K in N_2 and CO_2.

The PSD's of chars prepared in CO_2 were found to change with the temperature as shown in figure 6. The peak of the PSD is shifted from 82.6 µm for sieved coal to 96.2 µm at 1273 K and 112.1 µm at 1473 K and 1673 K. The corresponding weight based mean diameters are 75.8 µm, 90.4 µm, 105.6 µm and 113.7 µm.

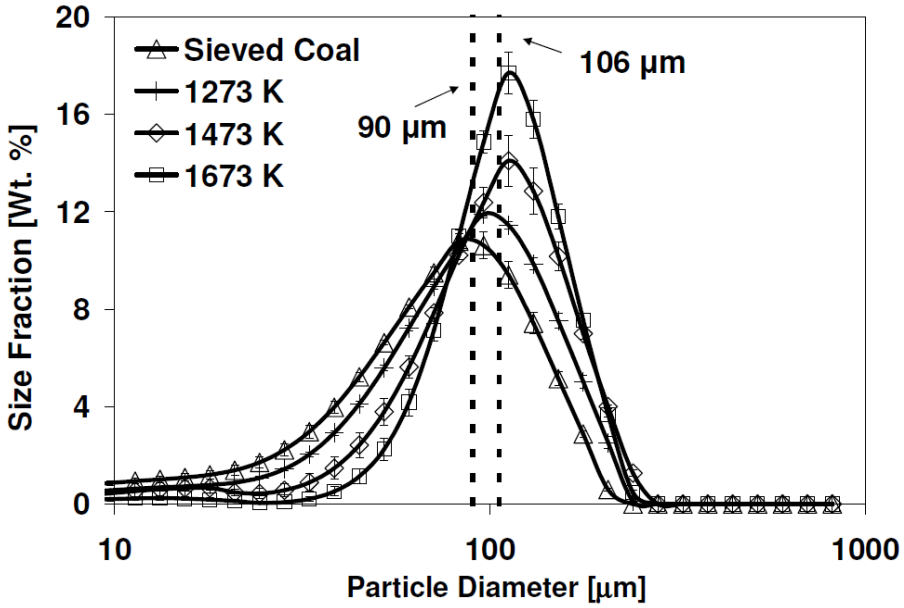

Figure 6 Particle size distributions of sieved coal and chars obtained in CO_2 at 1273 K, 1473 K and 1673 K.

That the peaks of the PSD's in figure 6 shifts towards higher values is a clear sign of swelling, which is expected behavior for a bituminous coal [13]. Fitting the weight based mean diameters to a second order polynomium yield equation (5) that describes the temperature dependent swelling ratio of the particles in the interval 1173 K – 1673 K.

$$SR = -1.375 \cdot 10^{-6} \cdot T^2 + 4.826 \cdot 10^{-3} \cdot T - 2.725 \quad (5)$$

It can also be seen from figure 6 that the amount of fines decreases as the temperature is raised. This is partly due to swelling but as fragmentation is also known to take place [13, 16], producing fines, some char oxidation has been taking place. The contribution of the fines to the overall weight of char is however relatively low with app. 7 Wt. % under 10 µm so if a slight consumption has been taking place it is not enough to cause large deviations in the determined volatile content in figure 4. Figure 7 show SEM images of the particles corresponding to the PSD's shown in figure 6 supporting that the amount of fines decrease with increasing temperature and that swelling is taking place.

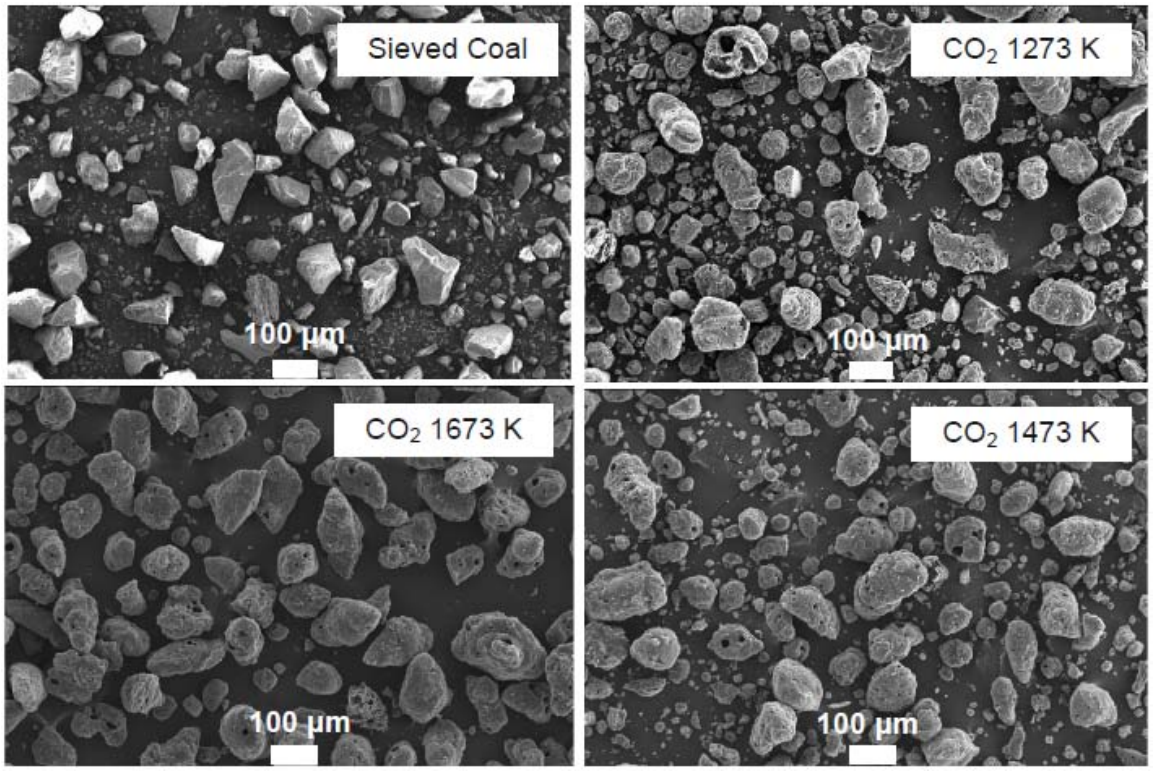

Figure 7 SEM images of the PSD's shown in figure 6.

3.3 Char combustion

The dependence of oxygen concentration on char conversion rate was found in both N_2 and CO_2 based atmospheres by plotting char conversion against oxygen concentration at fixed residence times. This can be seen in figure 8 using results obtained at 1373 K.

Figure 8 shows that there is no conspicuous difference in the influence of oxygen concentration on char conversion whether combustion is taking place in N_2 or CO_2 based atmospheres. Results obtained at 1173 K and 1273 K confirms this conclusion. That there is no apparent change in the dependence of oxygen concentration on char conversion indicates that the kinetic parameters governing char consumption is not changed when N_2 is replaced with CO_2 under similar conditions. In figure 9 conversion profiles, obtained at 1173 K and app. 27.8 vol. % O_2, supports the conclusion based on figure 8. In figure 10 char conversion profiles obtained at 1373 K and app. 6.1 vol. % O_2, which is expected to cause the combustion to take place in Zone II, does not show apparent differences in conversion rate either.

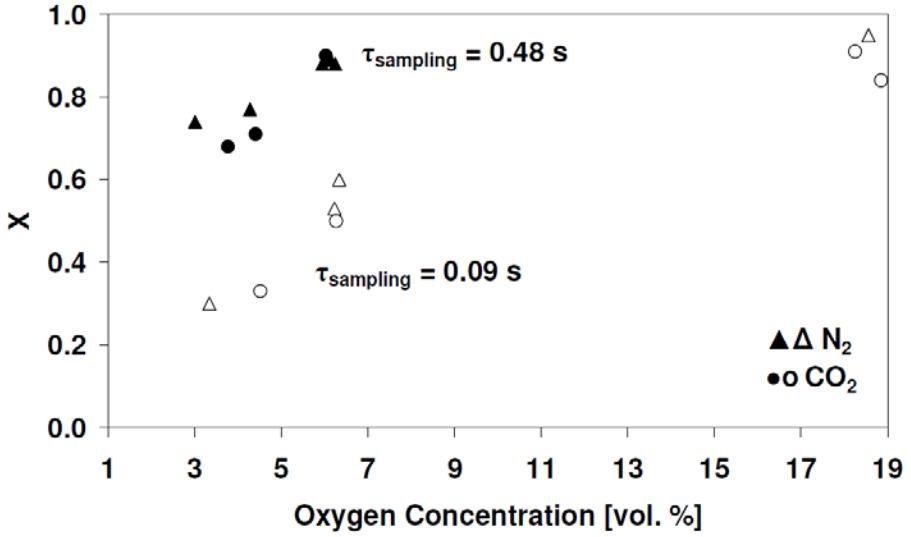

Figure 8 Char conversions vs. oxygen concentrations at 1373 K for two different sampling residence times. $\lambda \sim 2.4 - 10.2$.

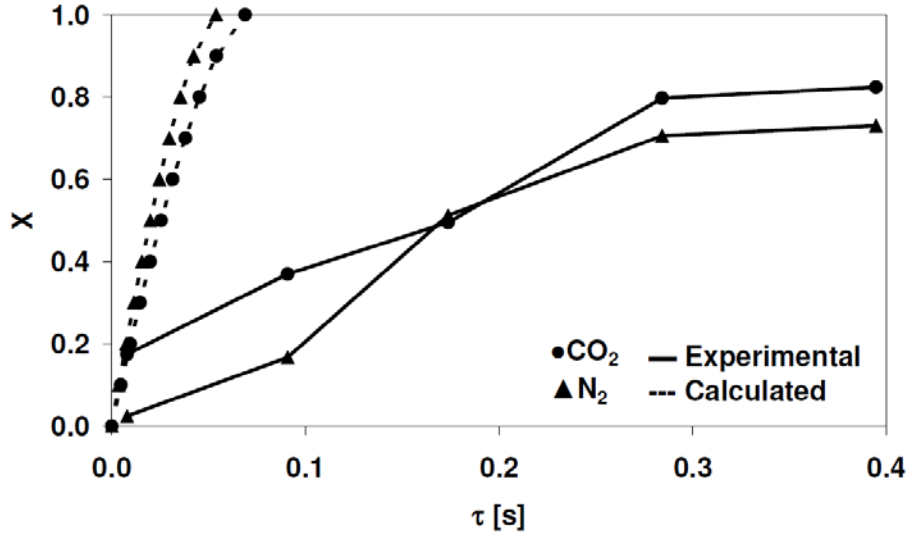

Figure 9 Char conversion profiles obtained at 1173 K. The calculated profiles are found for a shrinking sphere in zone III using equation (6). (● 27.9 vol. % O_2)(▲ 27.7 vol. % O_2). Oxygen concentrations are the averages of the local concentrations measured in each experiment. $\lambda \sim 15$.

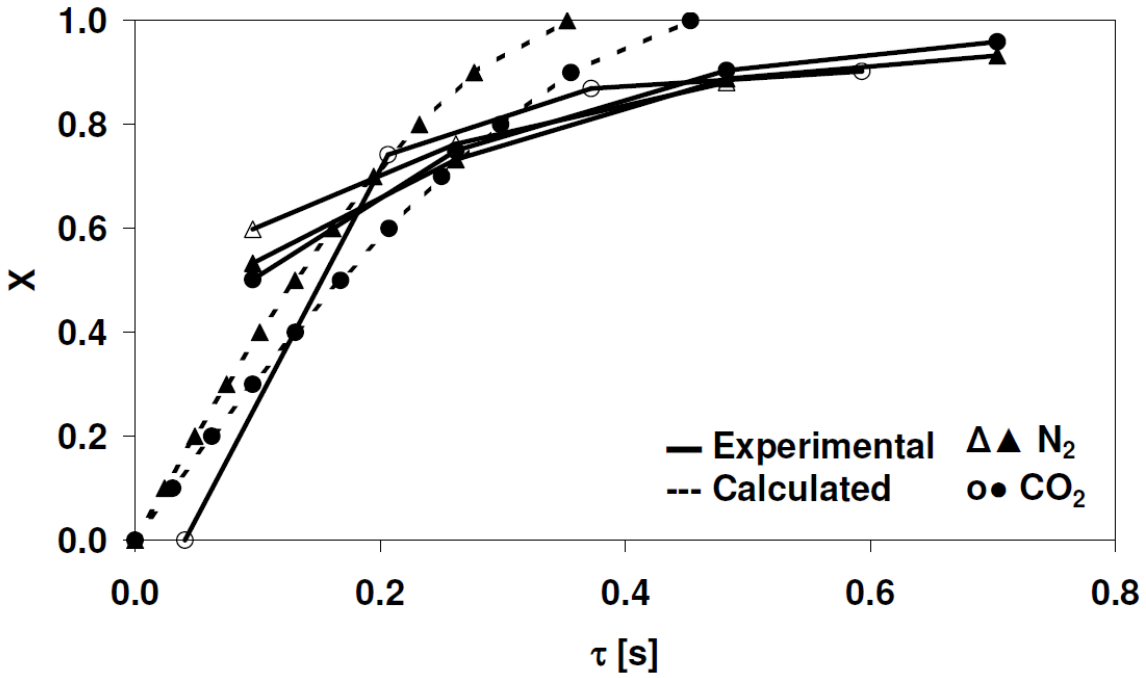

Figure 10 Char conversion profiles obtained at 1373 K. The calculated profiles are found for a shrinking sphere in zone III using equation (6). (▲ 6.2 vol. % O_2)(Δ 6.3 vol. % O_2)(● 6.1 vol. % O_2)(o 5.9 vol. % O_2). Oxygen concentrations are the averages of the local concentrations measured in each experiment. $\lambda \sim 4.1$.

In figures 9 and 10 the dashed conversion profiles are calculated for a shrinking particle burning in Zone III using equation (6) and the residence time τ ($\tau_{sampling} - \tau_{dev}$). Equation (5) is used to calculate the actual mean particle radius, R_0, from the mass mean diameter of the sieved coal. The bulk oxygen partial pressure, P_b, is found from the average of the measured local concentrations. Values of particle density and molar mass, ρ_p and M_p, are set to 1000 kg m^{-3} and 12 g mol^{-1} as approximate values for a graphite particle with a porosity of 50 %. The binary diffusion coefficient, D_m, is found at the reactor temperature, T_b, using Chapman-Enskog's equation [12]. Calculations show initially a lower conversion rate than found from experiments. This stresses the uncertainty inherent in this method of determining experimental combustion regimes as the calculated conversion profiles are restricted to one representative particle size whereas figures 5, 6 and 7 shows that several particle sizes and different morphologies are in fact present. That the experimental conversion profiles initially increases steeper than the calculated is

most likely caused by rapid conversion of the smaller particle sizes, a phenomenon that is not captured by the calculations.

$$\tau = \frac{1}{2} \cdot \left(\frac{R \cdot T_b \cdot \rho_p \cdot R_0^2}{2 \cdot D_m \cdot P_b \cdot M_p} \right) \cdot \left(1 - \left(1 - X \right)^{\left(\frac{2}{3}\right)} \right) \qquad (6)$$

The possible effect of CO_2 gasification on char conversion is often discussed in the oxy-fuel literature [4,5,6,7,10] In neither figure 9 or 10 this effect has been ascertainable but the temperatures have also been quite low and the oxygen excess quite high for this reaction to contribute significantly to the overall char conversion rate. In order to provoke an effect of CO_2 gasification, experiments have also been carried out at higher temperatures and lower oxygen concentrations. Figure 11 show conversion profiles obtained at 1573 K and 1673 K in oxygen concentrations between 3.1 and 3.7 vol. %. At these conditions the effect of CO_2 gasification would be expected to appear if important for practical boiler operation.

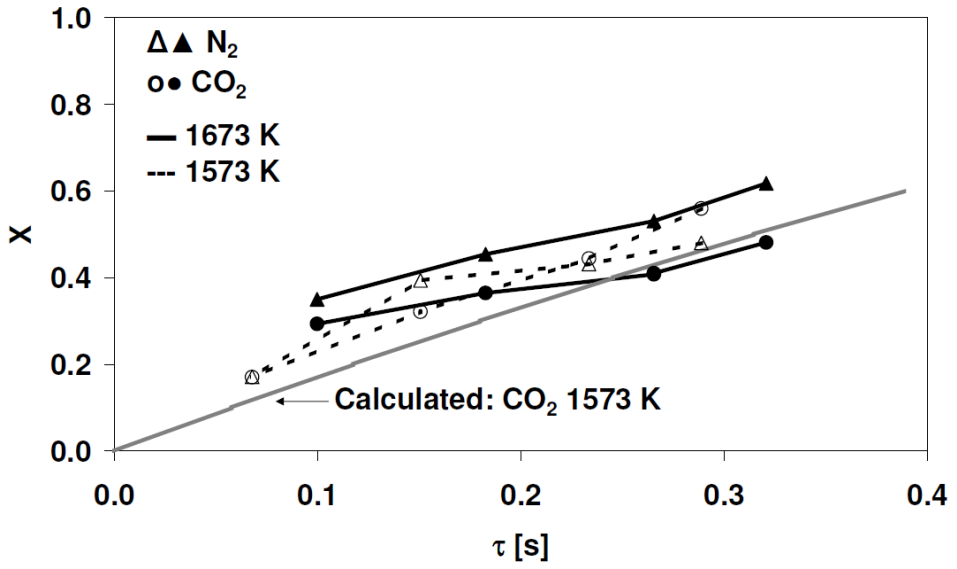

Figure 11 Char conversion profiles obtained at 1673 K and 1573 K. The calculated profile is found for a shrinking sphere in zone III using equation (6). (▲ 3.1 vol. % O_2)(Δ 3.4 vol. % O_2)(● 3.2 vol. % O_2)(o 3.7 vol. % O_2). Oxygen concentrations are the averages of the local concentrations measured in each experiment. $\lambda \sim 2$.

It can be seen from figure 11 that the conversion rates in N_2 generally are higher than in CO_2, which is likely caused by an app. 22 % lower diffusion coefficient of O_2 in CO_2 at these temperatures. The results strongly imply that CO_2 gasification does not have a practical effect on overall char conversion under suspension fired conditions for the investigated coal. In figure 11 the conversion profile found in CO_2 at 1573 K crosses that found at 1673 K. The initial trend of the profiles obtained in N_2 is the same but the profile at 1573 K breaks off in the last two data points. That conversion takes place faster at 1573 K than at 1673 K seem contradictive at first. The conversion profile in figure 11, calculated using equation (6), does however imply that char consumption is taking place in Zone III meaning that even small differences in bulk oxygen concentrations and particle swelling has a significant influence. Figure 12 show conversion profiles calculated using equation (6) and the experimental conditions in figure 11.

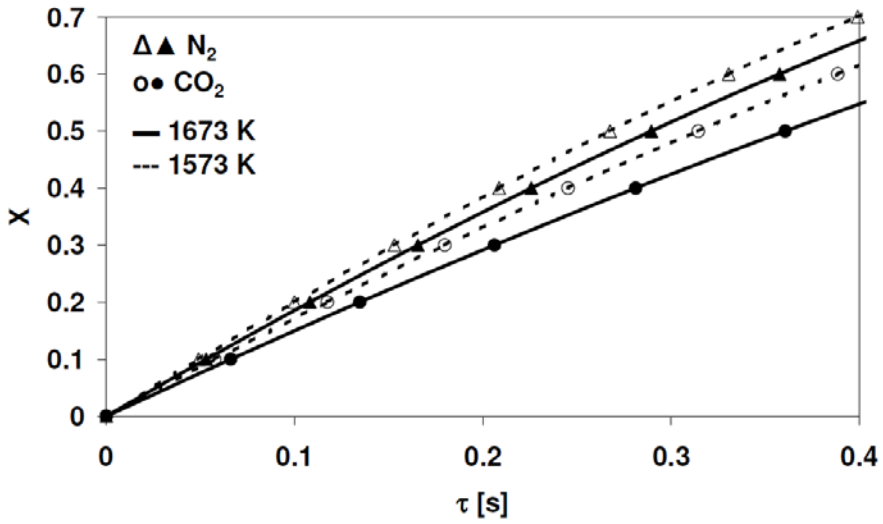

Figure 12 Calculated char conversion profiles for a shrinking sphere in Zone III using equation (6).

That conversion rates in figure 12 are faster at the lower temperature illustrates the importance of the increased particle size at 1673 K, caused by an increase in swelling ratio, and the slightly higher experimental oxygen concentrations at 1573 K. These two factors outweigh the increase in O_2 diffusion coefficient from 1573 K to 1673 K and results in a faster char conversion rate at 1573 K.

4. Conclusion

Devolatilization and combustion of a bituminous coal have been studied in both N_2 and CO_2 based atmospheres under suspension fired conditions. Results have been obtained in the temperature range 1173 K – 1673 K using inlet oxygen concentrations of 5 – 28 vol. % and sampling residence times up to app. 1 s. No noticeable differences have been found in volatile yield between N_2 and CO_2 based environments and SEM images and N_2-BET surface areas of char obtained at 1673 K also show no differences between N_2 and CO_2 based atmospheres. This indicates that char properties are not influenced by the gas atmosphere for the investigated bituminous coal. The differences observed in the literature are believed to be caused by differences in particle temperature histories and long residence times, which can induce CO_2 gasification of reactive coals. With respect to char conversion, the data show no indication of char gasification by CO_2 and the rate of char conversion is identical at temperatures up to 1373 K in O_2/N_2 and O_2/CO_2 atmospheres. Experiments at 1573 K and 1673 K and low oxygen concentrations between 3.1 and 3.7 vol. % have however shown that the lower molecular diffusion coefficient of O_2 in CO_2 compared to N_2 becomes important when reaction is taking place under the influence of external mass transfer limitations leading to slower burnout in O_2/CO_2. Comparison of experimental char conversion profiles and profiles calculated for a shrinking sphere have shown the importance of considering the entire PSD and char morphology when modeling char oxidation.

Acknowledgement

The research leading to these results has received funding from the European Community's Research Fund for Coal and Steel (RFCS) under contract n° RFCR-CT-2006-00007, project FRIENDLYCOAL, and is also sponsored by the Danish Agency for Science, Technology and Innovation. The support and funding from these entities are greatly valued.

References

[1] Davison J. Performance and costs of power plants with capture and storage of CO_2. Energy 2007;32:1163-6.

[2] Figueroa JD, Fout T, Plasynski S, McIlvried H, Srivastava RD. Advances in CO_2 capture technology-The U.S. department of energy's carbon sequestration program. Int J Greenhouse Gas Control 2008;2:9-0

[3] Buhre BJP, Elliot LK, Sheng CD, Gupta RP, Wall TF. Oxy-fuel combustion technology for coal-fired power generation. Prog Energy Combust Sci. 2005;31:283-7

[4] Rathnam RK, Elliot LK, Wall TF, Liu Y, Moghtaderi B. Differences in reactivity of pulverized coal in air (O_2/N_2) and oxy-fuel (O_2/CO_2) conditions. Fuel Process Technol 2009;90:797-2

[5] Al-Makhadmeh L, Maier J, Scheffknecht G. Coal pyrolysis and char combustion under oxy-fuel conditions. 34'Th international technical conference on coal utilization & fuel systems, Clearwater Florida 2009

[6] Borrego AG, Alvarez D. Comparison of chars obtained under oxy-fuel and conventional pulverized coal combustion atmospheres. Energy Fuels 2007;21:3171-9

[7] Li Q, Zhao C, Chen X, Wu W, Li Y. Comparison of pulverized coal combustion in air and in O_2/CO_2 mixtures by thermo-gravimetric analysis. J Anal Appl Pyrolysis 2009;85:521-8

[8] Duan L, Zhao C, Zhou W, Qu C, Chen X. Investigation on coal pyrolysis in CO_2 atmosphere. Energy Fuels 2009;23:3826-0

[9] Jamil K, Hayashi J-i, Li C-Z. Pyrolysis of Victorian brown coal and gasification of nascent char in CO_2 atmosphere in a wire-mesh reactor. Fuel 2004;83:833-3

[10] Várhegyi G, Szabó P, Jakab E, Till F. Mathematical modeling of char reactivity in Ar-O_2 and CO_2-O_2 mixtures. Energy Fuels 1996;10:1208-4

[11] Bejarano PA, Levendis YA. Single-coal-particle combustion in O_2/N_2 and O_2/CO_2 environments. Combust Flame 2008;153:270-7

[12] Bird RB, Stewart WE, Lightfoot EN. Transport Phenomena, 2nd ed. John Wiley & Sons, Inc; 2002

[13] Yu J, Lucas JA, Wall TF. Formation of the structure of chars during devolatilization of pulverized coal and its Thermoproperties. Prog Energy Combust Sci 2007;33:135-0

[14] Molina A, Shaddix CR. Ignition and devolatilization of pulverized bituminous coal particles during oxygen/carbon dioxide combustion. Proc Combust Inst 2007;31:1905-2

[15] Ballester J, Jiménez S. Kinetic parameters for the oxidation of pulverized coal as measured from drop tube tests. Combust Flame 2005;142:210-2

[16] Chen W.-H, Du S.-W, Yang T.-H. Volatile release and particle formation characteristics of injected pulverized coal in blast furnaces. Energy Convers Manage 2007;48;2025-3

Article II

Coal Char Reactivity: A Thermogravimetric Study on Chars Obtained in O_2/N_2 and O_2/CO_2 in an Entrained Flow Reactor Under Suspension Fired Conditions and in a TGA

Coal Char Reactivity: A Thermogravimetric Study on Chars Obtained in O_2/N_2 and O_2/CO_2 in an Entrained Flow Reactor Under Suspension Fired Conditions and in a TGA.

Jacob Brix, Morten Storgaard Petersen, Jesper Banke Grossmann, Peter Glarborg, Peter Arendt Jensen, Anker Degn Jensen*

Department of Chemical and Biochemical Engineering, Building 229 Søltofts Plads, 2800 Kgs. Lyngby, Denmark

**Corresponding Author: e-mail: aj@kt.dtu.dk, Fax: +45 45 88 22 58, Phone: +45 45 25 28 41*

Abstract

Intrinsic kinetics for combustion and gasification of coal char has been studied by ThermoGravimetric Analysis (TGA) in O_2/N_2 and O_2/CO_2 at 5 vol. % O_2 and in CO_2/N_2 at 80 vol. % CO_2. Chars were prepared in situ in the TGA in N_2 or in an Entrained Flow Reactor (EFR) in either O_2/N_2 or O_2/CO_2 under suspension fired conditions. The experiments did not reveal a change in char combustion reactivity with O_2 when N_2 was replaced with CO_2 during char formation and combustion. Gasification was seen in the TGA at temperatures above app. 1100 K in an O_2 free environment but in the presence of O_2 char consumption was completed below 1000 K. A gradual deactivation towards O_2 of chars produced in the EFR at progressively increasing temperatures was observed in the TGA. Combustion reactivity profiles of chars partly combusted in the EFR at high O_2 concentrations showed two distinct peaks indicating phases of different reactivity. This is attributed to high particle peak temperatures in the EFR that cause a molten/deactivated phase to form. An Arrhenius expression including the effect of deactivation is presented for both combustion and gasification.

Keywords: Oxy-fuel, Combustion, TGA, EFR, Char, Kinetics

1. Introduction

In the global political and scientific communities, it is a growing concern that anthropogenic CO_2 emissions seem to cause increasing temperatures on earth. As a result research programs to pursue alternative energy production technologies are initiated all over the world, many of which are focusing on the emission of CO_2 from fossil fuel combustion. Today fossil fuels account for approximately 85 %[1,2] of the power and heat production worldwide wherefore new technologies, not presently mature, are unlikely to substitute fossil fuels such as coal the next several decades[3]. To accommodate this, power plants today relaying on conventional coal combustion are under strain to reduce their emissions through technological innovation.

A new technology that could prove able to reduce power plants CO_2 emissions markedly is the oxy-fuel combustion process. In oxy-fuel combustion, O_2 is separated from air before the boiler and mixed with recycled flue gas to obtain a plant exit stream of almost pure CO_2[3,4]. This CO_2 stream can subsequently be stored in suitable geological formations such as depleted oil and gas reservoirs or saline aquifers[2,4].

Being an emerging technology many technical aspects still need to be clarified if oxy-fuel combustion is to be industrialized. A key aspect for industrialization is the clarification of coal and char combustion characteristics, and a question often raised is whether CO_2 gasification may contribute to char conversion or changes in char reactivity. To address these issues, experimental methods for reliable kinetic measurements must be established as the feature of CO_2 as a reactant that can influence devolatilization and char conversion is highly dependent on operating conditions. Furthermore, char formation and deactivation in O_2/N_2 and O_2/CO_2 must also be elucidated.

Li *et al.*[5] investigated pulverized bituminous coal pyrolysis and combustion in N_2 and CO_2 based atmospheres. They used a TGA at heating rates of 10, 20 and 30 K min^{-1}, a maximum temperature of 1273 K and particle sizes in the ranges < 48 μm, 48 – 74 μm and 74 – 90 μm. For their combustion experiments they used O_2 concentrations of 21, 30, 40 and 80 vol. % in CO_2 or air. From pyrolysis experiments Li *et al.*[5] saw an effect of CO_2 gasification at temperatures above 1073 K that resulted in a faster sample mass loss than in N_2. The quantitative effect of CO_2 gasification was small, however, and the overall pyrolysis mass loss rate was lower than 2.5 wt. % min^{-1} even at 1273 K. This is

consistent with results of Várhegyi *et al.*[6] and Rathnam *et al.*[7] who also saw a small quantitative effect of gasification above 1030 - 1073 K at similar conditions. Duan *et al.*[8] conducted TGA pyrolysis with a bituminous coal (< 100 μm) using either N_2 or CO_2 and heating rates of 10, 30, 50 or 70 K min^{-1}. Peak temperatures of 973 K, 1073 K, 1173 K or 1273 K were reached in their experiments. When N_2 was replaced with CO_2, Duan *et al.*[8] saw increases in weight loss of as much as 8 wt. % at 1273 K and gasification was initiated already at 753 K. This initiation temperature is much lower than found by Li *et al.*[5], Várhegyi *et al.*[6] and Rathnam *et al.*[7] and could indicate that the char used by Duan *et al.*[8] was particularly reactive. Even though CO_2 gasification was observed by Li *et al.*[5], Várhegyi *et al.*[6], Rathnam *et al.*[7] and Duan *et al.*[8], their results can not be transferred directly to industrial conditions as residence times used by the authors were from 10 min. and up whereas industrial scale pyrolysis is finished in a few hundred milliseconds.

In the presence of O_2 Li *et al.*[5] found an app. 7 % lower conversion rate in O_2/CO_2 than in O_2/N_2 at 21 vol. % O_2, which they attributed to a characteristic difference between N_2 and CO_2 based combustion. Further analysis of their data by the present authors yields activation energies in the range 20 – 50 kJ mol^{-1}, however; well below the values typically reported in the literature for char combustion under kinetic control. This implies that the difference encountered by Li *et al.*[5] arise from mass transfer limitations in their TGA. Using a char obtained from Drop Tube Furnace (DTF) pyrolysis of a low rank coal at 1673 K in N_2 Li *et al.*[9] also found that mass transfer influenced their TGA reactivity measurements resulting in activation energies of 82.46 kJ mol^{-1} and 74.66 kJ mol^{-1} in O_2/CO_2 and O_2/N_2 respectively.

Várhegyi *et al.*[6] conducted TGA experiments at O_2 concentrations between 5 and 100 vol. % using either Ar or CO_2 as balance gas under careful control of the combustion regime to ensure a kinetically controlled reaction. Using two different bituminous coals and a lignite coal Várhegyi *et al.*[6] did not find an effect of CO_2 when O_2 was present at heating rates of 10, 20 and 50 K min^{-1} to a maximum temperature of 1223 K. Similar experiments by Liu[10] and Rathnam *et al.*[7] support the conclusion of Várhegyi *et al.*[6]. In O_2/CO_2 Liu[10] found an activation energy of 127.8 kJ mol^{-1} for bituminous char and 138.0 kJ mol^{-1} for anthracitic char, both of which are consistent with literature findings in O_2/N_2[11]. Rathnam *et al.*[7] used a bituminous char pyrolized in a DTF at 1673 K in N_2,

similar to the work of Li *et al.*[9], whereas Liu[10] prepared his chars at the same conditions as proximate analysis. Even though results of Li *et al.*[5], Li *et al.*[9], Várhegyi *et al.*[6], Liu[10] and Rathnam *et al.*[7] do not suggest that gasification is influencing intrinsic kinetics, it is not possible from their experiments to foresee a potential effect at suspension fired conditions as only Rathnam *et al.*[7] and Li *et al.*[9] prepared their chars in high temperature setups and both in N_2.

Zolin *et al.*[11] investigated the reliability of kinetic measurements by comparing TGA reactivities of a suite of coals, ranking from subbituminous to low volatile bituminous, with reactivities found from EFR experiments. Their TGA experiments were carried out isothermally in the temperature interval 723 – 923 K at 20 vol. % O_2 using in situ pyrolysis at 1173 K in N_2 to prepare chars from 90 – 105 μm coal samples. EFR reference experiments were carried out at 6 and 12 vol. % O_2 with coal particles in the size range 106 – 125 μm and combustion temperatures of approximately 1673 K. For most of the coals tested a good consistency in the trend of relative reactivities found in the TGA and EFR was seen, even though the absolute reactivity for individual coals deviated between the two setups. Zolin *et al.*[11] found that for some of the coals the reactivity dropped significantly when shifting the TGA with the EFR compared to the behavior of the other coals. This was explained by the authors with a high content of inertinite compared to vitrinite in these coals, causing a more severe deactivation at EFR conditions. The reactivity measured from TGA experiments were generally significantly higher than that measured from EFR experiments, witnessing of significant thermal deactivation of the char in the EFR. Zolin et al.[11] also saw deviations in reactivity between the TGA and EFR experiments caused by the catalytic effect of mineral matter in the TGA. The work of Zolin *et al.*[11] illustrates the inherent uncertainty that exists when kinetic parameters derived from TGA experiments where both pyrolysis and char oxidation is performed at low temperatures and heating rates are used at suspension fired conditions; a conclusion that is supported by the similar work of Manquais *et al.*[12] and from measurements of ignition temperatures in similar setups by Faúndez *et al.*[13].

The short review above shows that there is a need for a consistent TGA analysis of char reactivity in O_2/CO_2 and O_2/N_2 combustion for chars formed at high temperatures in the relevant gas atmospheres. The experimental link between suspension fired conditions and

intrinsic kinetics needs to be carried out in both O_2/CO_2 and O_2/N_2 at all conditions. This paper presents a reactivity study carried out on char formed in a TGA and in an EFR at suspension fired conditions in both N_2 and CO_2 based atmospheres. From reactivity profiles consistent kinetic expressions for combustion and gasification are derived that allows extrapolation to temperatures of relevance in industrial boilers.

2. Experimental

All experiments presented here have been carried out in a thermogravimetric analyzer of the type Netzsch STA 449 F1 where gaseous atmospheres have been created by mixing bottled gases. Samples were placed in alumina crucibles and positioned automatically on a highly sensitive balance located in a chamber that was purged with 20 ml min^{-1} of N_2. This N_2 made up 20 vol. % of the total flow in all experiments. The weight of the sample and the crucible temperature were recorded continuously as reaction progressed. Temperature programs dictating heating rates and maximum temperatures were specified for the Netzsch STA 449 F1 and for each program a calibration curve was made to ensure that possible fluctuations caused by the TGA did not influence the experimental measurements. By repetition of experiments the deviation in weight losses was found to be less than 1 %.

Three different types of experiments have been carried out. The first type of experiment, with particles of El Cerrejón coal sieved into the size ranges 63 – 90, 90 – 106 and 150 - 180 μm, was done to establish experimental conditions where mass transfer limitations did not influence the combustion rate and to investigate at what temperature CO_2 gasification could be expected to influence the sample consumption rate. The influence of mass transfer limitations were checked by calculating the observed reaction rate and crucible diffusion rate at each measured data point, and was found to be less than a few percent at the point of maximum rate for all experiments. The ultimate and proximate analysis of the unsieved coal is shown in table 1. The coal particles in all of these experiments were pyrolized in situ using N_2 and heating rates between 5 and 20 K min^{-1} to a maximum temperature of 1273 K. After pyrolysis the samples were allowed to cool to a temperature of 473 K at what point a heating rate of 5 or 10 K min^{-1} were used for non-isothermal char combustion at 5 vol. % O_2 in N_2 or CO_2. The maximum temperature

of char combustion was 1373 K in all experiments and to evaluate the influence of sample mass on combustion regime samples of 2, 5 and 10 mg were used.

Table 1 Proximate and ultimate analysis of the coal used for experiments.

Proximate Analysis		**Value**
Upper heating value	MJ/kg ar	28.19
Effective heating value	MJ/kg ar	27.09
Moisture	Wt. % ar	5.0
Ash	Wt. % ar	9.6
Volatiles	Wt. % ar	34.9
Ultimate Analysis		
Carbon	Wt. % ar	68.9
Hydrogen	Wt. % ar	4.61
Oxygen (diff.)	Wt. % ar	9.82
Nitrogen	Wt. % ar	1.44
Sulfur	Wt. % ar	0.62

The second type of experiments were conducted using chars obtained from devolatilization and combustion of 90 – 106 μm El Cerrejón coal particles in an electrically heated EFR designed to simulate suspension firing. The EFR has a cylindrical reaction zone of 2 m in length and a diameter of 0.08 m and particle sampling was done through an adjustable probe which ensured accurate determination of particle residence times during the experiments. Though the coal was sieved to achieve a narrow size range, the actual size distribution obtained was broader as shown by a laser based measurement on the sieved coal, and the mass based mean diameter was 75.8 μm[14]. The combustion experiments in the EFR were carried out isothermally at reactor temperatures of 1173 - 1673 K using inlet O_2 concentrations between 5 - 28 vol. % in either N_2 or CO_2. Devolatilization experiments were carried out in the same temperature interval in N_2 or CO_2 with app. 5 vol. % O_2 to overcome problems with tar clogging the sampling lines and ventilation. The EFR experiments are described in detail elsewhere[14]. Based on

experience from the first type of TGA experiments a heating rate of 5 K min^{-1} was used to reach a maximum temperature of 1123 K and sample masses between 1.2 and 1.5 mg were combusted in 5 vol. % O_2 in either N_2 or CO_2 to ensure that the process took place in zone I and to avoid over temperatures of the particles.

The third type of experiment was carried out using the same char as in the second type of experiments, the same heating rate and the same sample masses. However the gas atmosphere consisted of 80 vol. % CO_2 and 20 vol. % N_2 and the peak temperature was 1473 K.

In the following, the reactivity, listed in the figures as $d(X)/dt$, is defined by equation (1) where m_0 is the initial mass of char (dry and ash-free) and m is the mass of char at time t (dry and ash-free).

$$\frac{d(X)}{dt} = -\frac{1}{m_0} \cdot \frac{d(m)}{dt} \qquad (1)$$

3. Results

3.1 Influence of CO_2 gasification in TGA experiments

The relative influence of CO_2 gasification on char conversion in TGA experiments was discussed in the introduction and for reliable conclusions to be drawn with respect to char oxidation by O_2 it is important to evaluate this effect in the present experiments. Figure 1 shows the effect of gasification in the presence and absence of O_2. The figure shows an effect of CO_2 gasification at temperatures above approximately 1100 K, which is consistent with the results of Li *et al.*[5], Várhegyi *et al.*[6] and Rathnam *et al.*[7]. This effect is however also seen to be negligible when O_2 is added to the system as the temperature window of char conversion is lowered significantly. This is consistent with the observations of Várhegyi *et al.*[6] and Rathnam *et al.*[7]. The same conclusion can be drawn from figure 2 that shows reactivity profiles of char obtained by devolatilization in the EFR at 1673 K in N_2. As all the combustion experiments in this study is carried out at 5 vol. % O_2 where no differences are seen to exist when either N_2 or CO_2 is used as carrier gas the remaining of the combustion experiments presented here have been carried out in O_2/N_2.

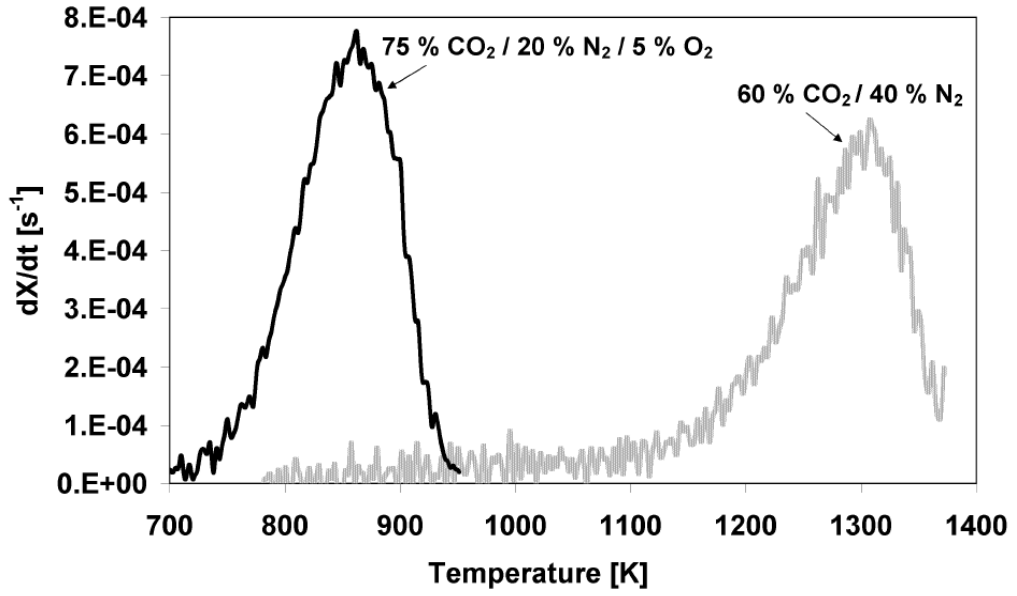

Figure 1 Reactivity of 63 – 90 μm coal particles pyrolized in N_2 using a heating rate of 20 K min^{-1} to a maximum temperature of 1273 K after which combustion/gasification is taking place from 473 K – 1373 K at a TGA heating rate 5 K min^{-1}. Sample masses were 5 mg.

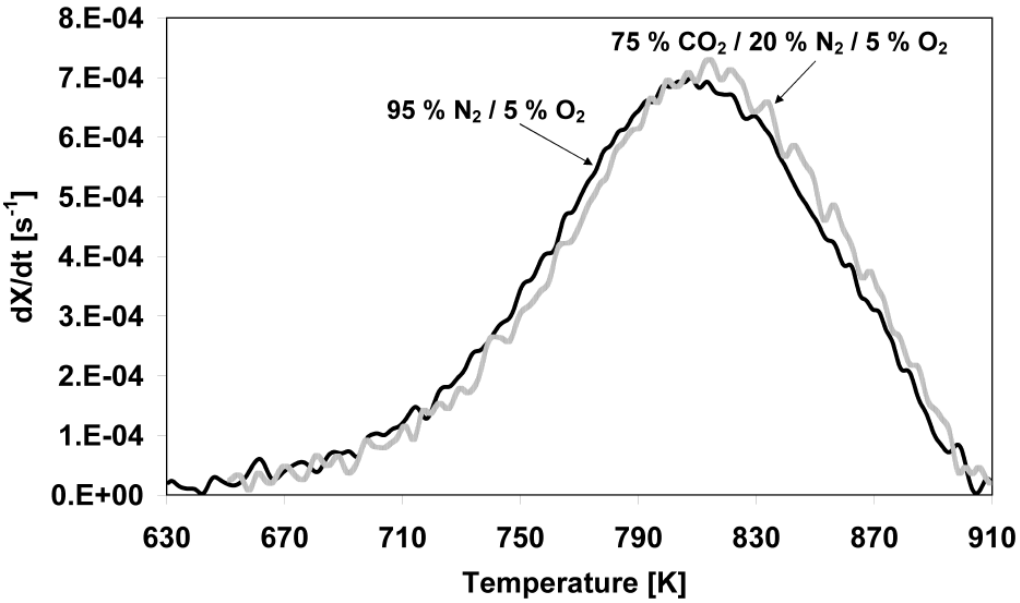

Figure 2 Combustion reactivity of EFR char obtained from devolatilization at 1673 K in N_2. A TGA heating rate of 5 K min^{-1} has been used to reach a maximum temperature of 1123 K. Sample masses were within 1.3 – 1.4 mg.

3.2 Combustion Reactivity of EFR Chars

When experiments to investigate char conversion are carried out under conditions resembling those found in a suspension fired boiler the influence of mass transfer phenomena make direct conclusions on intrinsic combustion reactivities difficult. To evaluate changes in intrinsic combustion reactivity when N_2 is replaced with CO_2 at suspension fired conditions a series of TGA experiments have been conducted on chars sampled in the EFR. Figure 3 shows combustion TGA reactivity profiles of chars obtained by devolatilization at 1573 K and 1673 K in N_2 or CO_2 in the EFR. It is seen from the figure that the switch of carrier gas from N_2 to CO_2 at the high temperatures where the chars were formed does not cause a significant change in combustion reactivity. The small differences in combustion reactivity between N_2 and CO_2 chars observed in figure 3 are within the experimental repeatability of the EFR as discussed in[14] and particle to particle variations in the small sample masses used in the TGA.

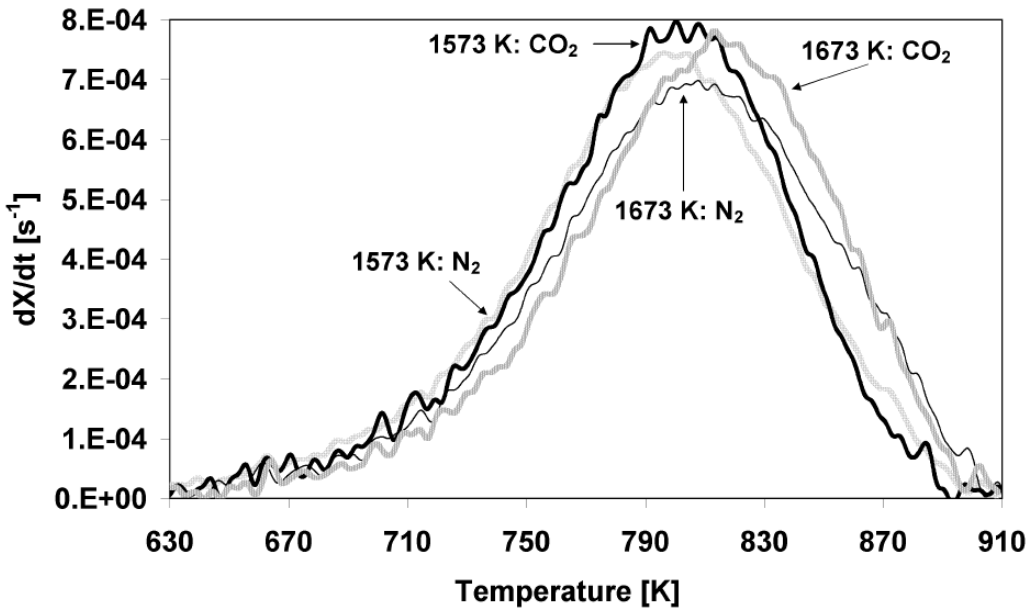

Figure 3 Combustion reactivity of EFR char obtained from devolatilization at 1573 K and 1673 K in N_2 and CO_2. A TGA heating rate of 5 K min^{-1} has been used to reach a maximum temperature of 1123 K in 5 vol. % O_2 and 95 vol. % N_2. Sample masses were within 1.2 – 1.5 mg.

The findings from figure 3 are consistent with related work on the same coal under suspension fired conditions[14,15] and they support conclusions that physical properties such

as densities and heat capacities of N_2 and CO_2[16] and their influence on flame propagation speed[17] are more likely to account for changes in ignition between O_2/CO_2 and O_2/N_2 atmospheres rather than the ability of CO_2 to react with the coal/char particles. In the related work[14,15], where the coal was combusted under suspension fired conditions in O_2/N_2 and O_2/CO_2, it was found that CO_2 gasification did not influence neither devolatilization nor char conversion. However it is also important to stress that different ignition and combustion characteristics in O_2/CO_2 and O_2/N_2 are found for coals of different ranks[18].

In figure 4 and figure 5 the development of intrinsic combustion reactivity is followed as conversion is progressing in the EFR.

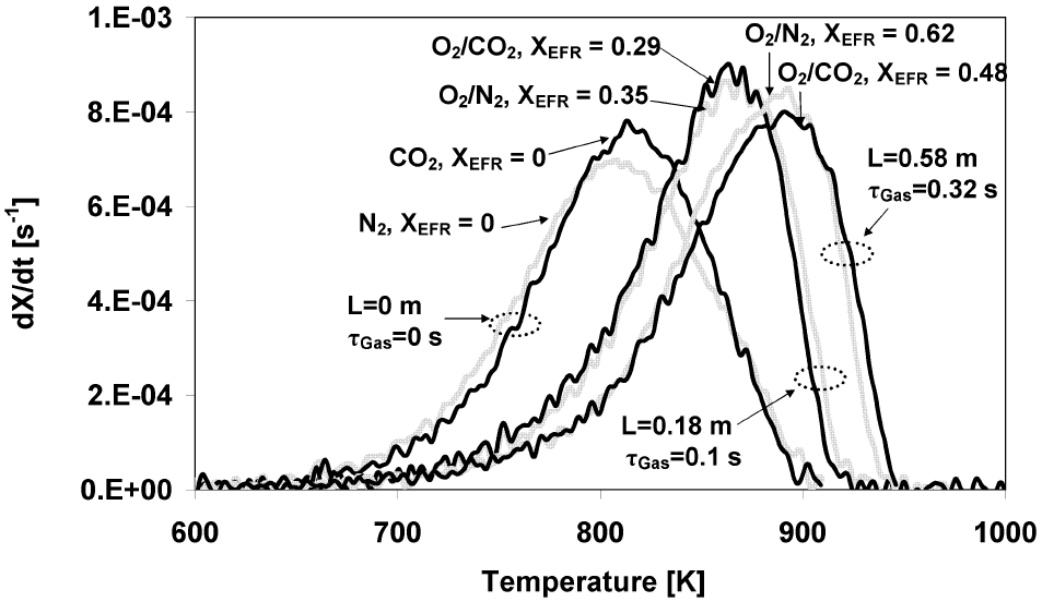

Figure 4 Combustion reactivity of EFR char obtained from devolatilization at 1673 K in N_2 and CO_2 and from combustion at 1673 K in 3.1 – 3.2 vol. % O_2 in N_2 or CO_2. A TGA heating rate of 5 K min^{-1} has been used to reach a maximum temperature of 1123 K in 5 vol. % O_2 and 95 vol. % N_2. Sample masses were within 1.2 – 1.5 mg.

Figure 4 shows combustion reactivity profiles of char devolatilized at 1673 K and char partly combusted at 1673 K and 3.1 – 3.2 vol. % O_2 (measured at the sampling positions) in N_2 and CO_2 based atmospheres. The degree of char conversion in the EFR is listed for each of the profiles in figure 4. It is seen from these values that the char conversions are 21 and 29 % higher in O_2/N_2 relative to O_2/CO_2. This is consistent with a combustion

process in the EFR that takes place in zone III as the diffusion coefficient of O_2 in N_2 is approximately 22 % higher than in CO_2 at 1673 K. That EFR conversion of the chars in figure 4 takes place in or close to zone III is supported by our modeling results[15] that further showed particle peak over-temperatures below 60 K due to the low oxygen concentrations. The results in figure 4 show that there are no differences in reactivity of the chars formed in O_2/N_2 or O_2/CO_2 when sampled at the same position in the EFR. Lower char reactivity is seen however as the EFR residence time is increasing, which could imply an effect of ash inhibition, thermal annealing or a gradual depletion of sites with higher reactivity.

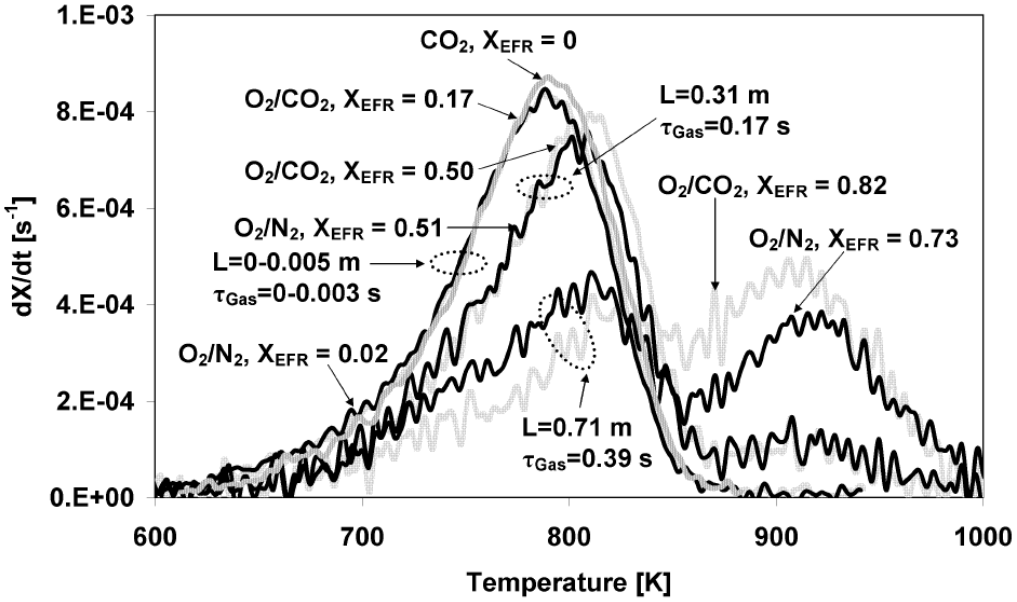

Figure 5 Combustion reactivity of EFR char obtained from devolatilization at 1173 K in CO_2 and by combustion at 1173 K in 27.7 – 27.9 vol. % O_2 in N_2 or CO_2. A TGA heating rate of 5 K min^{-1} has been used to reach a maximum temperature of 1123 K in 5 vol. % O_2 and 95 vol. % N_2. Sample masses were within 1.2 – 1.5 mg.

Figure 5 shows combustion reactivity profiles of char devolatilized at 1173 K in CO_2 and char partly combusted at 1173 K and 27.7 – 27.9 vol. % O_2 (measured at the sampling positions) in N_2 and CO_2 based atmospheres. It is seen from the figure that the combustion reactivity of devolatilized char (X = 0) and that of char sampled shortly after devolatilization (X = 0.17, X = 0.02) show a single peak whereas a second peak at around 900 K starts to appear for chars sampled with conversion around X = 0.50. At the highest

degrees of conversion the char clearly consists of two constituents of different reactivity. Zolin et al.[19] found the formation of two constituents with different reactivity after heat treatment of different fuels in a TGA to high temperatures, but did not provide a detailed explanation for this behavior. Zhang et al.[19] reported similar observations, which they attributed to the existence of a mineral cluster phase formed by a melt of inorganic components and trapped volatiles arising from a fierce devolatilization. The organic fraction in contact with the minerals forms an ordered phase of low reactivity[19]. That conditions in the EFR for these experiments exist for the formation of such a phase is supported by complementary work from the present authors[15]. Here it was found from modeling of single particle combustion that high particle peak temperatures (~ 1773 K) were reached shortly after heterogeneous ignition suggesting the existence of a second devolatilization. According to the model some particles reached their peak temperature at heating rates as high as 20000 K s^{-1}. Scanning Electron Microscopy (SEM) images also showed intact particles at high overall degrees of char conversion[15]. In figure 5 the development of a second phase is seen to proceed identically in O_2/N_2 and O_2/CO_2 with a peak temperature that is unchanged as char conversion in the EFR progress.

3.3 Kinetics of EFR Char Combustion and Gasification

An important feature of the thermogravimetric analyzer is its capability to combust well defined sample masses in the absence of mass transfer limitations. For this reason it is often used to extract intrinsic kinetic parameters for combustion and gasification of coal and char.

Figure 6 and figure 7 shows Arrhenius plots for combustion and gasification of EFR chars obtained by devolatilization in CO_2**,** respectively, along with the results of linear regression for each char. Due to a limited amount of char available from the EFR experiments[14] only three Arrhenius plots are shown in figure 7 for gasification by CO_2. Reaction rates covering char consumption between 10 % and 90 % conversion in the TGA are represented in both figures. The rate constants have been found from equation (2) with a specific char surface area, S_0, of 240 m^2 g^{-1} found from BET measurements[15].

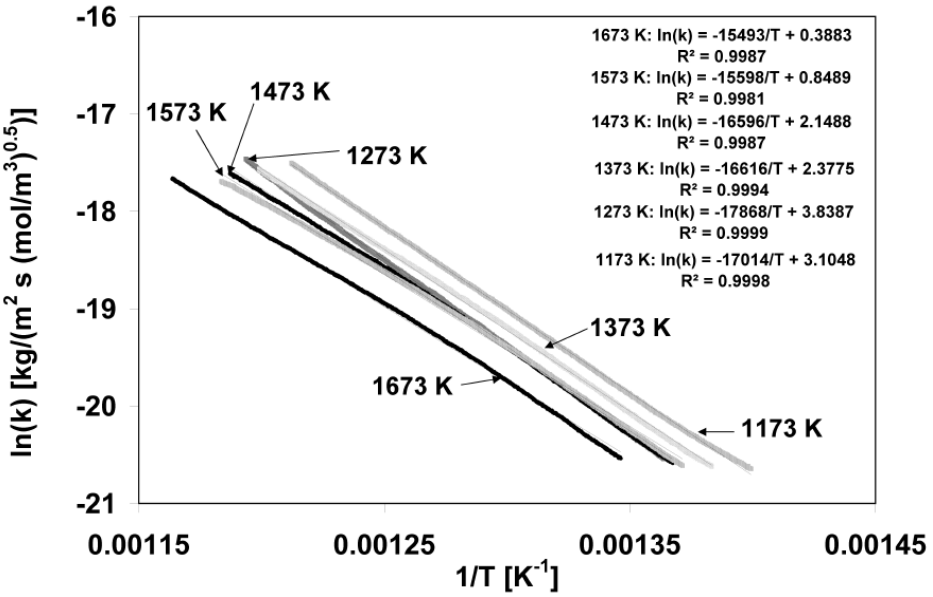

Figure 6 Arrhenius plots of combustion rate constants for char obtained by devolatilization in the EFR in CO_2.

The concentration of O_2 or CO_2, C, are found using the temperature measurements at each data point. The kinetic parameters found from the TGA data have been used in modeling work at the conditions of the EFR[15] and a decision must therefore be made for the choice of reaction orders n. As reaction orders are known to vary with temperature, intrinsic reaction orders found in the TGA would cause erroneous predictions under suspension fired conditions. For combustion intrinsic reaction orders between 0.5 – 1 have been reported for the temperature interval used in the TGA[20] while intrinsic reaction orders between 0 – 1, though with the majority being 0, have been reported at the temperature interval used in the EFR[21]. To make the kinetic parameters as consistent as possible when they are to be used at high temperatures a reaction order of 0.5 has been chosen for use in equation (2). For gasification, intrinsic reaction orders found in the literature varies around 0.5[22,23] and this value of reaction order has therefore been chosen for use in equation (2).

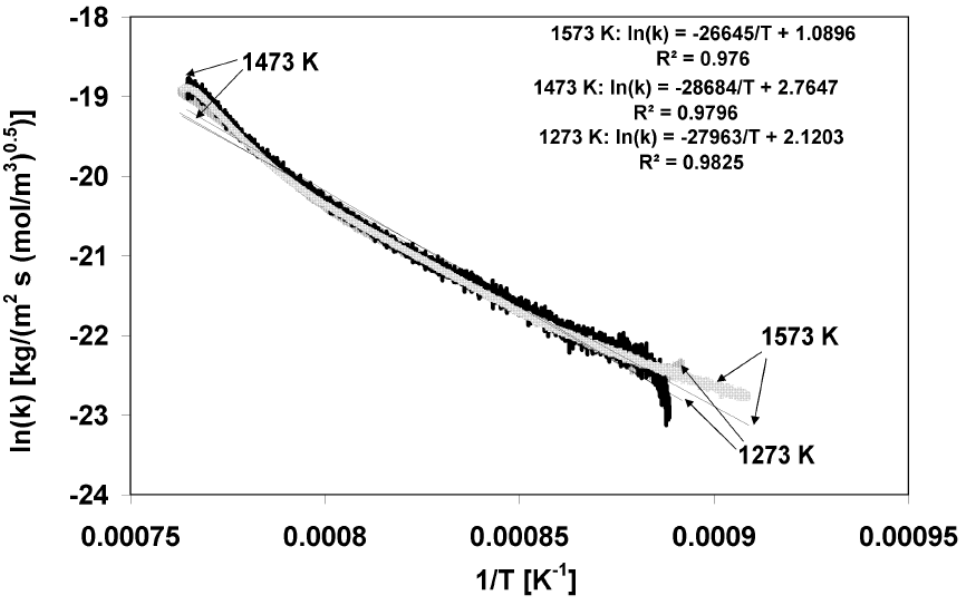

Figure 7 Arrhenius plots of gasification rate constants for char obtained by devolatilization in the EFR in CO_2.

Linear regression on the data in figure 6 and figure 7 yields activation energies, E_A, and pre-exponential factors, A_0, corresponding to an Arrhenius type power law expression as defined by equation (2).

$$k = A_0 \cdot e^{-E_A/RT} = \frac{d(X)}{dt} \cdot (1-X)^{-1} \cdot S_0^{-1} \cdot \left(C^n\right)^{-1} \qquad (2)$$

The curvature seen in figure 7 does suggest that Langmuir-Hinshelwood expressions could be used to better fit the Arrhenius plots in the figures. The purpose of this study is however to obtain kinetic expressions suitable for detailed reactor modeling[15] and the regression constants shown in figure 6 and 7 indicate that power law kinetics will describe reaction rates sufficiently well.

Similar activation energies are found for combustion of chars formed in the EFR at the different devolatilization temperatures but a variation is seen in the pre-exponential factors. As char consumption between X = 0.1 – 0.9 is taking place in a narrow temperature window of 110 – 130 K an average combustion temperature, T_{avg}, is used to

define a standardized reactivity of the individual chars. Using equation (3) a new pre-exponential factor, k_0, was calculated for each char using the average activation energy of all chars, $E_{A,Avg}$ = 137.5 kJ mol^{-1}. These new pre-exponential factors are shown in figure 8 in an Arrhenius plot and they show a decreasing trend as the devolatilization temperature at which the chars were formed increases.

$$k_0 = A_0 \cdot \exp\left(\frac{1}{R \cdot T_{Avg}} \cdot \left(E_{A,Avg} - E_A\right)\right) \tag{3}$$

The trend in the pre-exponential factors in figure 8 is a measure of deactivation caused by the increasing char formation temperatures. Linear regression on the data in figure 8 (i.e. ln(k_0) vs 1/T) yields a deactivation energy, E_D, of 20.5 kJ mol^{-1} and a pre-exponential factor, k_0^*, of 1.44 kg m^{-2} s^{-1} (mol m^{-3})$^{-0.5}$.

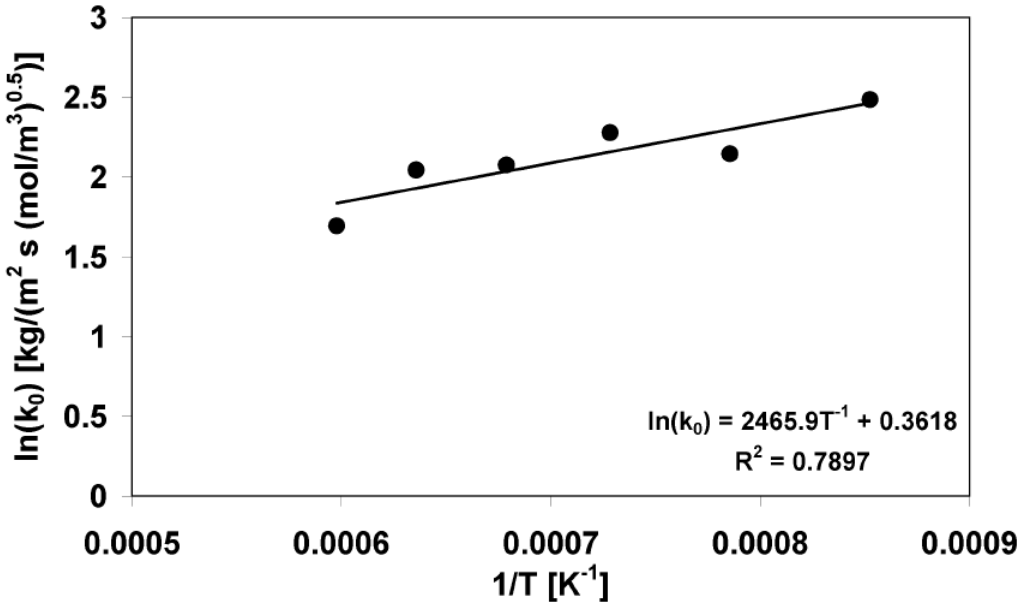

Figure 8 Arrhenius plot of the new pre-exponential factors for combustion found from equation (3).

In figure 7 it is seen that similar activation energies are found for gasification of each of the chars and furthermore that the difference in reactivity between the chars is very small.

The reason for the small difference in reactivity is probably that the range of devolatilization temperatures covered by the chars is rather narrow. Senneca and Salatino[24] did show that CO_2 gasification reactivity is influenced by thermal deactivation although to a much lower extent than reactivity towards oxygen. However, based on the present data the gasification reaction was modeled without taking deactivation into account. Fitting of the data gave a deactivation energy of 0 kJ mol^{-1}, an average pre-exponential factor, k_0, of 7.33 kg m^{-2} s^{-1} (mol m^{-3})$^{-0.5}$ and an average activation energy of 230.8 kJ mol^{-1}.

From the kinetic analysis of combustion and gasification above, a general Arrhenius expression that includes thermal deactivation can be defined as in equation (4) with the kinetic parameters listed in table 2.

Table 2 Intrinsic kinetic parameters to be used in (4).

Species/Property	**n**	**E_D [kJ mol^{-1}]**	**E_A [kJ mol^{-1}]**	**k_0* [kg m^{-2} s^{-1} (mol m^{-3})$^{-0.5}$]**
O_2	0.5	20.5	137.5	1.44
CO_2	0.5	0	230.8	7.33

When equation (4) is used T^* is the highest temperature a particle has reached during its conversion, which assumes a rapid deactivation to a pseudo steady value at any given T^*. This means that thermal deactivation, which is the governing mechanism of deactivation under oxidizing conditions, is accounted for in equation (4) throughout the particles life time. For gasification the deactivation part in equation (4) will cancel and the expression will reduce to a normal Arrhenius expression, i.e. $k_0 = k_0^*$

$$k = k_0^* \cdot \exp\left(\frac{E_D}{R \cdot T^*}\right) \cdot \exp\left(\frac{-E_A}{R \cdot T}\right) \qquad (4)$$

The rate constant in (4) has been used successfully to simulate combustion in O_2/N_2 and O_2/CO_2 based atmospheres in the EFR as discussed by these authors elsewhere[15].

4. Conclusion

Combustion and gasification of char has been studied in a ThermoGravimetric Analyzer (TGA). Chars were prepared from in situ pyrolysis in the TGA using N_2 and from devolatilization and combustion in O_2/N_2 and O_2/CO_2 in an Entrained Flow Reactor (EFR) under suspension fired conditions. From experiments on TGA chars in CO_2/N_2 and $O_2/CO_2/N_2$ it was found that the influence of CO_2 gasification during combustion in the TGA was negligible in the temperature window where the chars were converted.

Combustion reactivity profiles of EFR chars did not reveal any differences between chars obtained by devolatilization in N_2 and CO_2. The development of two char constituents with different reactivity was seen when combustion in the EFR was taking place at high O_2 concentrations of about 28 vol. %. This is attributed to high particle peak temperatures that cause a highly deactivated phase, possibly composed of organic as well as inorganic components, to form in some particles.

Intrinsic kinetics in terms of Arrhenius parameters for combustion and gasification were obtained from reactivity profiles of char formed at temperatures between 1173 K and 1673 K in the EFR. For combustion it was found that significant char deactivation was taking place in the EFR as the reactor temperature increased and the kinetic expression for combustion therefore includes a deactivation term. For the chars investigated with respect to CO_2 gasification no deactivation was observed and so this reaction was described by a simple Arrhenius expression.

Acknowledgement

The research leading to these results has received funding from the European Community's Research Fund for Coal and Steel (RFCS) under contract n° RFCR-CT-2006-00007, project FRIENDLYCOAL, and is also sponsored by the Danish Agency for Science, Technology and Innovation and Energinet.dk. The support and funding from these entities are greatly valued.

References

(1) Davison, J. *Energy*. **2007**, 32, 1163-1176.

(2) Figueroa, J. D.; Fout, T.; Plasynski, S.; McIlvried, H.; Srivastava, R. D. *Int J Greenhouse Gas Control*. **2008**, 2, 9-20.

(3) Buhre, B. J. P.; Elliot, L. K.; Sheng, C. D.; Gupta, R. P.; Wall, T. F. *Prog Energy Combust Sci*. **2005**, 31, 283-307.

(4) Toftegaard, M. B.; Brix, J.; Jensen, P. A.; Glarborg, P.; Jensen, A. D. *Prog Energy Combust Sci*. **2010**, 36, 581-625.

(5) Li, Q.; Zhao, C.; Chen, X.; Wu, W.; Li, Y. *J. Anal. Appl. Pyrolysis.* ***2*****009**, 85, 521-528.

(6) Várhegyi, G.; Szabó, P.; Jakab, E.; Till, F.; Richard, J-R. *Energy Fuels*. **1996**, 10, 1208-1214.

(7) Rathnam, R. K.; Elliott, L. K.; Wall, T. F.; Liu, Y.; Moghtaderi, B. *Fuel Process. Technol*. **2009**, 90, 797-802.

(8) Duan, L.; Zhao, C.; Zhou, W.; Qu, C.; Chen, X. *Energy Fuels*. **2009**, 23, 3826-3840.

(9) Li, X.; Rathnam, R. K.; Yu, J.; Wang, Q.; Wall, T.; Meesri, C. *Energy Fuels*. **2010**, 24, 160-174.

(10) Liu, H. *Energy Fuels*. **2009**, 23, 4278-4285.

(11) Zolin, A.; Jensen, A.; Pedersen, LS.; Dam-Johansen, K.; Tørslev, P. *Energy Fuels*. **1998**, 12, 268-276.

(12) Manquais, K. L.; Snape, C.; McRobbie, I.; Barker, J.; Pellegrini, V. *Energy Fuels.* **2009**, 23, 4269-4277.

(13) Faúndez, J.; Arenillas, A.; Rubiera, F.; García, X.; Gordon, A. L.; Pis, J. J. *Fuel*. **2005**, 23, 2172-2177.

(14) Brix, J.; Jensen, P. A.; Jensen, A. D. *Fuel*. **2010**, 89, 3373-3380.

(15) Brix J et al. *Fuel* (**2011**), doi:10.1016/j.fuel.2011.01.021

(16) Molina, A.; Shaddix, C. R. *Proc Combust Inst*. **2007**, 31, 1905-1912.

(17) Suda, T.; Masuko, K.; Sato, J.; Yamamoto, A.; Okazaki, K. *Fuel*. **2007**, 86, 2008-2015.

(18) Bejarano, P. A.; Levendis, Y. A. *Combust Flame*. **2008**, 153, 270-277.

(19) Zhang, H.; Pu, W-X.; Ha, S.; Li, Y.; Sun, M. *Fuel*. **2009**, 88, 2303 – 2310.

(20) Hurt, R. H.; Haynes, B. S. *Proc Combust Inst*. **2005**, 30, 2161-2168.

(21) Hurt, R. H.; Calo, J. M. *Combust Flame*. **2001**, 125, 1138-1149.

(22) Kajatani, S.; Hara, S.; Matsuda, H. *Fuel*. **2002**, 81, 539-546.

(23) Liu, H.; Luo, C.; Toyota, M.; Uemiya, S.; Kojima, T. *Fuel Process. Technol*. **2006**, 87, 769-774.

(24) Senneca, O.; Salatino, P. *Proc. Comb. Inst*. **2002**, 29, 485-493.

Article III

Modeling Char Conversion under Suspension Fired Conditions in O_2/N_2 and O_2/CO_2 Atmospheres

Modeling Char Conversion under Suspension Fired Conditions in O_2/N_2 and O_2/CO_2 Atmospheres

Jacob Brix, Peter Arendt Jensen, Anker Degn Jensen*

Department of Chemical and Biochemical Engineering, Building 229 Søltofts Plads, 2800 Kgs. Lyngby, Denmark
**Corresponding Author: e-mail: aj@kt.dtu.dk, Fax: +45 45 88 22 58, Phone: +45 45 25 28 41*

Abstract

The aim of this investigation has been to model combustion under suspension fired conditions in O_2/N_2 and O_2/CO_2 mixtures. Experiments used for model validation have been carried out in an electrically heated Entrained Flow Reactor (EFR) at temperatures between 1173 K and 1673 K with inlet O_2 concentrations between 5 and 28 vol. %. The COal COmbustion MOdel, COCOMO, includes the three char morphologies: cenospheric char, network char and dense char each divided between six discrete particle sizes. Both combustion and gasification with CO_2 are accounted for and reaction rates include thermal char deactivation, which was found to be important for combustion at high reactor temperatures and high O_2 concentrations. COCOMO show in general good agreement with experimental char conversion profiles at conditions covering zone I-III. From the experimental profiles no effect of CO_2-gasification on char conversion has been found. COCOMO does however suggest that CO_2-gasification in oxy-fuel combustion at low O_2 concentrations can account for as much as 70 % of the overall char consumption rate during combustion in zone III.

Keywords: Oxy-fuel, Combustion, Char, Modeling

1. Introduction

There is an increasing global focus on the anthropogenic CO_2 emission to the atmosphere due to its claimed effect on the earth's climate. This focus has caused fossil fuelled power plants, to explore technologies that will allow them to keep using fossil fuels, such as coal, as a feedstock while reducing CO_2 emissions markedly. One technology is oxy-fuel combustion in which near pure O_2 is mixed with recycled flue gas at the entrance to the boiler, thereby creating a plant exit stream of almost pure CO_2 [1]. This CO_2 stream can subsequently be sent to storage in geological formations such as saline aquifers or depleted oil and gas fields [2].

An important part of the scale up process of the oxy-fuel technology is clarifying differences in char conversion rates between this technology and conventional air-blown combustion. As it is the time required for char conversion that determines the size of a boiler and its heat release profile it is also important that predictive modeling tools are developed.

There exist many attempts to model char combustion in the literature [3-10]. Many of the models are very detailed in their description of char morphology, particle size, fragmentation, ash inhibition, thermal char deactivation and film layer mass transport of O_2, which also means that their outcome is depending on a wide range of parameters that are often related to specific experimental conditions and equipment. A more detailed model does however in general do a better job in predicting the combustion process than simple global models.

In their Char Burnout Kinetic (CBK) model Hurt *et al.* [4] described the oxidation of coal char and thereby estimated the fly ash carbon content. The model includes thermal annealing, statistical kinetics and char densities as well as ash inhibition. The ability of the model to predict a decrease in conversion rate at high degrees of conversion ($X > 90$ %), where many other models fail, were mostly due to the inclusion of ash inhibition. The effect of ash inhibition or ash retention on the conversion rate were also investigated by Shaddix and Murphy [5] using a shrinking sphere approach. They showed that low or even negative apparent Arrhenius reaction orders could be expected at the late stages of char combustion ($X > 70$ %). Shaddix and Murphy [5] did not find that ash retention caused a decrease in char conversion rate at conversions below approximately 90 %. On

the contrary the lower carbon density caused by the retention of ash caused slightly higher conversion rates in the earlier stages of combustion than did predictions without ash retention.

In the development of the CBK model Hurt *et al.* [11] examined the effect of coal heterogeneity and found that a distribution of pre-exponential Arrhenius factors, accounting for the heterogeneity of a Particle Size Distribution (PSD), improved burnout predictions especially during zone I combustion, where no mass transport limitations exist and conversion rate is determined only by chemical kinetics, and in the case of broad PSD's. The estimation of kinetic parameters is often a cause for concern in modeling. It has been found that the intrinsic reactivity of bituminous char decreases as the particle temperature and heating rate during pyrolysis increases. This is due to an increased graphitization of the char leading to more basal planes that have a lower content of active carbon sites [12]. The effect of thermal deactivation along with an exact determination of intrinsic kinetic parameters, obtained in zone I, needs to be accounted for in trustworthy kinetic expressions that are to be used for combustion across zone I – III where mass transfer limitations on reactants gradually cause concentration gradients to form in the particles as the effective concentrations on their surfaces approach zero.

An important feature of many detailed combustion models is the presence of char of different morphologies. Cloke *et al.* [6] conducted Drop Tube Furnace (DTF) experiments at 1573 K, 1423 K and 1273 K using pulverized coal in the size range 106 – 125 μm at 5 % O_2. The coal was first devolatilized at the different temperatures using 1 % O_2. Through digital images, taken under a microscope and analyzed by a computer, they divided the chars into three categories; cenospheric char, network char and mixed char, the latter category being predominately dense. Similar char classifications are suggested by other researchers [7,13,14]. The char size distribution was described by Cloke *et al.* [6] using 8 discrete intervals covering particles between 0 and 150 μm. With char morphology as input in the CBK model they found relatively good agreement between simulations and experimental results, though with a tendency of under prediction by the model. This under prediction was attributed to an over estimation of ash inhibition in the beginning of the process, i.e. the opposite of what was found by Shaddix & Murphy [5]. This contradiction witness of the sensitivity of detailed models to inputs

such as ash/char porosities, pore sizes, turtoisities and the way in which phenomena such as ash inhibition are described. In a later paper Cloke *et al.* [7] conducted similar experiments at 1573 K using 15 different coals. The chars were classified from image analysis both as individual coals and as a collected standardized set of input data covering all coals. Results of predicted char burnout showed reasonable agreement with experimental results when both types of char classification were used as model input, suggesting that a generalized morphological description of char can enhance the accuracy of model predictions without the need for specific experimental measurements.

Experimental char conversion data obtained under oxy-fuel combustion at high temperatures have been published by several authors [15-19] and low temperature data are also available in the literature [17,20-22]. Data obtained at high temperatures at conditions that are encountered in industrial boilers are contradictory regarding the effect of CO_2 gasification. In addition the effect of CO_2 gasification suggested by some TGA investigations appear more likely to be caused by the long residence times and low O_2 concentrations used in the experiments.

In the present investigation char consumption from reaction with both O_2 and CO_2 is included in a detailed single particle combustion model as an attempt to elucidate under what conditions CO_2-gasification can be expected to contribute to fuel conversion. Model predictions are compared with an extensive data set covering suspension fired O_2/N_2 and O_2/CO_2 combustion under a wide range of conditions. Conclusions are hereafter drawn from particle conversion rates, temperature histories and optical appearances determined by Scanning Electron Microscopy (SEM).

2. Experimental

The experiments were carried out in an electrically heated EFR and are previously described in the literature [15]. All data on char conversion presented in this text is taken directly from this reference. The reactor is cylindrical and measures 2 meters in length, 0.08 m in diameter and is shown schematically in figure 1 along with its utilities. The reaction zone is heated by 7 electrical heating elements and can reach temperatures up to 1773 K. On top of the reactor a 0.8 m long gas preheater, consisting of two heating elements, preheats the secondary gas stream to a prescribed temperature. Coal is fed to

the reactor at a constant rate of 50 g hr^{-1} using a dosing system consisting of a silo and a screw feeder connected to a vibration transporter. Coal injection into the top of the reaction zone is done through a water cooled probe that goes through the center of the gas preheater.

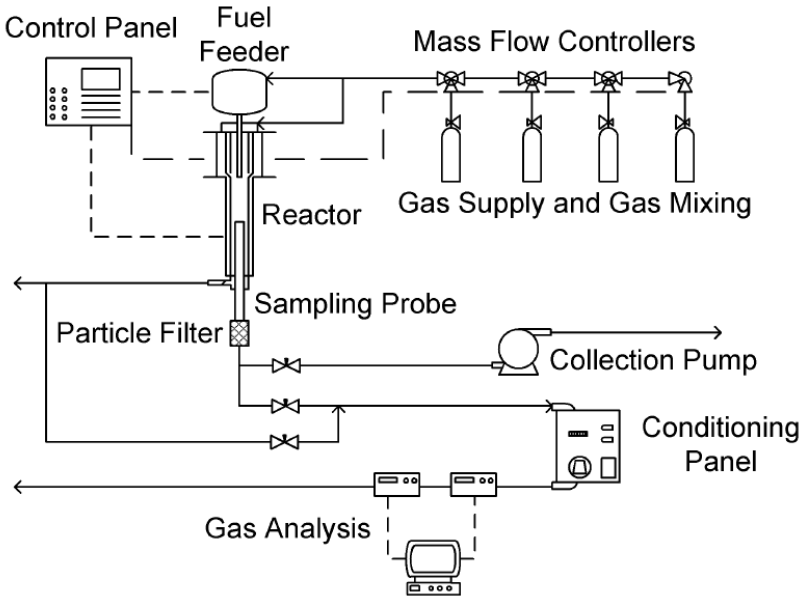

Figure 1 Experimental setup. Solid lines indicate tubes and dashed lines indicate wires for control and data logging. All streams leaving the setup is sent to a central ventilation system.

During experiments char has been sampled at different reactor positions using a water cooled sampling probe with an outer radius of 0.017 m. The sampling end of this probe is shaped as a funnel. Sampling has been done iso-kinetically with an average gas velocity of 1.81 m s^{-1} in all the experiments. Through the probe, gas sampling for analysis for CO, CO_2 and O_2 has also been done at each sampling point. Except when experiments were carried out in air all gaseous environments used in the experiments were created by mixing bottled gases.

Experiments were carried out in the temperature interval 1173 K – 1673 K with increments of 100 K. Inlet O_2 concentrations were in the range 5 – 28 vol. %, corresponding to stoichiometric ratios between 2 and 15, with either N_2 or CO_2 as carrier gas. O_2 concentrations given in this paper are however lower, as these are measured after complete devolatilization and are the concentrations experienced by the burning char

particles. During experiments the aim has been to obtain char conversion profiles at near constant O_2 concentrations, in order to use them for model validation. The only consideration towards stoichiometry has therefore been to ensure sufficient amounts of O_2.

At each of the experimental temperatures a devolatilization experiment was also carried out in order to correct char conversion for volatile weight loss. Due to problems with tar clogging the probe the devolatilization experiments were carried out at approximately 5 vol. % O_2 corresponding to a stoichiometric ratio of approximately 3. This did however not affect coal mass losses [15] and the presence of O_2 during devolatilization was not found to affect char reactivity [23].

Table 1 Proximate and ultimate analysis of the coal used for experiments. In the column "Corrected" the original data has been corrected for the ash content of the particle size fraction 90 – 106 μm.

Proximate Analysis		**Original**	**Corrected**
Upper heating value	MJ/kg ar	28.19	28.19
Effective heating value	MJ/kg ar	27.09	27.09
Moisture	Wt. % ar	5.0	5.2
Ash	Wt. % ar	9.6	5.9
Volatiles	Wt. % ar	34.9	34.9
Ultimate Analysis			
Carbon	Wt. % ar	68.9	71.73
Hydrogen	Wt. % ar	4.61	4.8
Oxygen (diff.)	Wt. % ar	9.82	10.23
Nitrogen	Wt. % ar	1.44	1.5
Sulfur	Wt. % ar	0.62	0.64

El Cerrejón coal sieved to the size range 90 – 106 μm has been used in all the experiments. Ash tracing on the sieved coal fraction revealed an ash content of 5.9 wt. %, which is lower than that of proximate analysis on the unsieved coal. The proximate and ultimate analysis of the coal in table 1 is therefore shown both as received from the lab

and corrected for ash content using the same fractional correction factor for all coal constituents.

3. Model Development

3.1 Classification of Char Morphology and Size

Both char morphology and its influence on conversion rates has been investigated by several authors [6,7,14,24-31].

Table 2 Char morphology categories found in the literature and the characteristics used to define them.

	Cloke *et al.* [6]	**Wu *et al.* [7]**	**Ma & Mitchell [13]**	**Yu *et al.* [14]**
Cenospheric char				
ε	> 71.48 %	> 68 %	> 70 %	> 80 %
δ_{Wall}	< 4.63 μm	55 % under 3 μm	< 10 μm (thin)	< 5 μm
Ψ	N/A	$\Psi \sim 0.65–0.73$	$\Psi > 0.85$	Spherical
Network char				
ε	38.83 -84.92 %	47-69 %	40-60 %	> 50 %
δ_{Wall}	4.13-6.89 μm	8–48 % under 3 μm	> 10 μm (medium)	Variable
Ψ	N/A	$\Psi \sim 0.47–0.82$	$\Psi > 0.8$	Variable
Dense/solid char				
ε	< 12.51 %	3-33 %	< 40 %	~ 50 %
δ_{Wall}	~ 13.01 μm	9–41 % under 3 μm	> 10 μm (thick)	> 5 μm
Ψ	N/A	$\Psi \sim 0.67–0.68$	$\Psi < 0.7$	Variable

Bailey *et al.* [25] and Shu & Xu [24] developed detailed char classification systems based on microscopy [24,25] and measurements of specific surface area and pore volume [24] and Yu *et al.* [14] reviewed the literature providing a thorough discussion on the classification of char. Common for these detailed classification systems is that they are difficult to apply when predicting the behavior of a practical system. In order to apply char morphology in predictive models each morphological group needs to be quantified and described with respect to porosity, density, size, geometry, specific surface area and abundance. Because of this, generalized morphologies as suggested by Cloke *et al.* [6], Wu *et al.* [7], Ma & Mitchell [13] and Yu *et al.* [14] are often used in modeling to lower

the requirement for input parameters. Common for the latter authors is that they divide the char into a cenospheric fraction, a network/mixed fraction and a solid/dense fraction. The generalized morphologies used by the authors are shown in table 2 along with key characteristics used to define each group.

Besides the characteristic parameters provided in table 2 knowledge on pore size/ pore size distribution, distribution of char between the categories, specific surface area, densities, char composition and PSD are important to know in modeling but the table clearly shows the challenges encountered when constructing a detailed combustion model founded on a description of char morphology. There is a general agreement that a highly porous, nearly spherical, cenospheric char is present. When dealing with network chars more disagreement can be found between the authors in table 2. Yu *et al.* [14] assumes quite porous chars of varying geometry. Wu *et al.* [7] and Ma & Mitchell [13] are in relative agreement on porosity and to some extent on wall thickness but Ma & Mitchell [13] assume more spherical chars than does Wu *et al.* [7]. Cloke *et al.* [6] defines network chars with a broad range of porosities but with wall thicknesses well in line with those of Wu *et al.* [7]. Also for dense/solid chars is there disagreement among the authors, especially with respect to porosities.

In this study char particles have been investigated by SEM as a mean to establish a qualitative description of the morphologies present.

Figure 2 A and B shows SEM images of char sampled at two different positions in the reactor at 1173 K in 27.9 vol. % O_2 in CO_2. At 37 % conversion the three morphologies of table 2 are all seen to be present. Even at 80 % conversion there are still particles present of distinctively different morphologies where some have surfaces with low macro porosity and some is almost fully consumed. Figure 2 C and D show SEM images of char obtained from devolatilization at 1673 K in N_2. Here both network and dense chars can be seen but the presence of char that does not fall easily into one category is seen in picture C. The network/cenosphere char in this picture has regions with large cavities and thin walls, characteristic of cenospheres, but it also has regions with a pore system resembling that of network chars. The inclusion of such a char into a practical morphological system must be based on judgment of its average wall thickness.

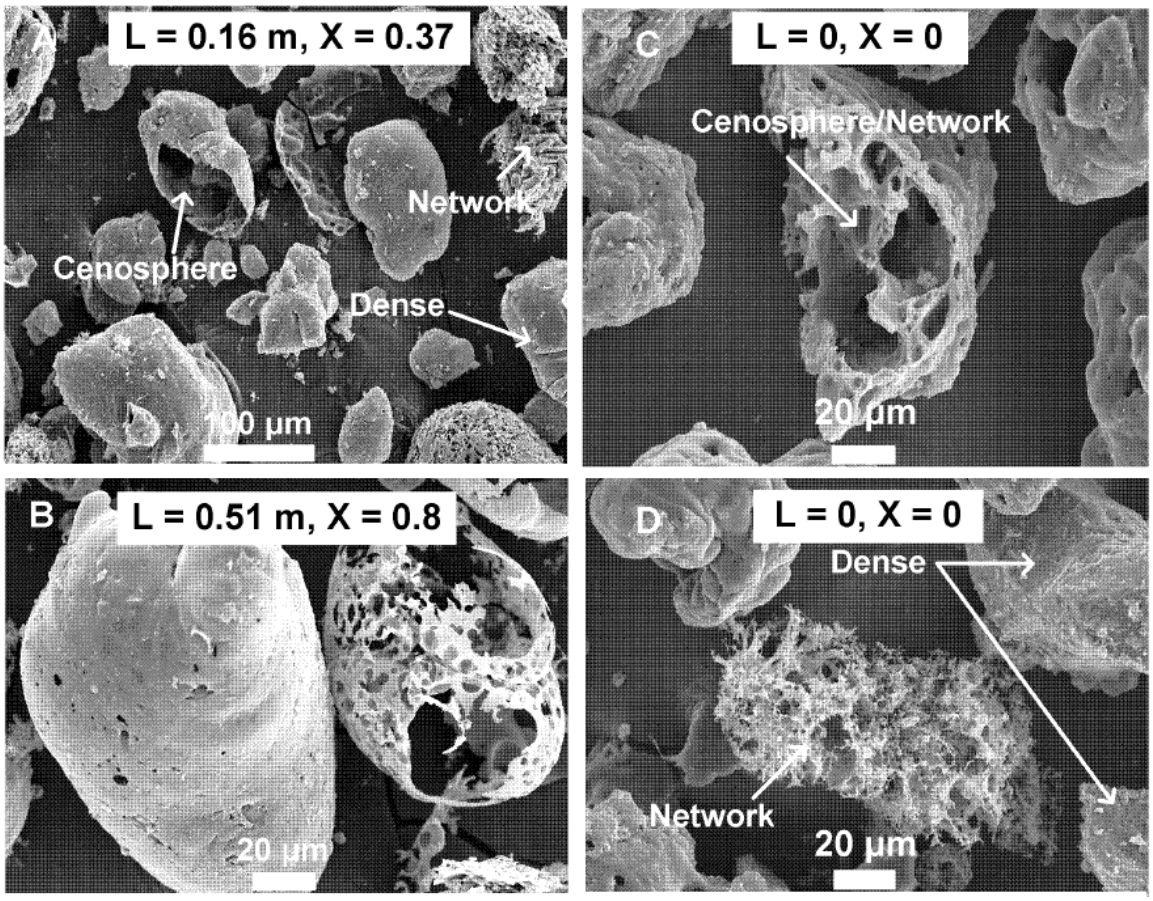

Figure 2 A & B: SEM images of chars obtained at 1173 K in CO_2 with an O_2 concentration of 27.9 vol. %. The O_2 concentration is the average of the local concentrations at each sampling position. $\lambda \sim 15$. C & D: SEM images obtained from devolatilization at 1673 K in N_2.

In table 2 the sphericity found for char particles belonging to different morphological categories varies between the authors. Figure 3 show SEM images of sieved coal and char formed at three different devolatilization temperatures. From the figure it can be seen that swelling is taking place at all three devolatilization temperatures thereby producing oval chars with a smooth surface whereas the raw coal particles are clearly fragments created mechanically from the milling of larger lumps.

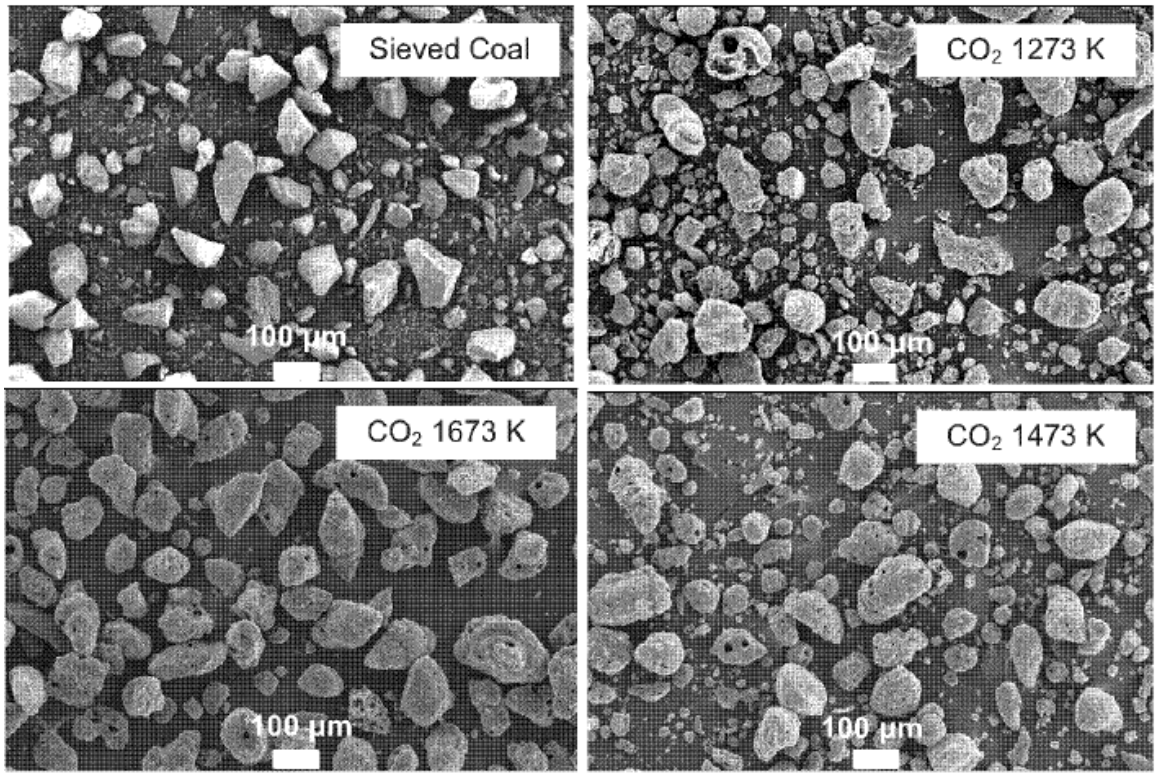

Figure 3 SEM images of sieved coal and chars obtained by devolatilization in CO_2 at 1273 K, 1473 K and 1673 K.

The structural changes taking place during the transformation from coal to char in figure 3 is due to the metaplast formed during devolatilization that allows rounder more spherical particles to evolve from the high internal particle pressures caused by the release and entrapment of volatiles [14,33]. Markings from the release of volatile bubbles can be seen on the surfaces of the chars in figure 2 and figure 3 where it has resulted in the formation of craters. Figure 3 also shows that even though the particles were sieved prior to experiments there still seems to be a fraction of small particles. This fraction seems to increase when devolatilization is carried out at 1273 K but its presence then appears to decrease as the devolatilization temperature increases. This is an indication of a decreased particle fragmentation rate compared to small particle conversion rate as the temperature goes up. Fragmentation of the sampled particles during SEM preparation and storage can however not be ruled out as a source of uncertainty and swelling may also play a role. Even if a slight consumption of fines, due to the presence of O_2 in the devolatilization experiments, has been taking place it will not affect the volatile weight losses significantly as the fines only makes up a few percent of the total mass. Regarding

the shape of the particles after devolatilization, figure 3 suggests that sphericities are varying though with a tendency that supports the higher values of table 2.

Based on the discussion above the chars in this study will be assumed perfect spheres falling into the three morphologies: cenospheric chars, network chars and dense chars as presented schematically in figure 4.

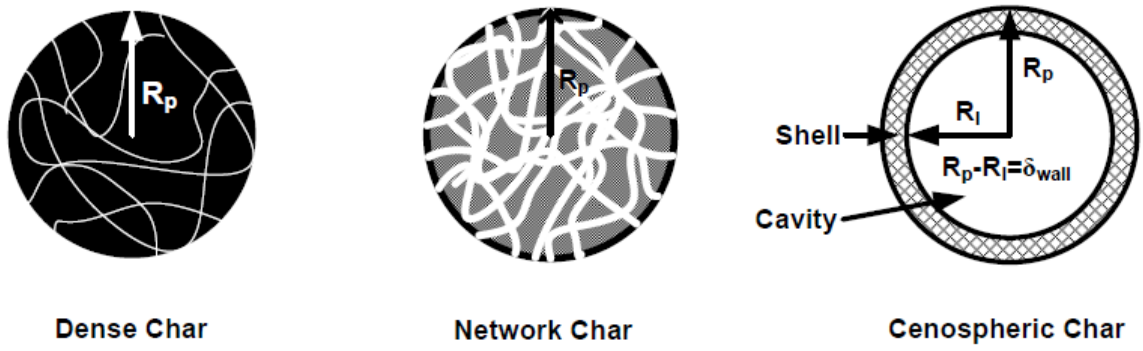

Figure 4 Schematics of char morphologies used to derive particle mass balances.

In [15] a correlation describing the char swelling ratio as a function of temperature was presented from PSD's of the char samples shown in figure 3. From these PSD's temperature dependent weight percents of six discrete particle sizes: 11.5 μm, 44.3 μm, 73.7 μm, 104.5 μm, 140 μm, 190.1 μm have been described by (1), which is valid in the temperature interval 1173 K – 1673 K. The temperature is that of the gas.

$$W\left(R_{p0,k}\right) = a_k \cdot T^2 + b_k \cdot T + c_k \tag{1}$$

Constants used in (1) for the six particle sizes are presented in table 3. The behavior of each particle size reflects the overall swelling described in [15]. The two smallest sizes decrease as the reactor temperature is increased whereas the remaining four particle sizes increase.

Table 3 Constants used in (1).

Particle Size/Constant	**a [K^{-2}]**	**b [K^{-1}]**	**c**
$W(11.5\,\mu m)$	$-6.25\cdot10^{-6}$	$3.1625\cdot10^{-3}$	13.902444
$W(44.3\,\mu m)$	$2.625\cdot10^{-5}$	$-1.095825\cdot10^{-1}$	114.05964
$W(73.7\,\mu m)$	$2.125\cdot10^{-5}$	$-7.38525\cdot10^{-2}$	86.277991
$W(104.5\,\mu m)$	$3.625\cdot10^{-5}$	$-8.35425\cdot10^{-2}$	70.905426
$W(140\,\mu m)$	$-1.25\cdot10^{-5}$	$6.2325\cdot10^{-2}$	-41.683113
$W(190.1\,\mu m)$	$-6.5\cdot10^{-5}$	$2.0149\cdot10^{-1}$	-143.46238

3.2 Model Equations and Solution Procedure

A COal COmbustion MOdel, COCOMO, has been implemented as a FORTRAN 77 code that calls on the CHEMKIN II [32] subroutine library for calculations of species enthalpies and stoichiometric coefficients in homogenous reactions, homogeneous reaction rates and bulk gas heat capacities used in the gas phase energy balance. The homogenous reaction mechanism encompasses 185 chemical species and 1173 reactions [34] although in the present simulations only CO oxidation to CO_2 is relevant. The heterogeneous reactions taking place in COCOMO are R 1 and R 2. The stoichiometric coefficients of R 1 are: $\Lambda_{1,k,l} = a/z_{k,l} + b/4 + d/2 - y/2 + e$, $\Lambda_{2,k,l} = \left(2/z_{k,l} - 1\right)a$, $\Lambda_{3,k,l} = 2\left(1 - 1/z_{k,l}\right)a$, $\Lambda_4 = b/2$, $\Lambda_5 = e$, $\Lambda_6 = d$, $\Lambda_7 = u$. The fuel to oxidizer ratio, accounting for the production of CO_2 relative to CO, is found as suggested by Norman *et al.* [35]: $z_{k,l} = \left(5000\cdot\exp\left(-6249/T_{p,k,l}\right) + 2\right)/\left(2500\cdot\exp\left(-6249/T_{p,k,l}\right) + 2\right)$. The stoichiometric coefficients of R 2 are: $\Lambda_8 = a - y$, $\Lambda_9 = 2a - y$, $\Lambda_{10} = b/2 - e$, $\Lambda_{11} = e$, $\Lambda_{12} = d/2$.

$$C_aH_bO_yN_dS_eA_u + \Lambda_{1,k,l}O_2 \rightarrow \Lambda_{2,k,l}CO_2 + \Lambda_{3,k,l}CO + \Lambda_4H_2O + \Lambda_5SO_2 + \Lambda_6NO + \Lambda_7A \quad \text{R 1}$$

$$C_aH_bO_yN_dS_eA_u + \Lambda_8CO_2 \rightarrow \Lambda_9CO + \Lambda_{10}H_2 + \Lambda_{11}H_2S + \Lambda_{12}N_2 + \Lambda_7A \quad \text{R 2}$$

In the present investigation the char is assumed only to consist of carbon and ash, specified as silicon dioxide. The possibility to include H, O, N and S in the char is included to increase the applicability of COCOMO in future investigations of NO_x and SO_x emissions.

In sections 3.2.1, 3.2.2 and 3.2.3 only the mass- and energy balances of COCOMO are presented. Auxiliary equations are found in Appendix A and a derivation of the mass balances is given in Appendix B.

3.2.1 Solid Mass Balances

There exist different classical approaches when heterogeneous gas-solid reactions are to be described mathematically [36-42]. The Grain Model (GRM), developed by Szekely and coworkers [39-41], considers the particles to be made from numerous small grains. Yagi & Kunii [42] presented the Unreacted Shrinking Core Model (USCM) where the gas-solid reaction is considered to take place on a well defined front between an ash layer and a solid core. Wen [36] also treated the USCM and discussed cases where the front between the ash layer and the core was not well defined or where reaction occurred homogeneously throughout the solid phase. Both the approaches of Wen [36] and Szekely and coworkers [39-41] are termed as Progressive or Volumetric Reaction Models (PRM's, VRM's). The surface area available for reaction in VRM's is also subject to modeling efforts though it is given by the grain packing in the GRM. An often used description of surface area development, especially when dealing with gasification, is the Random Pore Model (RPM) developed by Bhatia and Perlmutter [37,38]. This model takes pore expansion and fusion during reaction into account through the inclusion of a characteristic pore structural parameter and a logarithmic dependence on solid conversion. In processes where pore structural variation does not play an important role during reaction the char surface area is normally considered proportional to the mass of solid.

From TGA experiments [23] it was found that the conversion rates of char sampled in the EFR at all experimental temperatures are adequately described by a VRM. In the present model the char burning rate is modeled as taking place on both the particles interior and exterior surface while char consumption is modeled as a shrinking spherical particle

where the ash formed during reaction breaks of. The burning rate expression is therefore similar to that used for a porous catalyst while the accompanying char consumption takes place by radial shrinkage of the particle with no formation of an ash layer. This entails shrinking particles of constant particle density which ease calculations considerably. In the derivation of the particle mass balances both internal and external surface area is included, which yields a conversion rate for a cenospheric char described for each gaseous reactant by (2) and for all gaseous reactants by (3). The conversion rates for network and dense chars are described by the same equations when $\delta_0 = 1$. The first term in (2) describes the reaction rate in the interior of the particle while the second term accounts for the reaction rate at its exterior surface.

$$\frac{dX_{k,l,r}}{dL} = \frac{k_{k,l,r} \cdot \left(C_r^S\right)_{k,l}^{n_r}}{\nu_{s,k,l} + \nu_g} \cdot \left(S_0 \cdot \left(1 - X_{k,l}\right) \cdot \eta_{k,l,r} + \frac{3 \cdot \left(1 - X_k \cdot \left(1 - \left(1 - \delta_0\right)^3\right)\right)^{\left(\frac{2}{3}\right)}}{\rho_p \cdot R_{p0,k} \cdot \left(1 - \left(1 - \delta_0\right)^3\right)} \right) \tag{2}$$

$$\frac{dX_{k,l}}{dL} = \sum_r \frac{dX_{k,l,r}}{dL} \tag{3}$$

The effectiveness factor, $\eta_{k,l,r}$, is included in (2) to account for internal mass transfer resistance in the char particles. When mass transfer limitations cause internal concentration gradients of reactants to form inside the particles the effectiveness factor will gradually decrease from one to account for the internal surface area not accessible for reaction. In (2) the surface concentrations of the reactants are found from mass balances across the laminar gas film layer surrounding the particles as shown in (4).

$$k_{c,k,l,r} \cdot A_{p,k,l} \cdot \left(C_r^B - \left(C_r^S\right)_{k,l}\right) = \frac{\Lambda_{k,l,r} \cdot m_{p0,k,l}}{M_p} \cdot \frac{dX_{k,l,r}}{dL} \cdot \left(\nu_{s,k,l} + \nu_g\right) \tag{4}$$

The solution of (3) yields the conversion of a particle size belonging to one of the three morphologies. To calculate the total conversion of a morphological group or of all char (5) and (6) are used.

$$X_l = 1 - \sum_k \left(1 - X_{k,l}\right) \cdot \Theta_k \tag{5}$$

$$X_T = 1 - \sum_l \left(1 - X_l\right) \cdot \alpha_l \tag{6}$$

3.2.2 Solid Energy Balance

The energy balance for a burning char particle is given by (7). The energy balance takes into account convective heat transfer between the gas and particle, radiation between the particle and reactor wall and the heat generated by the oxidation and gasification of the particle. These are the general terms included in modeling studies [3,6,8,10,18].

$$\frac{dT_{p,k,l}}{dL} = \frac{-m_{p0,k,l} \cdot \left(\nu_{s,k,l} + \nu_g\right) \cdot \sum_r \frac{dX_{k,l,r}}{dL} \cdot \Delta H_{k,l,r} + A_{p,k,l} \cdot \left(h_{p,k,l} \cdot \left(T_g - T_{p,k,l}\right) + \bar{e} \cdot \sigma_{SB} \cdot \left(T_w^4 - T_{p,k,l}^4\right)\right)}{\left(\nu_{s,k,l} + \nu_g\right) \cdot m_{p,k,l} \cdot C_{p,k,l}} \tag{7}$$

The particle energy balance in (7) does not include radiation between particles of different sizes and morphologies due to the low coal feed rate used during the experiments.

3.2.3 Gas Phase Mass and Energy Balances

To account for changes in the gas temperature the energy balance in (8) is set up. This energy balance includes the heat generated by homogeneous reactions along with convective heat transfer with the particles and reactor wall. The mass balance in (9) accounts for both heterogeneous and homogeneous contributions.

$$\frac{dT_g}{dL} = A_R \cdot \left(\frac{\sum_{i=1}^{N_H} r_i \cdot \left(-\Delta H_i\right) + a_w \cdot h_w \cdot \left(T_w - T_g\right) + \sum_l \sum_k Q_{k,l}}{\sum_{j=1}^{N_G} F_j \cdot C_{p,j}} \right) \tag{8}$$

$$\frac{dF_j}{dL} = A_R \cdot \left(\sum_{i=1}^{N_H} \zeta_{j,i} \cdot r_i + \sum_r \sum_l \sum_k N_{k,l} \cdot \zeta_{j,k,l,r} \cdot r_{k,l,r} \right) \tag{9}$$

Even though the experiments presented in this study are carried out at conditions where the molar gas flow, its composition and its temperature are nearly constant the gas phase mass- and energy balance in (8) and (9) are included to enhance model accuracy and general applicability. In the present simulations the only significant gas phase reaction is CO oxidation and simulated gas temperatures are less than 30 K higher than the reactor wall at all times. In (8) the convective heat transfer between gas and particles is found as $Q_{k,l} = N_{k,l} \cdot h_{p,k,l} \cdot A_{p,k,l} \cdot \left(T_{p,k,l} - T_g\right)$. The reactor surface area pr. reactor volume, a_w, is found as $4 \cdot D_R^{-1}$.

3.3 Model Input Parameters

The model presented in (2) - (9) requires a range of input parameters, which are given in table 4 for the simulations presented here. Skeletal density, porosity and abundance of morphologies are found for El Cerrejón chars by the respective authors. The density is found by correcting the apparent value taken from Zolin *et al.* [43] with the porosity obtained from Cloke *et al.* [6]. Char porosities and morphology abundances of Cloke *et al.* [6] are found by DTF experiments at 1423 K, which is the average temperature used during the EFR experiments presented here. Cloke *et al.* [6] did not find strong effects of temperature on either porosity or abundance in the interval 1273 K – 1573 K. The values of tortuosity and char emissivity are used in combustion modeling by Charpenay *et al.* [44] and Mon & Amundson [45]. Weight fractions of discrete particle sizes are found from (1) and are assumed the same for all three morphologies.

Table 4 Input parameters used in the simulations.

Parameter	ρ_p [43]	S_0	$\bar{\tau}$ [44]	ε_N [6]	ε_D [6]	δ_0
Value	1453 [kg m^{-3}]	240 [m^2 g^{-1}]	2	38 %	19 %	0.05
Parameter	α_C [6]	α_N [6]	α_D [6]	$\bar{e}$ [44]	d_{pore}	$n_{O_2} = n_{CO_2}$
Value	0.2	0.71	0.09	0.93	1 μm	0.5

The value of the specific surface area is found as an average from N_2-BET measurements on the chars in figure 3, which yielded the specific surface areas: N_2-BET(1273 K) = 243 m^2 g^{-1}, N_2-BET(1473 K) = 200 m^2 g^{-1} and N_2-BET(1673 K) = 280 m^2 g^{-1}. The specific surface area is used for simulations in both N_2 and CO_2 [15].

$$k_{k,l,r} = A_{0,r} \cdot \exp\left(\frac{E_{D,r}}{R \cdot T_{p,d,k,l}}\right) \cdot \exp\left(\frac{-E_{A,r}}{R \cdot T_{p,k,l}}\right) \tag{10}$$

The rate constants used in (2) are found from the extended Arrhenius expression in (10) [23]. The expression includes a pre-exponential factor, $A_{0,r}$, which has a value of 1.4359 kg m^{-2} s^{-1} (mol m^{-3})$^{-0.5}$ when used for O_2 and a value of 7.3282 kg m^{-2} s^{-1} (mol m^{-3})$^{-0.5}$ when used for CO_2. The deactivation energy, $E_{D,r}$, is 20.5 kJ mol^{-1} for O_2 and 0 kJ mol^{-1} for CO_2 and an activation energy of 137.5 kJ mol^{-1} and 230.8 kJ mol^{-1} is used for O_2 and CO_2 respectively. It should be noted that a deactivation energy of 0 kJ mol^{-1} for CO_2 means that the gasification rate is not affected by thermal char deactivation though this is the case for the combustion rate. While this may strike as odd the kinetic data is a result of detailed data treatment on TGA reactivity profiles obtained with authentic EFR chars [23]. The deactivation temperature, $T_{p,d,k,l}$, is the highest temperature a particle has experienced at a given position in the reactor and is used assuming that the level of deactivation quickly adjusts to the experienced temperatures.

4. Comparison between Model and Experiments

Comparison between COCOMO and experimental profiles can be seen in figure 5 - figure 10 where data are collected for each experimental temperature. Simulated profiles found for O_2/CO_2 combustion are shown both with and without the contribution from CO_2 gasification in figure 9 and figure 10. It is only at these high temperature conditions that a detectable contribution from CO_2 gasification to overall char conversion is seen. In the remaining figures throughout the text CO_2 gasification is included in the simulations though it does not influence char conversion. In the following the ability of the model to predict the experimental data will be commented. The discussion of figure 5 and figure 6 will however be postponed as it prepares the ground for the detailed discussion of the data that will follow later in the text.

Figure 7 - figure 10 show in general a reasonable agreement between simulations and experimental data at all O_2 concentrations in both N_2 and CO_2. A tendency of under prediction by the model in figure 7 and figure 8 and a slight over prediction in figure 9 and figure 10 can however be seen, which are most likely caused by small variations in the abundance of morphologies and physical properties such as size and porosity. Figure 8 also shows the conversion profiles for each of the morphologies making up the total conversion profile. It can be seen from figure 8 that the presence of cenospheres, that predominantly burn in zone I, is very important for the steepness of the profile wherefore an increased cenosphere formation or an increase in porosity will increase the initial char conversion rate. Besides morphology, variations in particle size are also influencing the conversion rate. Figure 11 show conversion profiles and effectiveness factors for network chars of three different sizes belonging to the overall network conversion profile in figure 8. From figure 11 it is seen that the smallest particle size is rapidly converted in zone I. For a medium sized particle conversion is slower and takes place from near zone III to zone I throughout its consumption. The largest particle size present in the simulation is burning under almost complete external mass transfer control during the entire process. The strong influence of internal and external mass transfer control for the medium to large particles means that a faster overall char conversion would be achieved if a larger fraction of small particles is present, e.g. as a result of fragmentation.

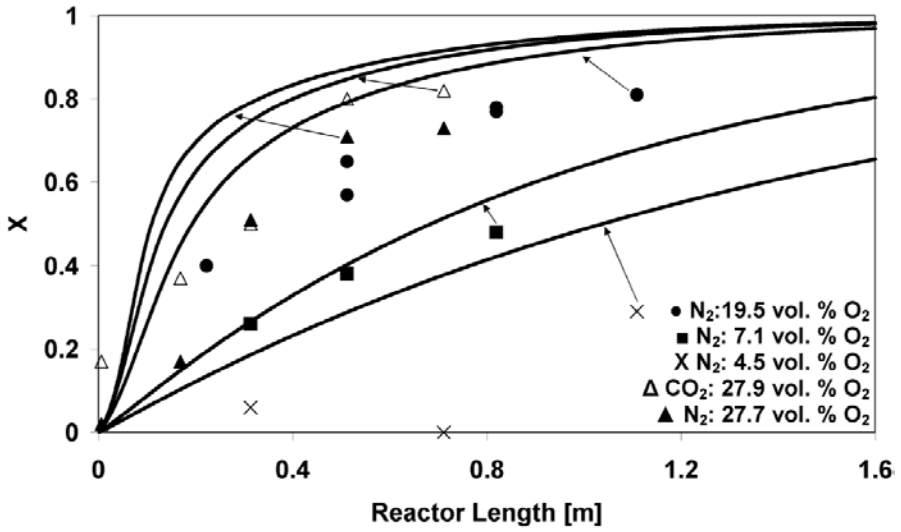

Figure 5 COCOMO profiles and experimental profiles obtained at 1173 K in N_2 and CO_2. The O_2 concentrations are the averages of the local concentrations at each sampling position. $\lambda \sim 2.7 - 15.2$.

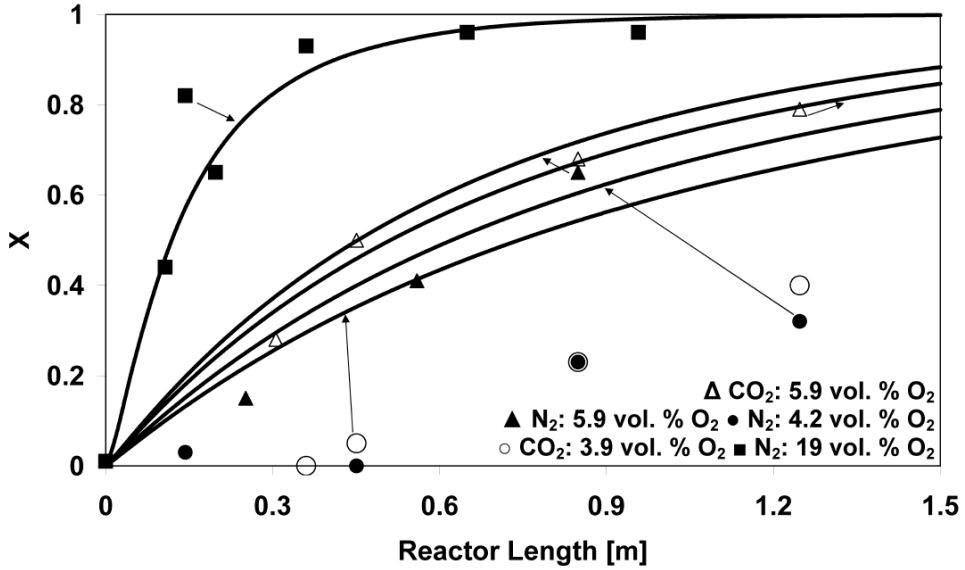

Figure 6 COCOMO profiles and experimental profiles obtained at 1273 K in N_2 and CO_2. The O_2 concentrations are the averages of the local concentrations at each sampling position. $\lambda \sim 2.5 - 10.5$.

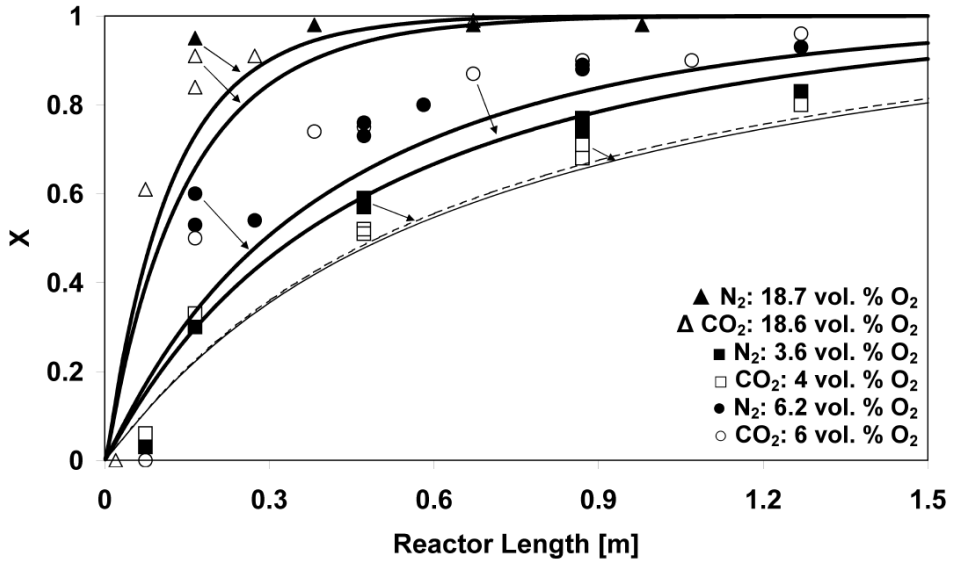

Figure 7 COCOMO profiles and experimental profiles obtained at 1373 K in N_2 and CO_2. The O_2 concentrations are the averages of the local concentrations at each sampling position. $\lambda \sim 2.3 - 9.8$.

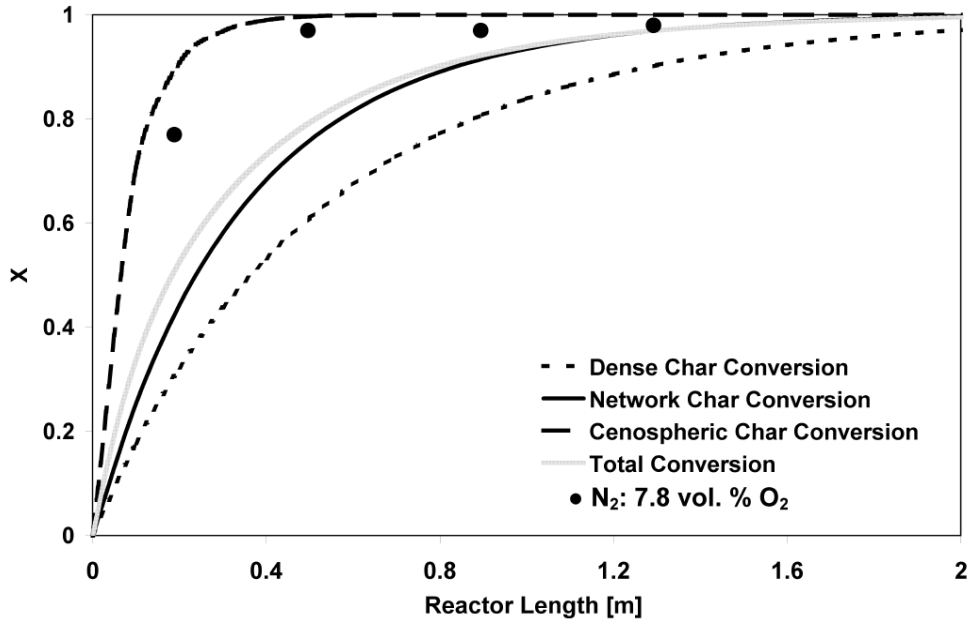

Figure 8 COCOMO profile and experimental profile obtained at 1473 K in N_2. The O_2 concentration is the average of the local concentrations at each sampling position. $\lambda \sim 3.7$. Also shown are COCOMO conversion profiles of each of the three morphologies.

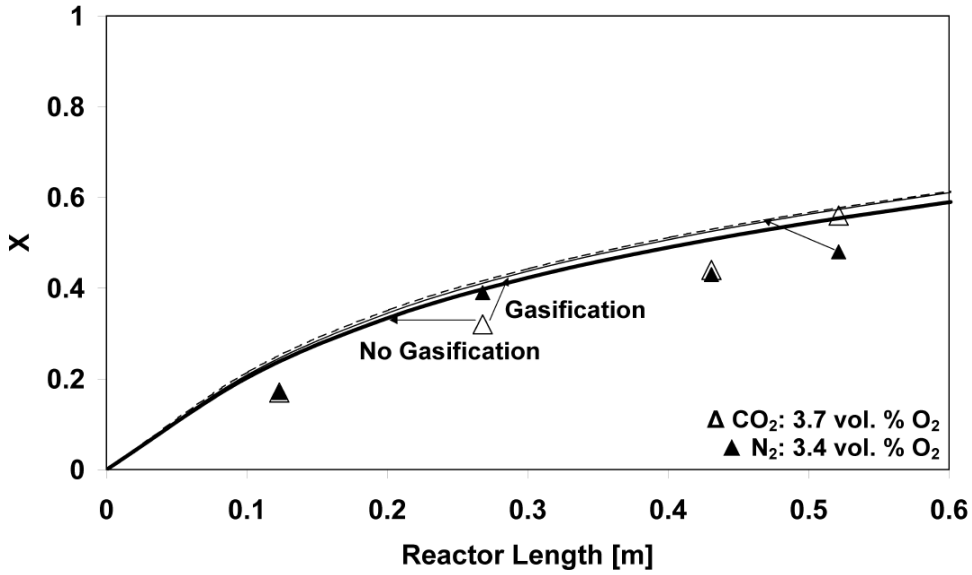

Figure 9 COCOMO profiles and experimental profiles obtained at 1573 K in N_2 and CO_2. The thin dashed line is the simulation in O_2/N_2 and the thin unbroken line is the simulation in O_2/CO_2 with gasification included. The O_2 concentrations are the averages of the local concentrations at each sampling position. $\lambda \sim 2$.

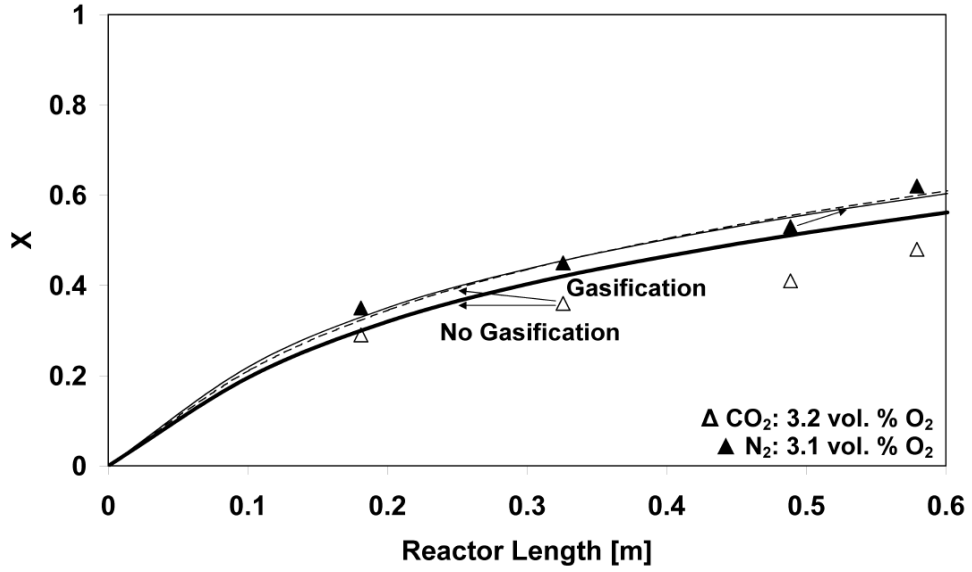

Figure 10 COCOMO profiles and experimental profiles obtained at 1673 K in N_2 and CO_2. The thin dashed line is the simulation in O_2/CO_2 with gasification included and the thin unbroken line is the simulation in O_2/N_2. The O_2 concentrations are the averages of the local concentrations at each sampling position. $\lambda \sim 1.9$.

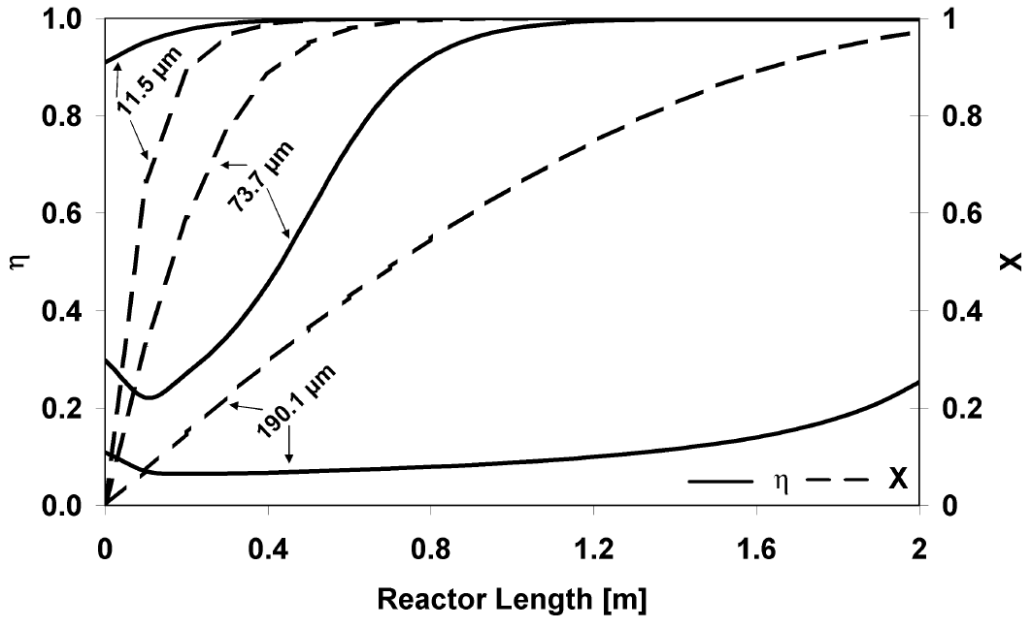

Figure 11 COCOMO conversion profiles and effectiveness factors for network particles at 1473 K and 7.8 vol. O_2 in N_2. The O_2 concentration is the average of the local concentrations at each sampling position. $\lambda \sim 3.7$.

In figure 9 and figure 10 COCOMO predicts an observable influence of CO_2 gasification on char conversion. In figure 9 this influence does not markedly change the conversion rate in O_2/CO_2, which is close to that in O_2/N_2, and in reasonable agreement with experimental data. In figure 10 the effect is more pronounced and does not tally with the experimental profiles. According to the experimental profiles in figure 10 the conversion rate in O_2/N_2 is significantly higher than in O_2/CO_2, suggesting an effect of O_2 diffusivity, which is approximately 22 % lower in CO_2 at these conditions. The simulated profiles show however that the conversion rates in O_2/N_2 and O_2/CO_2 are similar and that the conversion rate in O_2/CO_2 outpaces that in O_2/N_2 at conversions higher than approximately 50 %. The reason for the inconsistency between model and experiments can be found as a continuation of the discussion of figure 8 and figure 11 that illustrated the importance of variations in PSD and morphology abundances. Figure 12 and figure 13 show the calculated importance of CO_2 gasification for a small (44.3 µ) and large (140 µ) network particle respectively. In both figures a decrease in bulk O_2 concentration from 8 vol. % to vol. 4 % cause a more significant contribution from CO_2 gasification as

expected. Furthermore, as the particle temperature goes up CO_2 gasification becomes increasingly important. The reason for this behavior can be deduced from the internal effectiveness factors of O_2. At the higher temperatures the reaction with O_2 approaches zone III wherefore only moderate increases in consumption rate are gained as the temperature continues to increase. At these temperatures CO_2 gasification is taking place in zone I or zone II resulting in a fast increase in consumption rate as the temperature increase.

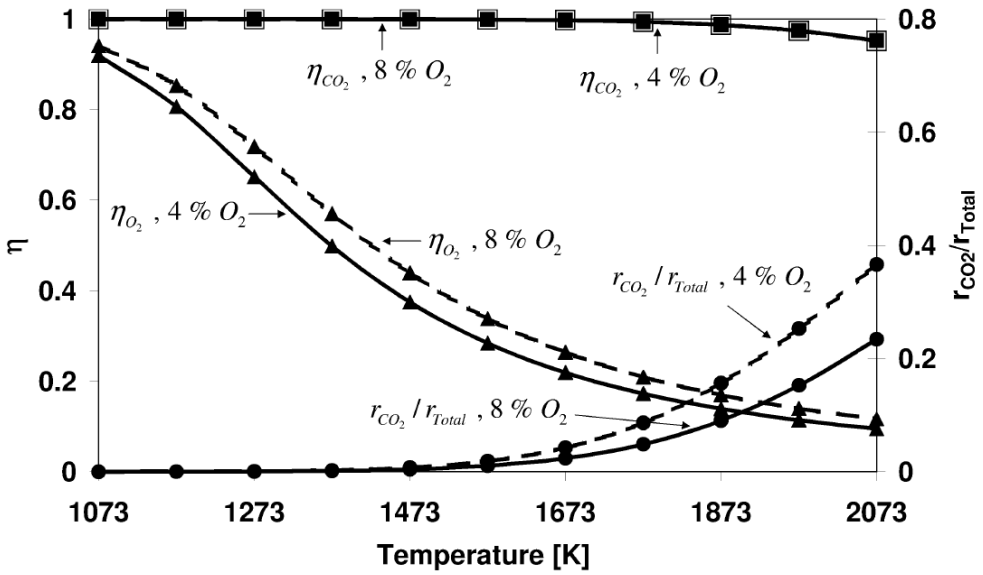

Figure 12 CO_2 gasification rate relative to overall char conversion rate and internal particle effectiveness factors at 4 and 8 vol. % O_2 and different particle temperatures. Network char, $T_g = T_p$, $\lambda = 1.05$, $d_p = 44.3$ μm, $\nu_s = 0$.

The crucial importance of O_2 combustion zone and zone III conversion rate (particle size and bulk O_2 concentration) illustrated in figure 12 and figure 13 means that even small variations in PSD, char porosity and abundance of morphologies between simulations and experiments can cause inconsistencies in overall char conversion rate as found in figure 10. Figure 9, figure 10, figure 12 and figure 13 do however show that CO_2 gasification can play a role when combustion is taking place in zone III.

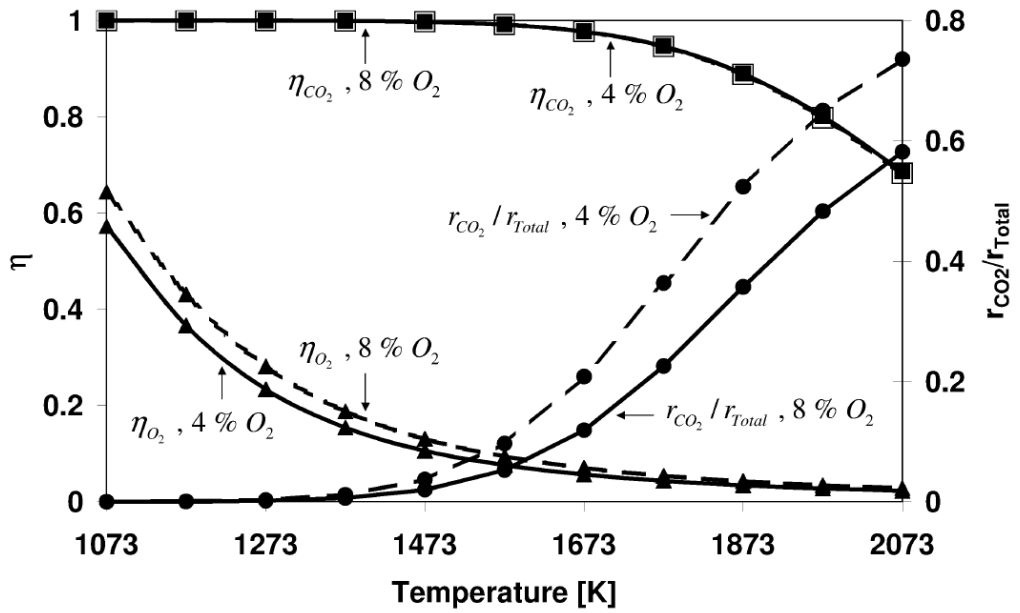

Figure 13 CO_2 gasification rate relative to overall char conversion rate and internal particle effectiveness factors at 4 and 8 vol. % O_2 and different particle temperatures. Network char, $T_g = T_p$, $\lambda = 1.05$, $d_p = 140$ μm, $\nu_s = 0$.

The discussion of the importance of CO_2 gasification, as indicated by the model, is however with the specific kinetic parameters used in the simulations [23]. These are based on TGA experiments at much lower temperatures causing significant extrapolation of the kinetics to the conditions used in the simulations. Though qualitatively unambiguous it must therefore be said that changes in kinetic rates can change the quantitative importance of CO_2 gasification at the conditions used in the preceding figures.

The differences between model predictions and experimental results in figure 5 and figure 6 are most significant for the lowest and highest O_2 concentrations. For a concentration of 4.5 vol. % O_2 in N_2 in figure 5 and for concentrations of 4.2 vol. % O_2 and 3.9 vol. % O_2 in N_2 and CO_2 in figure 6 the reaction appears delayed compared to the remaining experimental profiles. All three profiles were obtained at conditions similar to those used for the devolatilization experiments where an O_2 concentration of approximately 5 vol. % was used in order to overcome problems with tar clogging the sampling probe and reactor ventilation system. During sampling of devolatilized char it was reassured that no significant heterogeneous conversion took place that could result in

misleading values of volatile weight loss. This was done by sampling at reactor positions downstream of the actual sampling point and comparing char ash contents. From this it was found that no significant heterogeneous conversion took place, which indicates a delay between the end of devolatilization and onset of heterogeneous ignition under these conditions. This is not captured by the model in figure 5 and figure 6 wherefore a significant absolute error exists between model and experiments though the slope of the experimental conversion profiles are predicted quite accurately once reaction begins.

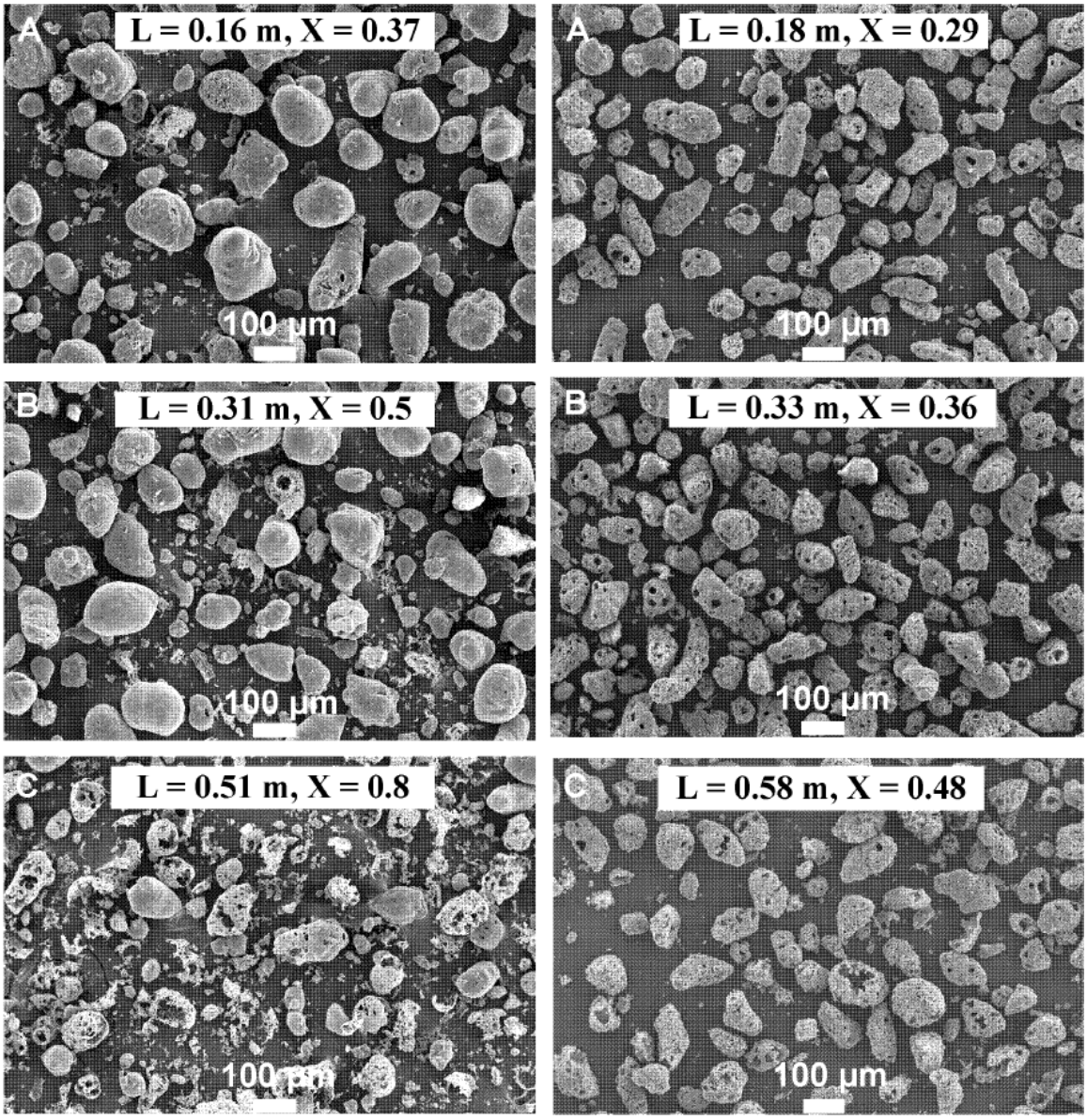

Figure 14 SEM images at three different degrees of conversion in CO_2. Left: T = 1173 K, 27.9 vol. % O_2. $\lambda \sim 15.2$. Right: T = 1673 K, 3.2 vol. % O_2. $\lambda \sim 1.9$.

In figure 5 the model over predicts the conversion rate at high O_2 concentrations though it captures the abrupt char deactivation that takes place at 70 – 80 % conversion. In figure 14 SEM images of char sampled at three different degrees of conversion at 1173 K and 27.9 vol. % O_2 (left panel) and 1673 K and 3.2 vol. % O_2 in CO_2 (right panel) shows that a fraction of non-reactive chars remain at 1173 K even at high overall degrees of conversion.

The behavior observed in figure 14 can be discussed on the basis of simulations. The deactivated particles of figure 14 are quite large and they appear to be present throughout the process. Figure 15 - figure 17 show the particle temperature profiles at 1173 K and 27.9 vol. % O_2 in CO_2 for cenospheres, network chars and dense chars respectively. From these figures it is seen that very high particle temperatures (1700 K – 1800 K) are reached shortly after ignition for 190.1 μm cenospheres, 73.7 μm, 104.5 μm, 140 μm and 190.1 μm network chars and 104.5 μm, 140 μm and 190.1 μm dense chars. These high temperatures will result in a second devolatilization and a distinct deactivation. For 190.1 μm cenospheres and 73.7 μm network chars, heating rates of approximately 20000 K s^{-1} and 12000 K s^{-1} are reached, which will facilitate an intense second devolatilization.

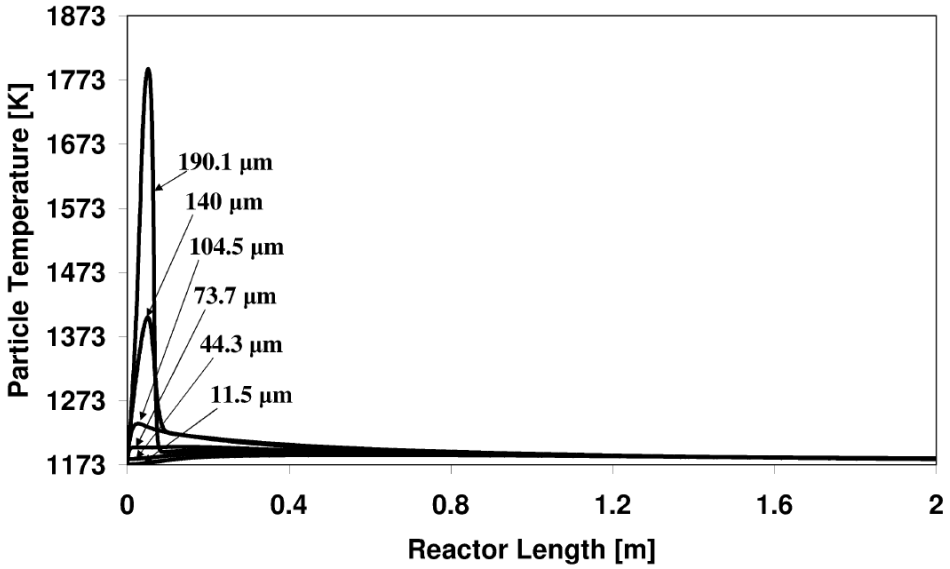

Figure 15 COCOMO temperature profiles for cenospheric char at 1173 K and 27.9 vol. % O_2 in CO_2. The O_2 concentration is the average of the local concentrations at each sampling position. $\lambda \sim 15.2$.

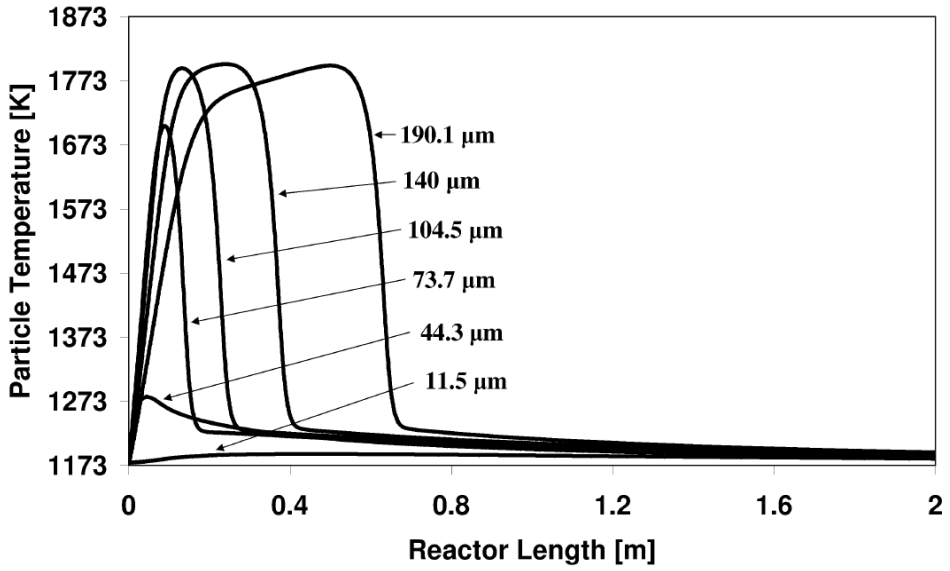

Figure 16 COCOMO temperature profiles for network char at 1173 K and 27.9 vol. % O_2 in CO_2. The O_2 concentration is the average of the local concentrations at each sampling position. $\lambda \sim 15.2$.

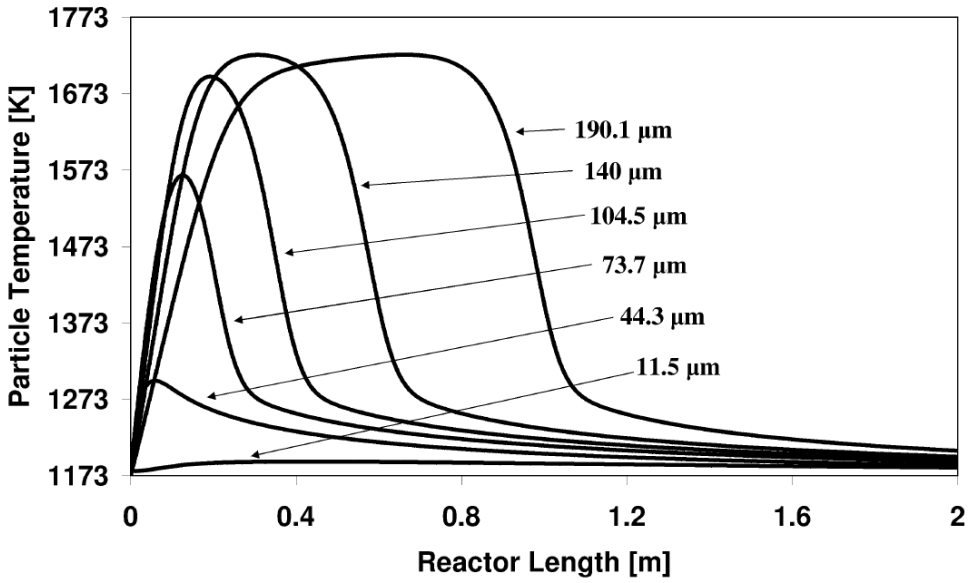

Figure 17 COCOMO temperature profiles for dense char at 1173 K and 27.9 vol. % O_2 in CO_2. The O_2 concentration is the average of the local concentrations at each sampling position. $\lambda \sim 15.2$.

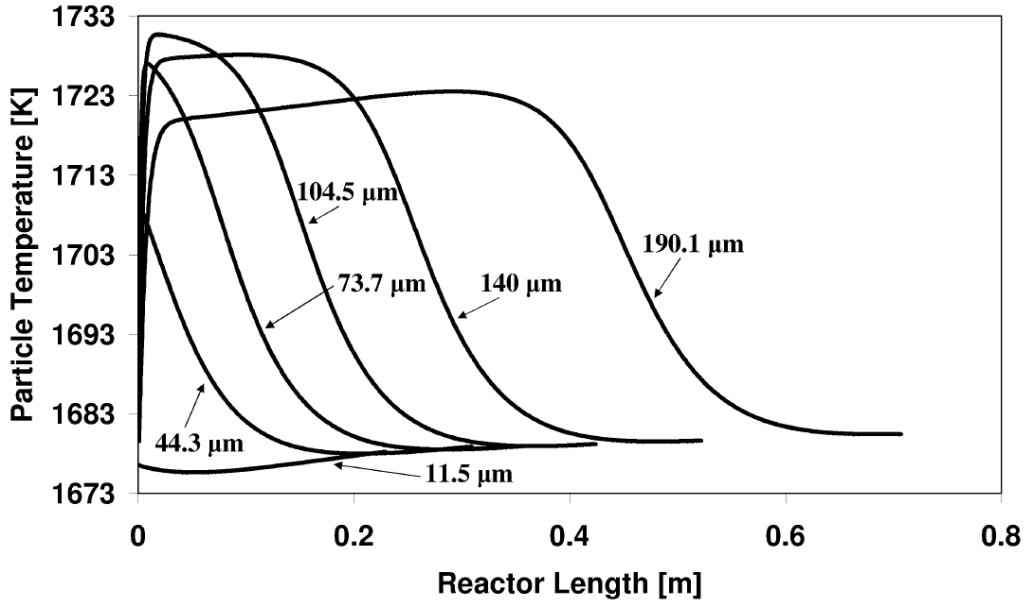

Figure 18 COCOMO temperature profiles for cenospheric char at 1673 K and 3.2 vol. % O_2 in CO_2. The O_2 concentration is the average of the local concentrations at each sampling position. $\lambda \sim 1.9$.

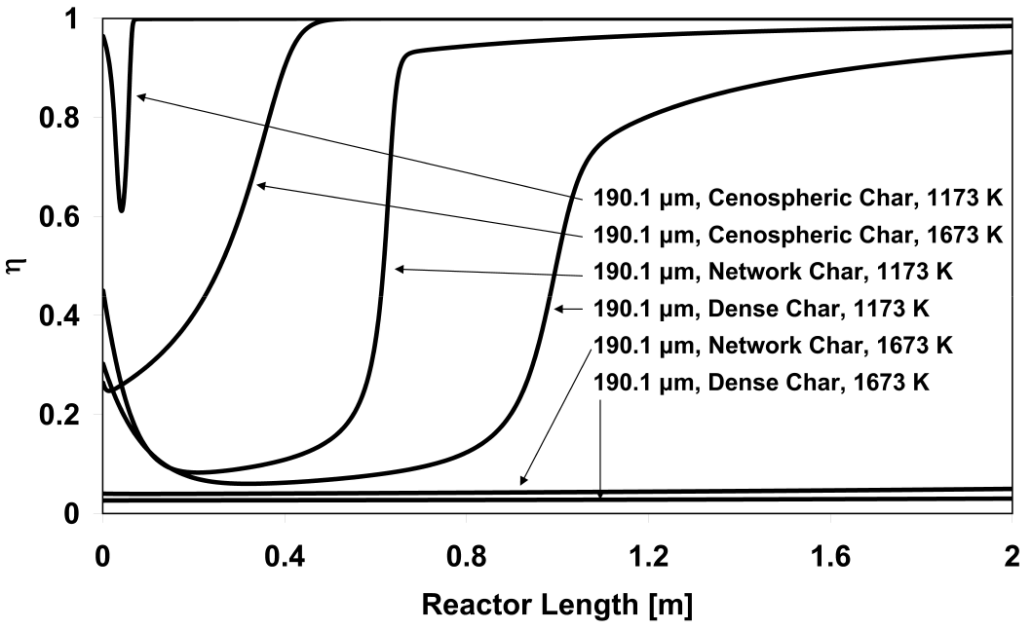

Figure 19 COCOMO effectiveness factor profiles at 1173 K, 27.9 vol. % O_2 in CO_2 and $\lambda \sim 15.2$ and at 1673 K, 3.2 vol. % O_2 in CO_2 with $\lambda \sim 1.9$ for 190.1 µm particles. The O_2 concentration is the average of the local concentrations at each sampling position.

Zhang *et al.* [46] found that when the three factors: high mineral content, high volatile content and high heating rate was met combustion was inhibited by the formation of an inactive mineral cluster phase. Zhang *et al.* [46] suggested that this phase is formed when liquid/volatile organic fractions are absorbed on the minerals thereby significantly reducing the void fraction in the particle, increasing the order in its structure and hence lowering its reactivity. The phase showed up as a second peak on TGA reactivity profiles in the work of Zhang *et al.* [46]. TGA measurements on the char sampled at 1173 K and 27.9 vol. % O_2 in CO_2 indeed also showed two distinct peaks in the reactivity profile [23] indicating that a separate highly inactive phase is present. This is not accounted for in COCOMO where char deactivates homogeneously and it therefore causes over predictions by the model when high particle temperatures are reached at high heating rates. The strong effect of particle temperature history on char conversion is made clear in figure 14 where SEM images of char conversions at 1173 K in 27.9 vol. % O_2 and at 1673 K and 3.2 vol. % O_2 in CO_2 are compared. Where the particles at 1173 K undergo substantial morphological changes due to the intense ignition, the particles at 1673 K seem to burn uniformly throughout the process. This is due to uniform particle temperatures illustrated for cenospheres in figure 18 where it is seen that the highest temperature difference between gas and particle is reached by 104.5 μm particles and is less than 60 K. This is the highest temperature difference between gas and particle for any particle size and morphology at 1673 K and 3.2 vol. % O_2 in CO_2. The cause of the differences in temperature histories of especially the larger particles between the two experiments are illustrated by the internal effectiveness factors in figure 19. In figure 19 it is seen that at a reactor temperature of 1173 K the combustion process starts in zone II for network and dense chars and in zone I for cenospheres. Since the devolatilization has taken place at 1173 K thermal deactivation of the particles have only been moderate at the onset of ignition and the high O_2 concentration enables efficient mass transfer across the gas film layer. This allows the particles to reach high peak temperatures before a combination of thermal char deactivation and external mass transfer limitations slows down the reaction rate. Figure 19 also shows that when ignition takes place at 1673 K cenospheres burn in zone II and dense and network chars burns in zone III where the low O_2 concentration hinders effective mass transfer across the gas film layer. Furthermore

figure 13 shows a more pronounced effect of CO_2 gasification at 1673 K and low O_2 concentration, which also drives down the particle temperatures. It is however not the main reason for the uniform temperature profiles in figure 18.

Figure 20 compares the collected experimental data points from figure 5 - figure 10 with model predictions, in total 108 data points. The data in figure 20 covers both combustion in zone I, zone II and zone III.

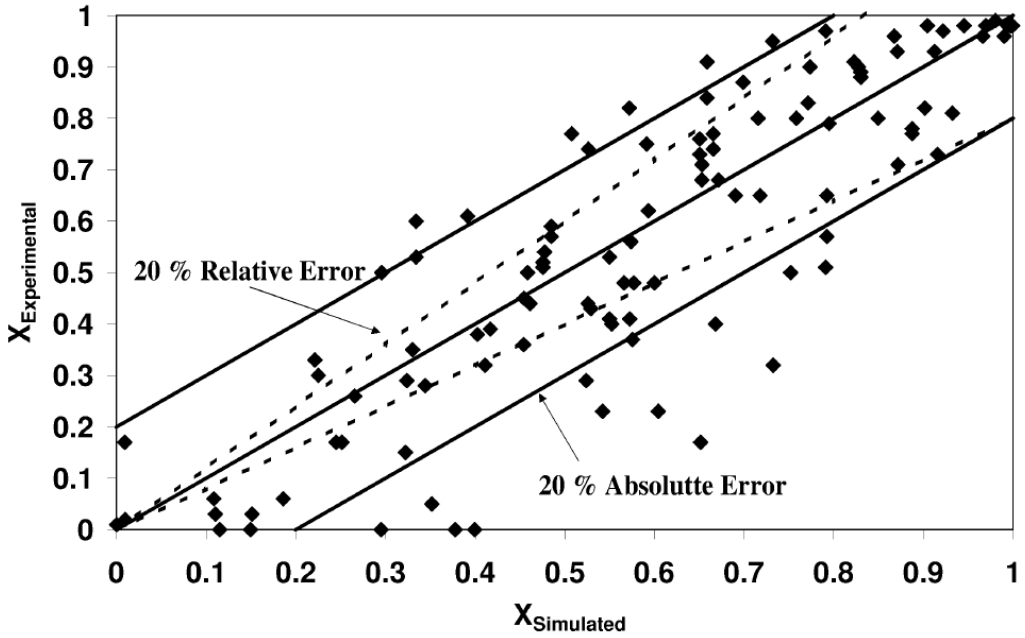

Figure 20 Comparison between COCOMO and experimental data.

It can be seen from figure 20 that the largest deviations between model and experiments come from over predictions by the model at experimental conversions below 40 %. The reasons for these deviations were discussed above in connection with the profiles of figure 5 and figure 6. Besides these data points figure 20 shows a reasonable consistency between model and experiments both in the dynamic part of the combustion at low char conversion and in the final burnout phase at high char conversion where much of the char is significantly deactivated.

5. Conclusions

A combustion model encompassing dense, network and cenospheric char each distributed between six discrete particle sizes have been compared to experimental char conversion profiles obtained in O_2/CO_2 and O_2/N_2 mixtures under suspension fired conditions. The model applies kinetic parameters for char oxidation and CO_2 gasification obtained from TGA experiments with char formed at the experimental temperatures under suspension fired conditions. The expressions for the rate constants include the effect of thermal char deactivation only for the reaction with O_2, since no deactivation was observed with CO_2. The kinetic expression for O_2 combustion has proven to work satisfactorily under a wide range of suspension fired conditions while that for CO_2 gasification show a slight over prediction at high temperatures.

In the temperature interval 1173 K – 1673 K reasonable consistency was found between experiments and simulations at inlet O_2 concentrations between 5 and 28 vol. %. At high O_2 concentrations and low reactor temperatures simulations showed that the larger particles of all three morphologies reached high over temperatures of up to 500 – 600 K shortly after ignition causing additional heating with rates as high as 20000 K/s for 190.1 μm cenospheres. SEM images of partly combusted char, sampled at these conditions showed large unreacted particles even at high overall degrees of conversion. It is suggested that these particles are formed during the intense heating from interactions between products of a secondary devolatilization and particle mineral matter though it is also possible that mineral matter itself affects char reactivity by ash layer inhibition. Due to the fraction of highly deactivated particles significant absolute deviation exists between model and experiment at low reactor temperature and high O_2 concentration as thermal char deactivation is modeled as homogeneous. When both reactor temperature and O_2 concentrations were low a delay between the end of devolatilization and onset of particle ignition also caused deviations.

From experimental profiles obtained in a range of operating conditions, covering zone I - III, no evidence suggesting an effect of CO_2-gasification on char conversion has been found. In fact the only indication of an effect of CO_2 on char conversion rate is seen in zone III where the lower diffusion coefficient of O_2 in CO_2 appears to slow down the reaction rate compared to O_2/N_2. Modeling does however suggest that CO_2 gasification

can contribute to char consumption when the O_2 concentration is low, the particle temperature high and combustion is taking place in zone III, especially for large particles. It is however questionable whether this effect will be of importance for industrial applications as the combinations of large particles, low O_2 concentrations and high particle temperatures are difficult to find in a specific position of a boiler. For particularly reactive coals, such as lignite coal, the window where CO_2 gasification is important could be wider, also encompassing common industrial conditions but further studies are needed on this topic.

Acknowledgement

The research leading to these results has received funding from the European Community's Research Fund for Coal and Steel (RFCS) under contract n° RFCR-CT-2006-00007, project FRIENDLYCOAL, and is also sponsored by the Danish Agency for Science, Technology and Innovation and from Energinet.dk under project PSO-7171. The support and funding from these entities are greatly valued.

Appendix A: Auxiliary Equations

To simplify the calculations of physical properties of the gas, not carried out by CHEMKIN II [32], it is assumed that only three gaseous species, N_2, O_2 and CO_2, are present in sufficient amounts during the experiments to influence the properties of the gas phase. Where multi component properties, indexed *mix*, are used calculations are based on bulk gas composition.

A.1 Equations Relating to Particle Geometries and Mass

An expression for the development of particle radius for a cenospheric char is given by (A 1) and for dense chars and network chars by (A 2).

$$R_{p,k} = R_{p0,k}\left(1 - X_k \cdot \left(1 - \left(1 - \delta_0\right)^3\right)\right)^{\left(\frac{1}{3}\right)} \tag{A 1}$$

$$R_{p,k,l} = R_{p0,k,l} \cdot \left(1 - X_{k,l}\right)^{\left(\frac{1}{3}\right)} \tag{A 2}$$

Geometric surface areas and volumes of the particles can be calculated immediately from (A 1) and (A 2). When the volume is used to calculate particle mass and effectiveness factor (A 1) can however not be applied directly as it does not take the cavity of a cenosphere into account. The expression for the volume of a cenosphere occupied by a continuous char matrix is given by (A 3).

$$V_{p,m,k} = \frac{4}{3} \cdot \pi \cdot R_{p0,k}^3 \cdot \left(1 - \left(1 - \delta_0\right)^3\right) \cdot \left(1 - X_k\right) \tag{A 3}$$

The apparent densities of the three char morphologies can be found from (A 4) - (A 6) where the skeletal density, ρ_p, is assumed to be the same for all particle sizes and morphologies.

$$\rho_{p,N}^{a} = \left(1-\varepsilon_{N}\right)\cdot\rho_{p} \tag{A 4}$$

$$\rho_{p,C,k}^{a} = \frac{\left(1-\left(1-\delta_{0}\right)^{3}\right)\cdot\left(1-\varepsilon_{N}\right)\cdot\rho_{p}\cdot\left(1-X_{k}\right)}{\left(1-X_{k}\cdot\left(1-\left(1-\delta_{0}\right)^{3}\right)\right)} \tag{A 5}$$

$$\rho_{p,D}^{a} = \left(1-\varepsilon_{D}\right)\cdot\rho_{p} \tag{A 6}$$

When the apparent density of cenospheric char is used to calculate the effectiveness factor and particle mass based on (A 3), (A 4) is applied instead of (A 5) as these calculations are based on particle volume occupied by a continuous matrix.

A.2 Effectiveness Factors and Diffusion Coefficients

Because the char oxidation rate is n'th order in O_2 concentration a generalized Thiele modulus, expressed in (A 7), is used to calculate the effectiveness factors, $\eta_{k,l,r}$ [47]. The volume of the particle and the apparent density refers to the fraction of particle occupied by a continuous matrix.

$$\phi_{k,l,r} = \frac{V_{p,k,l}}{A_{p,k,l}}\cdot\sqrt{\frac{n_{r}+1}{2}\cdot\frac{k_{k,l,r}\cdot\left(C_{r}^{S}\right)_{k,l}^{n_{r}-1}\cdot\rho_{p,k,l}^{a}\cdot S_{0}}{M_{p}\cdot D_{k,l,r}^{*}}} \tag{A 7}$$

The value of the effectiveness factor is found using (A 8), which is an approximation to the classical expression for a sphere [47], for all char morphologies.

$$\eta_{k,l,r} = \frac{1}{\sqrt{1+\phi_{k,l,r}^{2}}} \tag{A 8}$$

The effective diffusion coefficients of O_2 and CO_2 through the pore system of the char matrix, $D^*_{k,l,r}$, are found from (A 9) [47].

$$D^*_{k,l,r} = \frac{\varepsilon_l}{\tau} \cdot \left(\frac{1}{D_{K,k,l,r}} + \frac{1}{D_{mix,k,l,r}} \right)^{-1} \tag{A 9}$$

The Knudsen diffusion coefficient in (A 9) is found from (A 10) [47].

$$D_{K,k,l,r} = \frac{d_{pore}}{3} \cdot \left(\frac{8 \cdot R \cdot T_{p,k,l}}{\pi \cdot M_r} \right)^{0.5} \tag{A 10}$$

The molar diffusion coefficient of the reactant is calculated from (A 11) [47]. This equation is a simplification of Stefan-Maxwell's equation known as Wilke's equation and is derived for the diffusion of a key component through a stagnant mixture.

$$D_{mix,k,l,r} = \frac{1 - x_r}{\sum_{\substack{j \\ j \neq r}} \frac{x_j}{D_{k,l,j,r}}} \tag{A 11}$$

The bimolecular diffusion coefficients, $D_{k,l,j,r}$, used in (A 11) are calculated by Chapman-Enskog's relation, (A 12) [48], which includes the collision integral, $\Omega_{k,l,j,r}$, to account for intermolecular forces. The molar unit used here is [g mol^{-1}].

$$D_{k,l,j,r} = 1.8583 \cdot 10^{-7} \cdot \sqrt{T^3_{p,k,l} \cdot \left(\frac{1}{M_j} + \frac{1}{M_r} \right)} \cdot \frac{1}{P_{atm} \cdot \sigma^2_{j,r} \cdot \Omega_{k,l,j,r}} \tag{A 12}$$

$$\Omega_{k,l,j,r} = \frac{1.06036}{\left(\frac{\kappa \cdot T_{p,k,l}}{\varepsilon}\right)_{j,r}^{0.1561}} + \frac{0.193}{\exp\left(0.47635 \cdot \left(\frac{\kappa \cdot T_{p,k,l}}{\varepsilon}\right)_{j,r}\right)} + \frac{1.03587}{\exp\left(1.52996 \cdot \left(\frac{\kappa \cdot T_{p,k,l}}{\varepsilon}\right)_{j,r}\right)} + \frac{1.76474}{\exp\left(3.89411 \cdot \left(\frac{\kappa \cdot T_{p,k,l}}{\varepsilon}\right)_{j,r}\right)} \quad \text{(A 13)}$$

A.3 Equations Relating to Heat and Mass Transfer

The convective heat transfer coefficient between gas and particles are described by (A 14), which is valid for forced convection around a sphere submerged in a fluid [48].

$$h_{p,k,l} = \left(2 + 0.60 \cdot \mathrm{Re}_{p,k,l}^{\frac{1}{2}} \cdot \mathrm{Pr}_{p,k,l}^{\frac{1}{3}}\right) \cdot \left(\frac{\lambda_{mix,f,k,l}}{d_{p,k,l}}\right) \quad \text{(A 14)}$$

The particle Reynolds and Prandtl numbers are defined by (A 15) and (A 16) where the subscript *f* indicates that the physical properties of the gas are found at an average temperature between the particle and the bulk gas.

$$\mathrm{Re}_{p,k,l} = \frac{d_{p,k,l} \cdot \nu_{s,k,l} \cdot \rho_{mix,f,k,l}}{\mu_{mix,f,k,l}} \quad \text{(A 15)}$$

$$\mathrm{Pr}_{p,k,l} = \frac{C_{p,mix,f,k,l} \cdot \mu_{mix,f,k,l}}{\lambda_{mix,f,k,l}} \quad \text{(A 16)}$$

The heat transfer between the gas and reactor wall is taking place by forced convection in the laminar regime ($\mathrm{Re_g} < 4000$). The wall heat transfer coefficient, h_w, is described by (A 17) that applies for heat transfer in a circular tube [49].

$$h_w = 1.62 \cdot \mathrm{Re}_g^{\frac{1}{3}} \cdot \mathrm{Pr}_g^{\frac{1}{3}} \cdot \left(\frac{D_R}{L_R} \right)^{\frac{1}{3}} \cdot \left(\frac{\lambda_{mix}}{D_R} \right) \qquad \text{(A 17)}$$

In order to increase the applicability of the model (A 18) is also included to account for heat transfer between the gas and reactor wall in case of turbulent gas flow ($Re_g > 4000$) [49]. As it is the case for (A 17), (A 18) applies for heat transfer in a circular tube.

$$h_w = \left(0.023 \cdot \mathrm{Re}_g^{\frac{4}{5}} \cdot \mathrm{Pr}_g^{\frac{1}{3}} \right) \cdot \left(\frac{\lambda_{mix}}{D_R} \right) \qquad \text{(A 18)}$$

The Reynolds and Prandtl numbers of the gas are defined by (A 19) and (A 20) where the absence of the subscript *f* indicates that the physical properties of the gas are found at the bulk gas temperature.

$$\mathrm{Re}_g = \frac{D_R \cdot \hat{\nu}_g \cdot \rho_{mix}}{\mu_{mix}} \qquad \text{(A 19)}$$

$$\mathrm{Pr}_g = \frac{C_{p,mix} \cdot \mu_{mix}}{\lambda_{mix}} \qquad \text{(A 20)}$$

It should be noted that there exists a transitional interval, $Re_g \sim 2000 - 4000$, where the flow is shifting gradually from laminar to turbulent. The bulk gas Reynolds numbers during the experiments have however been between 400 and 1100 wherefore (A 17) has been used in all the simulations presented here.

In (A 14) - (A 20) heat capacities, viscosities and thermal conductivities of the gas are depending on temperature, which is also indicated by the subscripts on the Reynolds and Prandtl number. In addition these properties also depend on the composition of the gas. The pure component viscosities of N_2, CO_2 and O_2 are found from (A 21), which

originates from gas kinetic theory and includes the collision integral, Ω_j (A 22), to account for intermolecular forces [48]. The molar weight M_j is in the unit [g mol^{-1}].

$$\mu_j = 2.6693 \cdot 10^{-6} \cdot \frac{\sqrt{M_j \cdot T}}{\sigma_j^2 \cdot \Omega_j} \tag{A 21}$$

$$\Omega_j = \frac{1.16145}{\left(\frac{\kappa \cdot T}{\varepsilon}\right)_j^{0.14874}} + \frac{0.52487}{\exp\left(0.77320\left(\frac{\kappa \cdot T}{\varepsilon}\right)_j\right)} + \frac{2.16178}{\exp\left(2.43787\left(\frac{\kappa \cdot T}{\varepsilon}\right)_j\right)} \tag{A 22}$$

In (A 21) and (A 22) the temperature *T* is not indexed as this can be either the bulk gas or a film layer temperature. When used for film layer calculations the indexes *k* and *l* are used to account for particle size and morphology.

Using the pure component viscosity in (A 21) the Eucken equation (A 23) [48] and the Eucken correlation (A 24) [50] are used to find thermal conductivities of the pure components. The Eucken equation is used for N_2 and O_2 and the Eucken correlation is used for CO_2 as this was found to give the best fits with available data of thermal conductivities.

$$\lambda_j = \left(C_{p,j} + \frac{5}{4} \cdot \frac{R}{M_j}\right) \cdot \mu_j \tag{A 23}$$

$$\lambda_j = \left(C_{p,j} - R \cdot \left(1 - \frac{9}{4 \cdot M_j}\right)\right) \cdot \mu_j \tag{A 24}$$

From the pure component properties the thermal conductivity and viscosity of the mixture are found from (A 25) [51].

$$\mu_{mix}/\lambda_{mix} = \sum_j \frac{\mu_j/\lambda_j}{1+\frac{1}{x_j}\cdot\sum\limits_{\substack{h\\h\neq j}} x_h\cdot\Gamma_{j,h}} \tag{A 25}$$

$$\Gamma_{j,h} = \frac{1}{\sqrt{8}}\cdot\left(1+\frac{M_j}{M_h}\right)^{-\frac{1}{2}}\cdot\left(1+\left(\frac{\mu_j/\lambda_j}{\mu_h/\lambda_h}\right)^{\frac{1}{2}}\cdot\left(\frac{M_h}{M_j}\right)^{\frac{1}{4}}\right)^2 \tag{A 26}$$

The pure component heat capacities, necessary to calculate the Prandtl numbers and thermal conductivities are described by a second order polynomial given in (A 27) [52].

$$C_{p,j} = a_j + b_j\cdot T + c_j\cdot T^{-2} \tag{A 27}$$

Values used in (A 27) for the three gases are shown in table A 1 [52].

Table A 1 Constants used in (A 27) [52].

Component/Constant	**a [J K^{-1} kg^{-1}]**	**b [J K^{-2} kg^{-1}]**	**c [J K kg^{-1}]**
N_2	1020.71	$1342.86\cdot10^{-4}$	$-1785.71\cdot10^{3}$
CO_2	1004.55	$1997.73\cdot10^{-4}$	$-1959.09\cdot10^{4}$
O_2	936.25	$1306.25\cdot10^{-4}$	$-5218.75\cdot10^{3}$

As it was the case with (A 21) and (A 22) the temperature in (A 27) is not indexed as this can be either a particle film layer or bulk gas temperature. The heat capacity of the gas mixture is found from (A 28).

$$C_{p,mix} = \sum_j x_j\cdot C_{p,j} \tag{A 28}$$

Similar to (A 28) the mixture density is found from (A 29) where the temperature also can by either that of a particle film layer or the bulk gas.

$$\rho_{mix} = \frac{P \cdot \sum_j x_j \cdot M_j}{R \cdot T} \tag{A 29}$$

The mass transfer coefficient of the gas film layer, $k_{c,k,l,r}$, is found from (A 30) [48], which applies for a sphere experiencing forced convection in a fluid.

$$k_{c,k,l,r} = \left(2 + 0.60 \cdot \mathrm{Re}_{p,k,l}^{\frac{1}{2}} \cdot Sc_{p,k,l,r}^{\frac{1}{3}}\right) \cdot \left(\frac{D_{mix,f,k,l,r}}{d_{p,k,l}}\right) \tag{A 30}$$

The particle Reynolds and Schmidt's number is defined by (A 15) and (A 31).

$$Sc_{p,k,l,r} = \frac{\mu_{mix,f,k,l}}{\rho_{mix,f,k,l} \cdot D_{mix,f,k,l,r}} \tag{A 31}$$

The molar diffusion coefficient of the reactant, $D_{mix,f,k,l,r}$, is found from (A 11) using the film layer temperature to calculate bimolecular diffusion coefficients in (A 12) and (A 13).

A.4 Particle Slip Velocity, Heat Capacity, Enthalpy and Concentration

The slip velocity of a particle is used in both the mass and energy balances in section 3.2 and to calculate the Reynolds number of a particle in (A 15). The particle slip velocity is found in (A 32) - (A 34) as suggested by Haider & Levenspiel [53].

$$\nu_{s,k,l} = \frac{\nu^{\bullet}_{s,k,l}}{\left(\frac{\rho^2_{mix,f,k,l}}{g \cdot \mu_{mix,f,k,l} \cdot \left(\rho^a_{p,k,l} - \rho_{mix,f,k,l} \right)} \right)^{\frac{1}{3}}} \tag{A 32}$$

$$\nu^{\bullet}_{s,k,l} = \left(\frac{1}{\frac{10.8323}{\left(d^{\bullet}_{p,k,l} \right)^{1.6486}} + \frac{0.626029}{\left(d^{\bullet}_{p,k,l} \right)^{0.41215}}} \right)^{1.21315} \tag{A 33}$$

$$d^{\bullet}_{p,k,l} = d_{p,k,l} \cdot \left(\frac{g \cdot \rho_{mix,f,k,l} \cdot \left(\rho^a_{p,k,l} - \rho_{mix,f,k,l} \right)}{\mu^2_{mix,f,k,l}} \right)^{\frac{1}{3}} \tag{A 34}$$

In (A 32) and (A 34) values of film layer viscosity is found from (A 25), film layer density is found from (A 29) and apparent particle densities are found from (A 4) - (A 6). In the solid energy balances it is necessary to describe the solid heat capacity as a function of particle temperature. This relationship is described by Coimbra and Queiroz [54] in (A 35) - (A 38). In (A 36) the characteristic Einstein temperature, θ_1, which is a measure of the energy in atomic vibrations, has a constant value of 380 K.

$$R^x = R \cdot \left(\sum_{j=0}^{N} \frac{w_j}{M_j} \right) \tag{A 35}$$

$$EF_{i,k,l} = \left(\frac{\theta_i}{T_{p,k,l}} \right)^2 \cdot \frac{\exp\left(\frac{\theta_i}{T_{p,k,l}} \right)}{\left(\exp\left(\frac{\theta_i}{T_{p,k,l}} \right) - 1 \right)^2} \tag{A 36}$$

$$\theta_2 = \frac{Q_{LHV}}{R^x} \cdot \left(\frac{9 - 4.973 \cdot \left(1 - VM_{daf} \right)}{100} \right) \tag{A 37}$$

$$C_{p,k,l} = 3 \cdot R^{x} \cdot \left(\frac{EF_{1,k,l}}{3} + \frac{2 \cdot EF_{2,k,l}}{3} \right) \quad \text{(A 38)}$$

In (A 37) the volatile content is zero in all of the simulations as the equation is used on devolatilized char. The lower heating value, Q_{LHV}, is 32.75 MJ kg^{-1} corresponding to the oxidation of one kg carbon to carbon dioxide at standard conditions.
The solid enthalpy, used to calculate the particle heat of reaction, will be approximated as that of graphite [34].

$$H_{p,k,l} = 2.286 \cdot T_{p,k,l} - 1099.5 \quad \text{(A 39)}$$

The concentration of a particle fraction defined by size and morphology will change down the reactor as the slip velocity of that fraction will decrease during its consumption. The concentration of a particle fraction defined by size and morphology is given by (A 40).

$$N_{l,k} = \frac{\tilde{m}_{Char} \cdot \alpha_l \cdot \Theta_k}{V_{p0,k} \cdot \rho^{a}_{p0,l} \cdot \left(\nu_{s,k,l} + \nu_g \right) \cdot A_R} \quad \text{(A 40)}$$

A.5 Gas Velocities

The linear velocity of the section of the laminar gas front where particles are sampled during experiments is given by (A 41). The average linear gas velocity in the reactor is calculated as (A 42).

$$\nu_g = \frac{\hat{\nu}_g \cdot \left(2 \cdot R_R^2 - R_F^2 \right)}{R_R^2} \quad \text{(A 41)}$$

$$\hat{\nu}_g = \frac{F_T \cdot R \cdot T_g}{A_R \cdot P} \tag{A 42}$$

Appendix B: Derivation of Particle Mass Balances

The particle mass balances for cenospheres, network chars and dense chars are derived in the following. All mass balances include reaction on both exterior and interior surfaces but consumption is taking place after a shrinking spheres model. To describe the development of interior surface the volumetric reaction model is used for all char morphologies.

B.1 Cenospheric Char

The mass balance for a cenospheric char particle is based on continuous char matrix and its derivation proceeds as shown below.

$$\frac{dm_{p,k,r}}{dt} = -\left(m_{p,k} \cdot S_k \cdot k_{k,r} \cdot \left(C_r^S\right)_k^{n_r} \cdot \eta_{k,r} + A_{p,k} \cdot k_{k,r} \cdot \left(C_r^S\right)_k^{n_r} \right) \Rightarrow$$

$$\frac{d\,\frac{4}{3} \cdot \pi \cdot \rho_p \cdot \left(R_{p,k}^3 - R_{p,k,I}^3\right)_r}{dt} =$$

$$-\left(\frac{4}{3} \cdot \pi \cdot \left(R_{p,k}^3 - R_{p,k,I}^3\right) \cdot \rho_p \cdot S_k \cdot k_{k,r} \cdot \left(C_r^S\right)_k^{n_r} \cdot \eta_{k,r} + 4 \cdot \pi \cdot R_{p,k}^2 \cdot k_{k,r} \cdot \left(C_r^S\right)_k^{n_r} \right) \Rightarrow$$

$$\frac{d\left(R_{p,k}^3 - R_{p,k,I}^3\right)_r}{dt} = -\left(\left(R_{p,k}^3 - R_{p,k,I}^3\right) \cdot S_k \cdot k_{k,r} \cdot \left(C_r^S\right)_k^{n_r} \cdot \eta_{k,r} + \frac{3 \cdot R_{p,k}^2}{\rho_p} \cdot k_{k,r} \cdot \left(C_r^S\right)_k^{n_r} \right) \tag{B 1}$$

Before continuing the derivation the differential in (B 1) must be redefined using particle conversion. This redefinition is shown in (B 2).

$$X_k = \frac{m_{p0,k} - m_{p,k}}{m_{p0,k}} \Rightarrow$$

$$X_k = 1 - \frac{\frac{4}{3}\cdot\pi\cdot\left(R_{p,k}^3 - R_{p,k,I}^3\right)\cdot\rho_{p,N}^a}{\frac{4}{3}\cdot\pi\cdot\left(R_{p0,k}^3 - R_{p,k,I}^3\right)\cdot\rho_{p,N}^a} \Rightarrow$$

$$X_k = 1 - \frac{\left(R_{p,k}^3 - R_{p,k,I}^3\right)}{\left(R_{p0,k}^3 - R_{p,k,I}^3\right)}$$

$$\left(R_{p,k}^3 - R_{p,k,I}^3\right) = \left(R_{p0,k}^3 - R_{p,k,I}^3\right)\cdot\left(1 - X_k\right) \qquad \text{(B 2)}$$

Substituting (B 2) into (B 1) yields (B 3), the last intermediate expression before the final formulation of the mass balance is achieved.

$$\frac{dX_{k,r}}{dt} = k_{k,r}\cdot\left(C_r^S\right)_k^{n_r}\cdot\left(\left(1 - X_k\right)\cdot S_0\cdot\eta_{k,r} + \frac{3\cdot R_{p,k}^2}{\rho_p\cdot\left(R_{p0,k}^3 - R_{p,k,I}^3\right)}\right) \qquad \text{(B 3)}$$

In order to express the radius in (B 3) as a function of char conversion the derivation below is made from (B 2). The definition $\delta_0 = \left(R_{p0,k} - R_{p,k,I}\right)/R_{p0,k}$ is utilized in the derivation.

$$\left(R_{p,k}^3 - R_{p,k,I}^3\right) = \left(R_{p0,k}^3 - R_{p,k,I}^3\right)\cdot\left(1 - X_k\right) \Rightarrow$$

$$R_{p,k} = \left(\left(R_{p0,k}^3 - R_{p,k,I}^3\right)\cdot\left(1 - X_k\right) + R_{p,k,I}^3\right)^{\left(\frac{1}{3}\right)} \Rightarrow$$

$$R_{p,k} = \left(R_{p0,k}^3 - R_{p0,k}^3\cdot X_k + R_{p,k,I}^3\cdot X_k\right)^{\left(\frac{1}{3}\right)} \Rightarrow$$

$$R_{p,k} = \left(R_{p0,k}^3\cdot\left(1 - X_k\right) + R_{p0,k}^3\cdot\left(1 - \delta_0\right)^3\cdot X_k\right)^{\left(\frac{1}{3}\right)} \Rightarrow$$

$$R_{p,k} = R_{p0,k}\left(1 - X_k\cdot\left(1 - \left(1 - \delta_0\right)^3\right)\right)^{\left(\frac{1}{3}\right)} \qquad \text{(B 4)}$$

Substituting (B 4) into (B 3) and using the definition of δ_0 the final form of the cenospheric mass balance is (2).

$$\frac{dX_{k,r}}{dL} = \frac{k_{k,r} \cdot \left(C_r^S\right)_k^{n_r}}{\nu_{s,k} + \nu_g} \cdot \left(S_0 \cdot \left(1 - X_k\right) \cdot \eta_{k,r} + \frac{3 \cdot \left(1 - X_k \cdot \left(1 - \left(1 - \delta_0\right)^3\right)\right)^{\left(\frac{2}{3}\right)}}{\rho_p \cdot R_{p0,k} \cdot \left(1 - \left(1 - \delta_0\right)^3\right)} \right) \tag{2}$$

B.2 Network Chars and Dense Chars

The derivation of the mass balance for a network chars and a dense chars is identical and proceeds as follow.

$$\frac{dm_{p,k,l,r}}{dt} = -\left(m_{p,k,l} \cdot S_{k,l} \cdot k_{k,l,r} \cdot \left(C_r^S\right)_{k,l}^{n_r} \cdot \eta_{k,l,r} + A_{p,k,l} \cdot k_{k,l,r} \cdot \left(C_r^S\right)_{k,l}^{n_r}\right) \Rightarrow$$

$$\frac{d\,\frac{4}{3} \cdot \pi \cdot \rho_p \cdot R_{p,k,l,r}^3}{dt} = -\left(\frac{4}{3} \cdot \pi \cdot R_{p,k,l}^3 \cdot \rho_p \cdot S_{k,l} \cdot k_{k,l,r} \cdot \left(C_r^S\right)_{k,l}^{n_r} \cdot \eta_{k,l,r} + 4 \cdot \pi \cdot R_{p,k,l}^2 \cdot k_{k,l,r} \cdot \left(C_r^S\right)_{k,l}^{n_r}\right) \Rightarrow$$

$$\frac{dR_{p,k,l,r}^3}{dt} = -\left(R_{p,k,l}^3 \cdot S_{k,l} \cdot k_{k,l,r} \cdot \left(C_r^S\right)_{k,l}^{n_r} \cdot \eta_{k,l,r} + \frac{3 \cdot R_{p,k,l}^2}{\rho_p} \cdot k_{k,l,r} \cdot \left(C_r^S\right)_{k,l}^{n_r} \right) \tag{B 5}$$

Before the derivation can continue the differential in (B 5) must be redefined using char conversion to express the particle radius. This definition is shown in (B 6).

$$R_{p,k,l} = R_{p0,k,l} \cdot \left(1 - X_{k,l}\right)^{\left(\frac{1}{3}\right)} \tag{B 6}$$

Substituting (B 6) into (B 5) yields the final form of the network- and dense char mass balances, shown in (B 7). It can be seen that (B 7) is identical to (2) when $\delta_0 = 1$.

$$\frac{dX_{k,l,r}}{dt} = k_{k,l,r} \cdot \left(C_r^S\right)_{k,l}^{n_r} \cdot \left(\frac{R_{p,k,l}^3}{R_{p0,k,l}^3} \cdot S_{k,l} \cdot \eta_{k,l,r} + \frac{3 \cdot R_{p,k,l}^2}{R_{p0,k,l}^3 \cdot \rho_p} \right) \Rightarrow$$

$$\frac{dX_{k,l,r}}{dL} = \frac{k_{k,l,r} \cdot \left(C_r^S\right)_{k,l}^{n_r}}{\nu_{s,k,l} + \nu_g} \cdot \left(S_0 \cdot \left(1 - X_{k,l}\right) \cdot \eta_{k,l,r} + \frac{3 \cdot \left(1 - X_{k,l}\right)^{\left(\frac{2}{3}\right)}}{\rho_p \cdot R_{p0,k,l}} \right) \qquad \text{(B 7)}$$

References

[1] Buhre BJP, Elliot LK, Sheng CD, Gupta RP, Wall TF. Oxy-fuel combustion technology for coal-fired power generation. Prog Energy Combust Sci. 2005;31:283-7

[2] Figueroa JD, Fout T, Plasynski S, McIlvried H, Srivastava RD. Advances in CO_2 capture technology-The U.S. department of energy's carbon sequestration program. Int J Greenhouse Gas Control 2008;2:9-0

[3] Murphy JJ, Shaddix CR. Combustion kinetics of coal chars in oxygen-enriched environments. Combust Flame 2006;144:710-9

[4] Hurt R, Sun J-K, Lunden M. A kinetic model of carbon burnout in pulverized coal combustion. Combust Flame 1998;113:181-1

[5] Murphy JJ, Shaddix CR. Effect of reactivity loss on apparent reaction order of burning char particles 2010;157:535-9

[6] Cloke M, Wu T, Barranco R, Lester E. Char characterisation and its application in a coal burnout model. Fuel 2003;82:1989-0

[7] Wu T, Lester E, Cloke M. A burnout prediction model based around char morphology. Energy Fuels 2006;20:1175-3

[8] Ballester J, Jiménez S. Kinetic parameters for the oxidation of pulverized coal as measured from drop tube tests. Combust Flame 2005;142:210-2

[9] Jiménez S, Ballester J. Study of the evolution of particle size distributions and it effects on the oxidation of pulverized coal. Combust Flame 2007;151:482-4

[10] Mitchell RE, Ma L, Kim BJ. On the burning behavior of pulverized coal chars. Combust Flame 2007;151:426-6

[11] Hurt RH, Lunden MM, Brehob EG, Maloney DJ. Statistical kinetics for pulverized coal combustion. 26'th Symposium (International) on Combustion 1996:3169-7

[12] Gale TK, Bartholomew CH, Fletcher TH. Effects of pyrolysis heating rate on intrinsic reactivities of coal char. Energy Fuels 1996;10:766-5

[13] Ma L, Mitchell R. Modeling char oxidation behavior under zone II burning conditions at elevated pressures. Combust Flame 2009;156:37-0

[14] Yu J, Lucas JA, Wall TF. Formation of the structure of chars during devolatilization of pulverized coal and its thermoproperties: A review. Prog Energy Combust Sci. 2007;33:135-0

[15] Brix J, Jensen PA, Jensen AD. Coal devolatilization and char conversion under suspension fired conditions in O_2/N_2 and O_2/CO_2 atmospheres. Fuel 2010;89:3373-0

[16] Bejarano PA, Levendis YA. Single-coal-particle combustion in O_2/N_2 and O_2/CO_2 environments. Combust Flame 2008;153:270-7

[17] Rathnam RK, Elliot LK, Wall TF, Liu Y, Moghtaderi B. Differences in reactivity of pulverized coal in air (O_2/N_2) and oxy-fuel (O_2/CO_2) conditions. Fuel Proc. Technol. 2009;90:797-2

[18] Molina A, Shaddix CR. Ignition and devolatilization of pulverized bituminous coal particles during oxygen/carbon dioxide coal combustion. Proc Combust Inst 2007; 31:1905 – 2

[19] Shaddix CR, Molina A. Particle imaging of ignition and devolatilization of pulverized coal during oxy-fuel combustion. Proc Combust Inst 2009;32:2091-8

[20] Li Q, Zhao C, Chen X, Wu W, Li Y. Comparison of pulverized coal combustion in air and in O_2/CO_2 mixtures by thermo-gravimetric analysis. J. Anal. Appl. Pyrolysis 2009;85:521-8

[21] Várhegyi G, Szabó P, Jakab E, Till F. Mathematical modeling of char reactivity in Ar-O_2 and CO_2-O_2 mixtures. Energy Fuels 1996;10:1208-4

[22] Liu H. Combustion of coal char in O_2/CO_2 and O_2/N_2 mixtures: A comparative study with non-isothermal thermogravimetric analyzer (TGA) tests. Energy Fuels 2009;23:4278-5

[23] Brix J et al. Coal char reactivity: A thermogravimetric study on chars obtained in O_2/N_2 and O_2/CO_2 in an entrained flow reactor under suspension fired conditions and in a TGA. Article in progress

[24] Shu X, Xu X. Study on morphology of chars from coal pyrolysis. Energy Fuels 2001;15:1347-3

[25] Bailey JG, Tate A, Diessel CFK, Wall TF. A char morphology system with applications to coal combustion. Fuel 1990;69:225-9

[26] Tsai C-Y, Scaroni AW. Reactivity of bituminous coal chars during the initial stage of pulverized-coal combustion. Fuel 1987;66:1400-6

[27] Tsai C-Y, Scaroni AW. The structural changes of bituminous coal particles during the initial stages of pulverized-coal combustion. Fuel 1987;66:200-6

[28] Gao H, Murata S, Nomura M, Ishigaki M, Qu M, Tokuda M. Experimental observation and image analysis for evaluation of swelling and fluidity of single coal particles heated with CO_2 laser. Energy Fuels 1997;11:730-8

[29] Gao H, Murata S, Nomura M, Ishigaki M, Tokuda M. Preliminary surface structure transition of coal particles during prepyrolysis with CO_2 laser. Energy Fuels 1996;10:1227-4

[30] Gale TK, Bartholomew CH, Fletcher TH. Decreases in the swelling and porosity of bituminous coals during devolatilization at high heating rates. Combust Flame 1995;100:94-0

[31] Fletcher TH. Swelling properties of coal chars during rapid pyrolysis and combustion. Fuel 1993;72:1485-5

[32] Kee RJ, Rupley FM, Miller JA. CHEMKIN II: A FORTRAN chemical kinetics package for the analysis of gas-phase chemical kinetics, Report No. SAND 89-8009, Sandia National Laboratories, 1989

[33] Oh MS, Peters WA, Howard JB. An experimental and modeling study of softening coal pyrolysis. AIChE Journal 1989;35:775-2

[34] Brix J. A model for entrained flow reactor gasification of solid fuels for syngas production. M.Sc. Thesis, Department of Chemical and Biochemical Engineering, CHEC Research Center, Technical University of Denmark, 2007:1-4

[35] Norman J, Pourkashanin M, Williams A. Modeling the formation and emission of environmentally unfriendly coal species in some gasification processes. Fuel 1997;76:1201-6

[36] Wen CY. Noncatalytic heterogeneous solid fluid reaction models. Ind. Eng. Chem 1968;9:34-4

[37] Bhatia SK, Perlmutter DD. A random pore model for fluid-solid reactions: I. Isothermal, kinetic control. AIChE Journal 1980;26:379-6

[38] Bhatia SK, Perlmutter DD. A random pore model for fluid-solid reactions: II. Diffusion and Transport Effects. AIChE Journal 1981;27:247-4

[39] Szekely J, Evans JW. A structural model for gas-solid reactions with a moving boundary. Chem. Eng. Sci. 1970;25:1091-7

[40] Szekely J, Evans JW. A structural model for gas-solid reactions with a moving boundary-II. Chem. Eng. Sci. 1971;26:1901-3

[41] Sohn HY, Szekely J. A structural model for gas-solid reactions with a moving boundary-III. A general dimensionless representation of the irreversible reaction between a porous solid and a reactant gas. Chem. Eng. Sci. 1972;27:763-8

[42] Yagi S, Kunii D. Studies on combustion of carbon particles in flames and fluidized beds. Fifth Symposium (International) on Combustion 1955:231-4

[43] Zolin A, Jensen A, Pedersen LS, Dam-Johansen K. A comparison of coal char reactivity determined from thermogravimetric and laminar flow reactor experiments. Energy Fuels 1998;12:268-6

[44] Charpenay S, Serio MA, Solomon PR. The prediction of coal char reactivity under combustion conditions. Twenty-Fourth Symposium (International) on Combustion 1992:1189-7

[45] Mon E, Amundson NR. Diffusion and reaction in a stagnant boundary layer about a carbon particle. 2. An extension. Ind Eng. Chem. Fundam. 1978;17:313-1

[46] Zhang H, Pu W-X, Ha S, Li Y, Sun M. The influence of included minerals on the intrinsic reactivity of char prepared at 900 ^{o}C in a drop tube furnace and a muffle furnace. Fuel 2009;88:2303-0

[47] Froment GF, Bischoff KB. Chemical reactor analysis and design, 2'nd edition. John Wiley & Sons, Inc; 1990

[48] Bird RB, Stewart WE, Lightfoot EN. Transport phenomena, 2'nd edition. John Wiley & Sons, Inc;2002

[49] Griskey RG. Transport phenomena and unit operations – A combined approach, 1'st edition, John Wiley & Sons, Inc;2002

[50] Gosse J. The thermal conductivity of pure polyatomic gasses at moderate pressure. Int. J. Heat Mass Transfer 1992;35:599-4

[51] Wilke CR. A viscosity equation for gas mixtures. J. Chem. Phys. 1950;18:517-9

[52] Laidler KJ, Meiser JH. Sanctuary BC. Physical chemistry, 4'th edition. Houghton Mifflin:2002

[53] Haider A, Levenspiel O. Drag coefficient and terminal velocity of spherical and nonspherical particles. Powder Technol. 1989;58:63-0

[54] Coimbra CFM, Queiroz M. Evaluation of a dimensionless group number to determine second-Einstein temperatures in a heat capacity model for all coal ranks. Combust Flame 1995;101:209-0

Symbols

A	Area $\left[m^2\right]$ or pre-exponential Arrhenius factor $\left[kg\ m^{-2}\ s^{-1}\left(mol\ m^{-3}\right)^{-0.5}\right]$
a	Polynomial coefficient $\left[K^{-2}\right]$ or $[\ ]$
b	Polynomial coefficient $\left[K^{-1}\right]$
C	Heat capacity $\left[J\ kg\ K^{-1}\right]$ or $\left[J\ mol^{-1}\ K^{-1}\right]$ or concentration $\left[mol\ m^{-3}\right]$
c	Polynomial coefficient $\left[K^2\right]$
D	Diffusion coefficient $\left[m^2\ s^{-1}\right]$ or diameter $[m]$
d	Char pore- or particle diameter $[m]$
E	Activation- or deactivation energy $\left[J\ mol^{-1}\right]$
EF	Einstein function
$\bar{e}$	Char emissivity
F	Gaseous flow rate $\left[mol\ s^{-1}\right]$
g	Gravity $\left[m\ s^{-2}\right]$
H	Enthalpy $\left[J\ mol^{-1}\right]$ or $\left[J\ kg^{-1}\right]$
ΔH	Reaction enthalpy $\left[J\ mol^{-1}\right]$ or $\left[J\ kg^{-1}\right]$
h	Heat transfer coefficient $\left[W\ m^{-2}\ K^{-1}\right]$
k	Rate constant $\left[kg\ m^{-2}\ s^{-1}\left(mol\ m^{-3}\right)^{-0.5}\right]$ or mass transfer coefficient $\left[m\ s^{-1}\right]$
L	Reactor length $[m]$
M	Molar mass $\left[kg\ mol^{-1}\right]$ or $\left[g\ mol^{-1}\right]$
m	Mass $[kg]$
N	Number quantity or particle concentration $\left[m^{-3}\right]$

n	Reaction order
P	Pressure $[Pa]$, $[Bar]$ or $[atm]$
Pr	Prandtl's number
Q	Convective heat transfer $\left[W\ m^{-3}\right]$ or heating value $\left[J\ kg^{-1}\right]$
R	Radius $[m]$ or gas constant $\left[J\ mol^{-1}\ K^{-1}\right]$ or $\left[J\ kg^{-1}\ K^{-1}\right]$
Re	Reynolds number
r	Reaction rate $\left[mol\ m^{-3}\ s^{-1}\right]$ or $\left[s^{-1}\right]$
S	Specific surface area $\left[m^2\ kg^{-1}\right]$
Sc	Schmidt's number
T	Temperature $[K]$
V	Volume $\left[m^3\right]$
VM	Volatile fraction
W	Initial weight percent of particle size k
w	Molar fraction of a char constituents $[daf]$
X	Char conversion
x	Molar fraction
z	Oxidizer to fuel ratio
α	Initial weight fraction of a char morphology
δ	Cenosphere wall thickness $[\mu m]$ or cenosphere wall thickness divided by cenosphere radius
ε	Char porosity
ε/κ	Lennard-Jones parameter $[K]$
ς	Stoichiometric coefficient
η	Internal particle effectiveness factor
Θ	Initial weight fraction of a particle size
θ	Einstein temperature $[K]$
Λ	Stoichiometric coefficient of heterogeneous reaction

λ	Thermal conductivity $\left[W\ m^{-1}\ K^{-1}\right]$
μ	Viscosity $\left[Pa\ s\right]$
ν	Linear velocity $\left[m\ s^{-1}\right]$
ρ	Skeletal density (unless indexed by superscript a) $\left[kg\ m^{-3}\right]$
σ_{SB}	Stefan-Boltzmann constant $\left[W\,m^{-2}\,K^{-4}\right]$
σ	Lennard-Jones parameter $\left[\AA\right]$
$\bar{\tau}$	Tortuosity
ϕ	Thiele modulus
Ψ	Particle Sphericity
Ω	Collisional integral

Subscripts

A	Activation
a	Stoichiometric coefficient of carbon in char
b	Stoichiometric coefficient of hydrogen in char
C	Cenospheric char
c	Mass transfer coefficient
D	Deactivation or dense char
d	Stoichiometric coefficient of nitrogen in char
daf	Dry and ash free basis
e	Stoichiometric coefficient of sulfur in char
F	Funnel of sampling probe
G	Index of all gaseous species
f	Gas film layer property
H	Index of all homogeneous reactions
h	Index of gaseous component
I	Cenosphere cavity radius
i	Index of homogeneous reaction

j	Index of gaseous component
K	Knudsen diffusivity
k	Index of initial particle size
LHV	Lower heating value
l	Index of char morphology
m	Relating property to mass
mix	Property of N_2, CO_2 and O_2 mixture
N	Network char
p	Particle property or constant pressure gas property
pore	Pore property
R	Reactor property
r	Index of gaseous reactant
s	Particle slip velocity
T	Total amount
u	Stoichiometric coefficient of ash in char
Wall	Wall of a particle
w	Reactor wall property
y	Stoichiometric coefficient of oxygen in char
0	Initial property

Superscripts

a	Apparent density
B	Bulk gas property
n	Reaction order
S	Particle surface property
*	Effective diffusivity
^	Mean gas flow
•	Dimensionless property
x	Based on mass
~	Flow in time

Article IV
Oxy-Fuel Combustion of Coal Char: Particle Temperature and NO Formation

Oxy-Fuel Combustion of Coal Char: Particle Temperature and NO Formation

Jacob Brix[1], Leyre Gómez Navascués[1], Joachim Bachmann Nielsen[1], Peter Løvengreen Bonnek[1], Henning Engelbrecht Larsen[2], Sønnik Clausen[3], Peter Glarborg[1], Anker Degn Jensen*[,1]

[1]*Department of Chemical and Biochemical Engineering – Technical University of Denmark, Building 229 Søltofts Plads, 2800 Kgs. Lyngby, Denmark*

[2]*Department of Photonics Engineering – Technical University of Denmark, Building 128, Frederiksborgvej 399, 4000 Roskilde*

[3]*Department of Plasma Physics and Technology – Technical University of Denmark, Building 128, Fredriksborgvej 399, 4000 Rosklide*

**Corresponding Author: e-mail: aj@kt.dtu.dk, Fax: +45 45 88 22 58, Phone: +45 45 25 28 41*

Abstract

The objective of this investigation is to examine differences in char-NO emissions between O_2/N_2 and O_2/CO_2 atmospheres. A laboratory scale fixed bed reactor, operated isothermally at 1073 K, has been used for combustion of millimeter-sized lignite- and bituminous char particles in 5 – 80 vol. % O_2. Particle temperatures and structural changes have been recorded by a Charged Coupled Device (CCD) camera during the experiments. Experiments have been carried out with both single and multiple particles of different sizes. Emissions from lignite char were not influenced by the change from N_2 to CO_2 whereas emissions from bituminous char were lower in O_2/CO_2. For both chars emissions decreased as the O_2 concentration or the particle size increased. An intermediate particle size, where emissions peaked was observed however for bituminous char. The CCD camera provided accurate in situ temperature measurements during the experiments and film recording proved a valuable tool for data interpretation. Results suggest that transport phenomena and kinetics alone can not account for changes in NO emissions between O_2/N_2 and O_2/CO_2. The effect of mineral catalysis and the presence of other N-containing species, such as HCN and NH_3, may also play a role.

Keywords: Oxy-fuel, Combustion, CCD Camera, Particle Temperature, NO

1. Introduction

In recent years the increased focus on anthropogenic CO_2 emission and its effect on the earth's climate have lead to research programs that aim at reducing the CO_2 emission from fossil fueled power and heat generation. An interesting technology in this context is oxy-fuel combustion, where recycled flue gas is mixed with near pure O_2 before the boiler entrance. This results in a plant exit stream of almost pure CO_2, ready for subsequent capture and sequestration [1,2].

The change from N_2 to CO_2 as the dominant gaseous species alters the characteristics of NO formation/reduction and gives promises of lower emissions [1-4]. Even though mechanisms of NO formation/reduction have been extensively studied for decades [5,6-17], several questions remain unanswered, making interpretation of results obtained under oxy-fuel conditions difficult. These questions relate to the effect of mineral catalysis in heterogeneous NO reduction [18-20], the effect of coal rank in heterogeneous NO reduction [16] and the effect of CO in heterogeneous NO reduction [19,21,22]. Recent results show that homogeneous kinetics of NO formation/reduction, which changes significantly under oxy-fuel conditions are fairly well described [23-28]. In order to utilize the potential of reduced NO emission in oxy-fuel combustion through primary measures knowledge of especially char-NO formation is therefore necessary.

The objective of the present work is to investigate char-NO emissions in N_2 and CO_2 atmospheres under a wide range of O_2 concentrations of relevance to both retrofit- and future oxy-fuel plants. The work comprises data from laboratory fixed bed combustion of millimeter-sized lignite- and bituminous char particles. Besides the effect of O_2 concentration the influence of particle size- and concentration is also investigated and a CCD camera has been used for continuously monitoring and recording of particle temperature and structure. The results are discussed in terms of mechanisms for NO formation from char nitrogen oxidation.

2. Experimental

2.1 Equipment

Experiments have been carried out in the laboratory scale fixed bed reactor shown schematically in figure 1. The reactor consists of an inner and outer quartz cylinder

heated by three electrical heating elements. In all experiments the reactor was operated isothermally at 1073 K, showing fluctuations of less than 10 K through its centerline. The reactor inlet gas was preheated in the annulus between the inner and outer quartz cylinder before it flowed through the inner quartz cylinder where it made contact with the particle, cf. figure 1. After the gas exited the reactor it was sent for analysis for CO, CO_2, O_2 and NO (not shown in figure 1). The time delay from the reactor exit to the gas analyzers were measured initially before starting experiments. In all experiments the particle rested on a 5 mm bed of 300 - 355 µm sand particles on top of a quartz frit to ensure its fixation during combustion and to protect the frit. Gaseous atmospheres were created by mixing bottled gases and the volumetric flow has been 1 Nl min^{-1} in all experiments with O_2 concentrations ranging between 5 and 80 vol. % in either N_2 or CO_2. The majority of the experiments have been conducted with a single particle, weighing between 1.3 – 543 mg, but a series of experiments with 5, 10, 15 and 20 particles in both O_2/N_2 and O_2/CO_2 have also been carried out to investigate the effect of particle concentration.

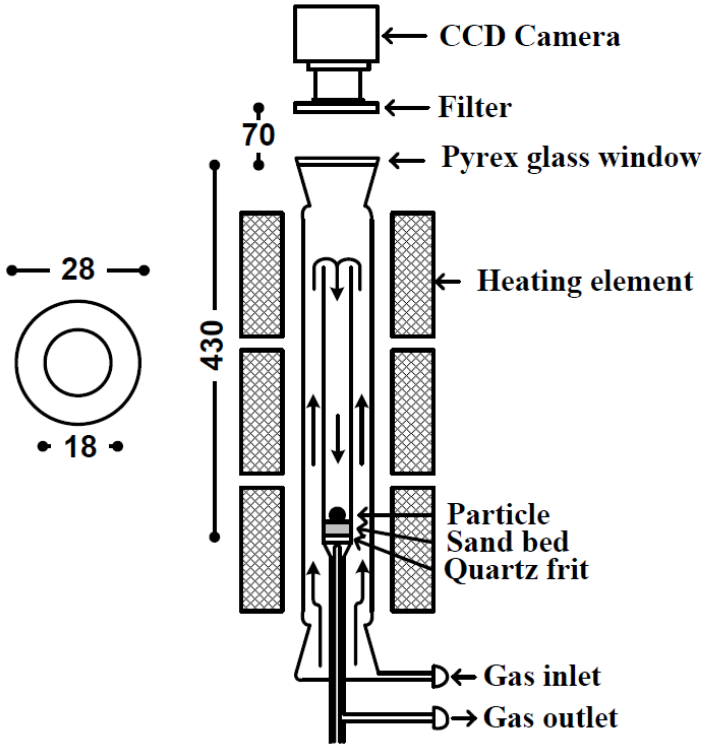

Figure 1 Experimental setup. Inlet gas is mixed from bottled gases and exit gas is sent for analysis for CO, CO_2, O_2 and NO. Length scale is millimeters.

A pyrex glass window was mounted on top of the reactor, directly above the bed, through which a 16 bit CCD camera measured the intensity of the Near Infra Red (NIR) radiation emitted by the particle. To ensure pure NIR measurements and to avoid saturation of the camera's light sensor, a filter was placed in front of the lens.

2.1.2 CCD Camera and Temperature Measurements

The CCD camera used was a Stingray F033 from Allied Vision Technologies and had a 14 bit analog to digital converter. An extra 2 bit of unsigned resolution was achieved by averaging a series of shutter intervals thereby providing a total of 2^{16} = 65536 digital levels that could be detected by the camera. The digital level is a measure of the photon radiation intensity. The maximum digital level corresponds to a saturation of the detector and its processing system and it therefore relates to the maximum measurable particle temperature. A filter, that only allows radiation in the wavelength interval 710 – 1100 nm (NIR) to reach the sensor, was placed in front of the camera. The camera was calibrated with the filter in the temperature interval 1023 K – 1873 K using a black body source. This temperature interval was adequate for the experiments presented here. The filter served two purposes; It avoided saturation of the camera at each temperature and it reduced the influence of scatter caused by background radiation. The relationship between particle temperature and camera response was modeled by integration of Planck's law over the wavelength interval of the filter. Constants accounting for the emissivity of the radiating source, the transmittance of the filter and optics and the camera sensitivity were established during calibration. The sensitivity of the temperature measurements towards potential changes in source emissivity, e.g. ash layer formation during combustion, were tested and found negligible (changes were a few K). Data acquisition during the experiments was done using a LabVIEW program developed specifically for this setup and output were given both as movies made up from still images and data files.

It is important to emphasize that because the camera was recording the NIR radiation from the part of the particles surface that was positioned in its view point reported temperatures are surface temperatures of this area. Throughout the text the term

"Maximum Particle Temperature" refers to the highest temperature measured during an experiment.

2.2 Fuels and Char Preparation

Experiments have been conducted using chars from bituminous El Cerrejón coal and from German Lausitz lignite coal. Proximate and ultimate analyses of these coals are shown in table 1.

Table 1 Proximate and ultimate analysis of the coals used in this study.* Calculated from muffle furnace pyrolysis at 1173 K in N_2.

	El Cerrejón (bit.)	**Lausitz (Lign.)**
Proximate Analysis		
LHV [MJ/kg]	24.70	20.43
Moisture [wt. % wet]	12.20	10.21
Volatiles [wt. % wet]	31.00	28.25*
Ash [wt. % wet]	11.30	4.85
Ultimate Analysis		
C [wt. % dry]	70.62	64.32
H [wt. % dry]	4.78	5.44
O [wt. % dry]	9.32	23.37
N [wt. % dry]	1.59	0.63
S [wt. % dry]	0.80	0.82
Cl [wt. % dry]	0.02	0.03

To prepare the chars, coals were dried at 378 K for app. 22 hours. Then the dry coals were sieved into the size intervals: 0.71 – 2 mm, 2 – 4 mm, 4 – 7 mm and 7 < mm. A size fraction of 1.7 – 2.36 mm bituminous coal particles was also prepared and used for experiments with several particles present in the reactor. Each of the size fractions were pyrolysed at 1173 K for 2 hours in N_2 to ensure that volatiles would not interfere with gas analysis during the experiments. During the pyrolysis no swelling was observed wherefore the size intervals remained intact. Pyrolysis was also carried out using CO_2 at

the same conditions. The resulting chars have not been used for combustion experiments, however, as gasification caused additional weight losses of 8 – 20 wt. % for bituminous coal and total conversion of the lignite coal.

The ash content of the char particles was found by ash tracing at 1073 K for 2 hours in air. The ash content varied with particle size for the bituminous coal with close to 20 wt. % for the smallest particles and around 6 wt. % for the largest. For lignite char the ash content was constant around 11 wt. % irrespective of size.

In order to calculate the fraction of char-N emitted as NO, elemental analysis was done on both lignite- and bituminous chars of different sizes. For none of the chars, char-N content deviated significantly between particles of different sizes with a near constant N-content of 1.537 wt. % for bituminous char and 0.727 wt. % for lignite char.

3. Results

3.1 Data Treatment

For each of the experiments conducted in this investigation a dataset consisting of O_2, NO, CO, CO_2 and particle temperature profiles has been obtained. Figure 2 and figure 3 show examples of these profiles for particle temperature, CO and NO during combustion of 2 – 4 mm bituminous char particles at 20 vol. % O_2.

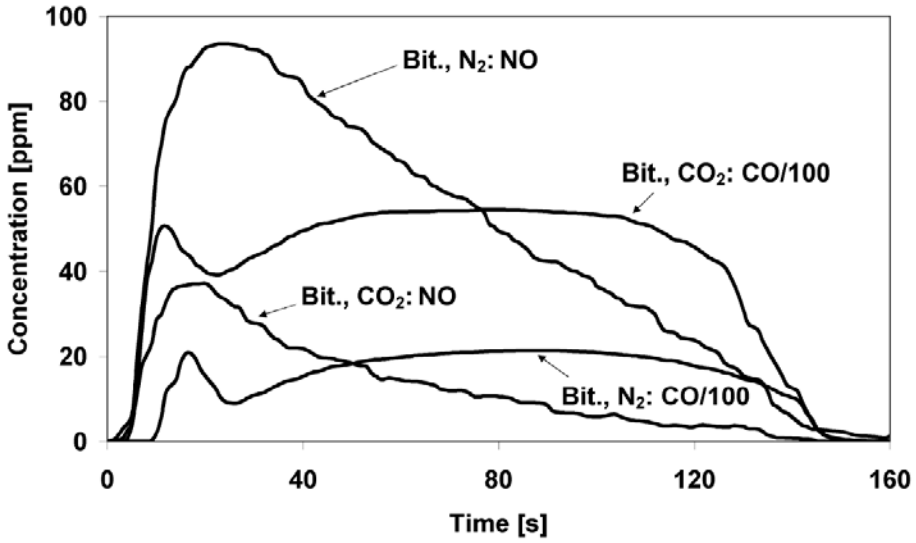

Figure 2 Concentration profiles from single particle combustion of bituminous char at 20 vol. % O_2 in N_2 and CO_2. d_p = 2 – 4 mm. $T_{reactor}$ = 1073 K.

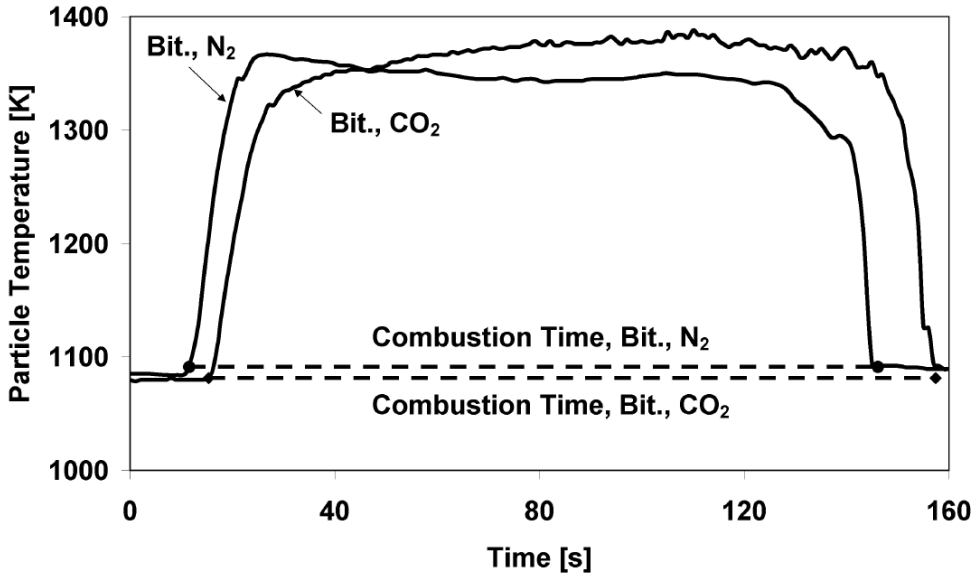

Figure 3 Particle temperature profiles from single particle combustion of bituminous char at 20 vol. % O_2 in N_2 and CO_2. d_p = 2 – 4 mm. $T_{reactor}$ = 1073 K.

In figure 3 the dashed bars indicate the combustion times of the particles used in the experiments. For all experiments presented in this text a combustion time has been estimated this way, using the transient behavior of the temperature profile. The NO emission measured during each experiment has been quantified using eq. 1 and eq. 2. For the integration in eq. 1 n_{NO} and $\bar{n}$ denotes the total molar amount of NO and the total molar flow in the reactor, respectively. C_{NO} is the measured concentration of NO in ppm and t is time.

$$n_{NO} = 10^{-6} \cdot \bar{n} \cdot \sum \left(t_i - t_{i-1} \right) \cdot \frac{\left(C_{NO,i} + C_{NO,i-1} \right)}{2} \qquad \text{Eq. 1}$$

$$Char\_N\ to\ NO\ [\%] = \frac{n_{NO} \cdot M_{NO}}{m_{particle} \cdot \alpha_N} \cdot 100\ \% \qquad \text{Eq. 2}$$

In eq. 2 the molar mass of NO, M_{NO}, the initial mass of the char particle, $m_{particle}$, and the weight fraction of nitrogen in the char, α_N, are used to calculate the fractional conversion of char-N to NO.

3.2 The Effect of O_2 Concentration

The effect of O_2 concentration on NO emission is shown in figure 4 for 2 – 4 mm particles. It is seen from the figure that emissions from lignite chars are similar in O_2/N_2 and O_2/CO_2 and that emission from bituminous chars in O_2/CO_2 is close to that of lignite char. The emission from bituminous chars in O_2/N_2, however, is higher than the previous at lower O_2 concentrations but approaches a similar level as the O_2 concentration increases. For lignite chars O_2 does not seem to have an influence on NO emission at concentrations above 20 vol. % whereas a slight effect is observed for bituminous char in O_2/CO_2 and a strong effect is observed for bituminous char in O_2/N_2.

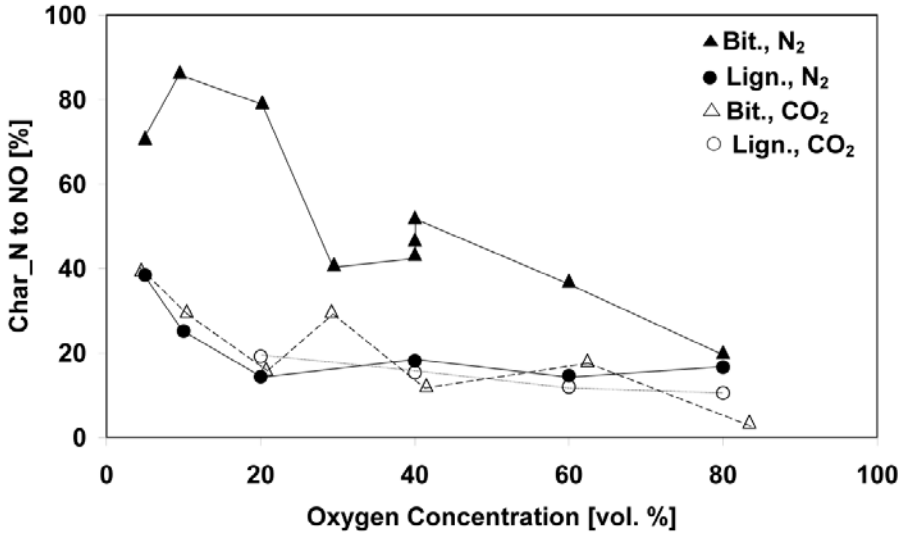

Figure 4 NO emissions from single particle combustion as a function of O_2 concentration. d_p = 2 – 4 mm. $T_{reactor}$ = 1073 K.

That the NO emission from a particle decreases with increasing O_2 concentration, can be sought explained by the increasing particle temperatures shown in figure 5. As the particle temperature increases the combustion rate will be limited by O_2 diffusion in the

particles interior, meaning that further increases in particle temperature mainly promotes NO reduction over char in the reducing interior of the particle [6,17,29].

Figure 5 also shows that higher particle temperatures are reached for bituminous char than for lignite char. This strikes as peculiar as the burnout times in figure 6 shows that the lignite is significantly more reactive. An unambiguous explanation for this is not known but factors such as conductive heat transfer between the sand bed and char particle and the influence of particle surface texture on temperature measurements are likely contributors.

In figure 4 it is seen that lignite char emissions are lower than for bituminous char when combustion is taking place in O_2/N_2. That the char-NO emission decreases with decreasing rank of the parent coal is previously reported in the literature [5,7,16,30]. It is generally believed to be due to the development of a more reactive char network structure upon pyrolysis for low rank coals [31], which increases NO-char reactivity as well as O_2-char reactivity [30,32]. When combustion is taking place in O_2/CO_2 figure 4 shows that NO emissions for bituminous char drop significantly whereas emissions from lignite char is hardly affected. Several factors can influence NO emission from a coal char. Ash minerals are known to have a catalytic effect on NO reduction mainly due to constituents such as Ca [10,33], Fe [19,33], Na [10,19,21,33] and K [10,33,34] and ash from low rank coals have been reported to have a higher catalytic activity [35]. CO is also known to enhance NO reduction on char [6,10,29], presumably through the removal of surface oxides [36,37] and/or through a surface catalyzed reaction [21,22]. The relative importance of CO is known to decrease with increasing temperatures [22,36,37] and to be promoted by the presence of mineral matter [19,22,37]. Even though the ash content of the lignite chars and bituminous chars in figure 4 is similar, differences in its composition could mean that effects of catalytic minerals and CO on NO reduction are different for each parent coal. For this to explain the trends in figure 4 it would mean that the enhancement of CO for lignite chars that are highly reactive due a char structure rich in active and/or catalytic sites is negligible whereas the enhancing effect of CO is significantly reducing the emission from bituminous chars. That the replacement of N_2 with CO_2 in fact yields a significant increase in CO concentration is shown in figure 2,

where the profiles could suggest that this increase is connected to a decrease in NO emission.

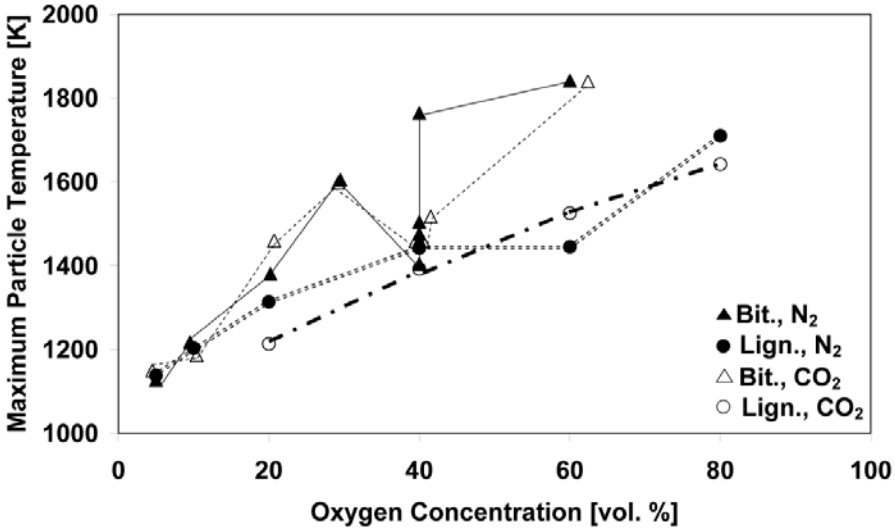

Figure 5 Maximum particle temperatures achieved during single particle combustion as a function of O_2 concentration. d_p = 2 – 4 mm. $T_{reactor}$ = 1073 K.

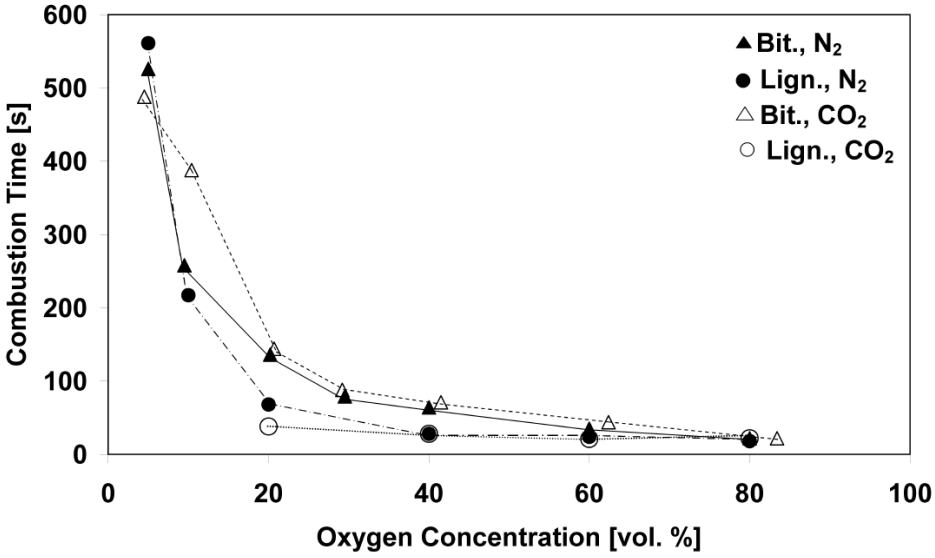

Figure 6 Burnout times for single particle combustion as a function of O_2 concentration. d_p = 2 – 4 mm. $T_{reactor}$ = 1073 K.

Some investigations have also sought to clarify the effect of CO_2 on NO emission/reduction though with conflicting results and always with a focus on CO_2 as a

gasifying reactant contributing to the abundance of surface oxides and gaseous levels of CO [22,38,39]. Should CO_2 gasification affect NO emission in the present case, it is unlikely however that it would only show in the profiles for bituminous chars, as figure 6 clearly shows that lignite char is more reactive. CO_2 could however be expected to affect NO emission through its influence on homogeneous reactions in the particle pore space and in its vicinity. The char particles in figure 4 were prepared at 1073 K but figure 5 shows that much higher peak temperatures are reached during combustion, meaning that nitrogen species such as NH_3 and especially HCN could be expected to evolve from a secondary pyrolysis. Furthermore HCN is often suspected to evolve as a primary product during char oxidation [9,40-43], even though this is not unambiguous [44]. The presence of NH_3 and/or HCN as gaseous species would cause a change in NO emission in CO_2 compared to N_2 due to reaction R 1, which suppresses the O/H radical pool while increasing the OH/H ratio. Reaction R 1 has been found to significantly inhibit HCN oxidation across a broad range of stoichiometries at temperatures similar to those of figure 5 [25] and it has been found to inhibit NO formation from NH_3 at lean conditions and promote it at rich conditions [23]. Besides the inhibited NO reaction pathways in CO_2 the presence of NH_3 and especially HCN means that NO reduction could take place in the gas phase inside the particle and in its vicinity. The role of homogeneous chemistry for char-NO evolution in oxy-fuel combustion has however not been clarified and it is also still widely disputed for air-blown combustion.

$$CO_2 + H \rightleftharpoons CO + OH \qquad \text{R 1}$$

The preceding discussion has dealt mostly with the influence of chemical and catalytic reactions on NO emission. However the use of the CCD camera also allow for a discussion on the development of particle structure during combustion. Figure 7 shows still images of a 3.5 mm bituminous char particle burning in 80 vol. % O_2 in N_2. It can be seen that glowing fragments appear on the sand bed the first seconds after ignition. This was seen for all the experiments carried out with bituminous char in 60 or 80 vol. % O_2 in both N_2 and CO_2 and it is believed to be caused by the rapid release of gases during a secondary devolatilization that is brought upon by a fierce heating. The heating itself may

also contribute to the fragmentation as thermal tensions will develop in the fragile char structure. A similar behavior was not observed for lignite char.

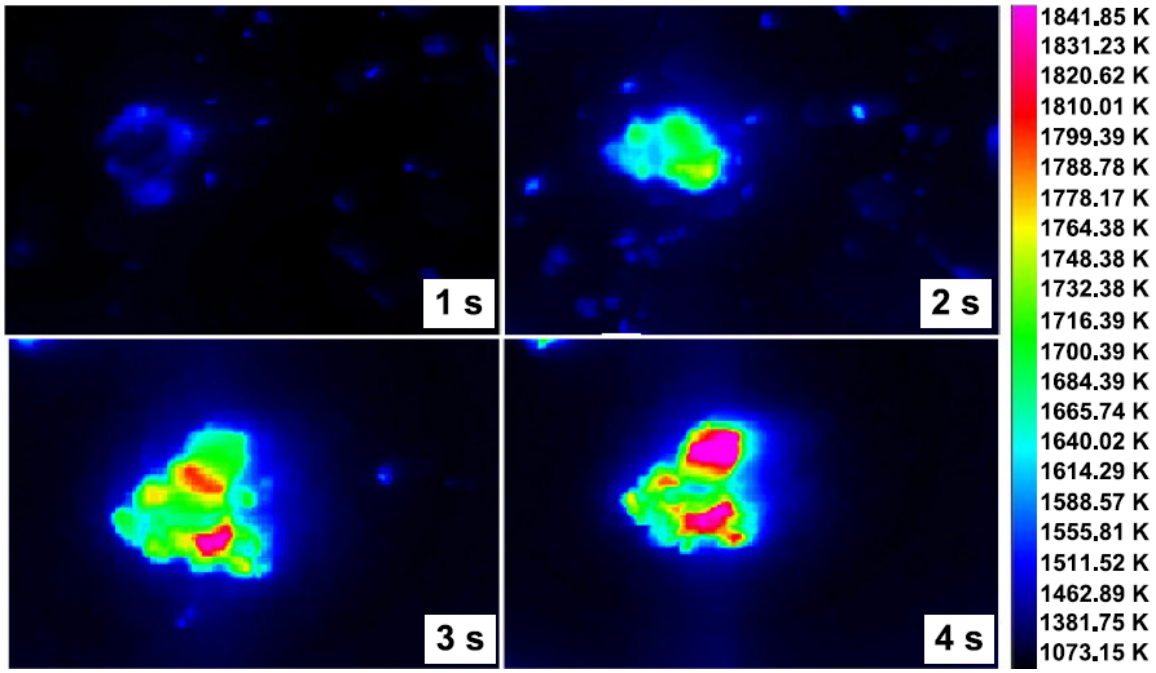

Figure 7 Still images of a single bituminous particle burning at 80 vol. % O_2 in N_2. d_p = 3.5 mm. $T_{reactor}$ = 1073 K. Time zero is ignition.

The initiation of a secondary devolatilization, indicated by figure 7, means that a variety of N-containing gases can in fact be expected to be present in the reactor, especially for bituminous char, (cf. the discussion above). Figure 7 also witness of the strength that visual recording of a combustion process has when structural modeling is to be attempted.

3.3 The Effect of Particle Concentration

The effect of the particle concentration on NO emission is shown in figure 8 for 1.7 – 2.36 mm bituminous char particles burning in 30 vol. % O_2. The figure shows a modest decrease in emission, from app. 60 % to 45 %, when combustion is taking place in N_2 whereas the emission in CO_2 is constant. In figure 9, that shows the peak temperature of the hottest particle in each experiment, it is seen that the temperature increases up to 150

K when the particle concentration increases from 5 to 20, though the increase is most pronounced for combustion in N_2.

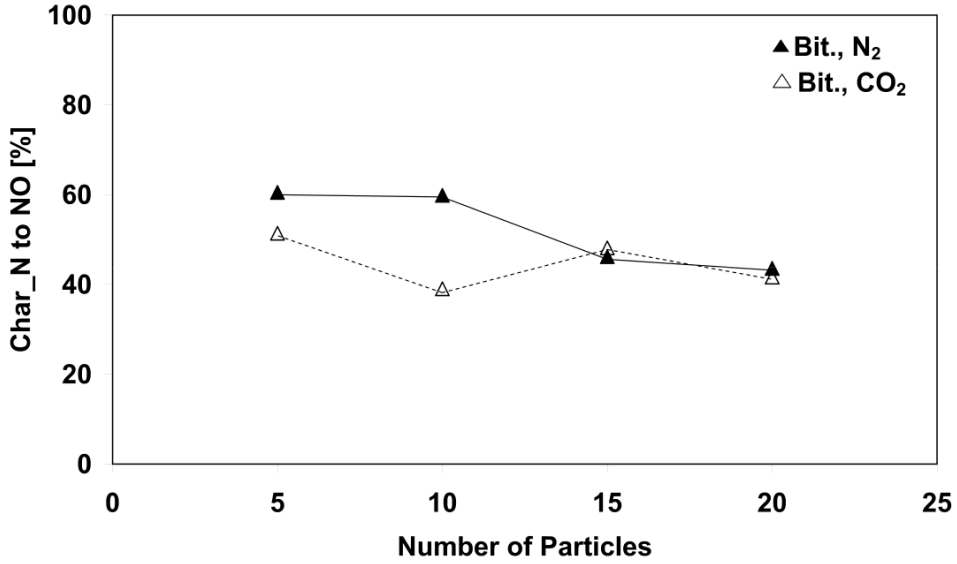

Figure 8 NO emissions from combustion of multiple particles at 30 vol. % O_2. d_p = 1.7 – 2.36 mm. $T_{reactor}$ = 1073 K.

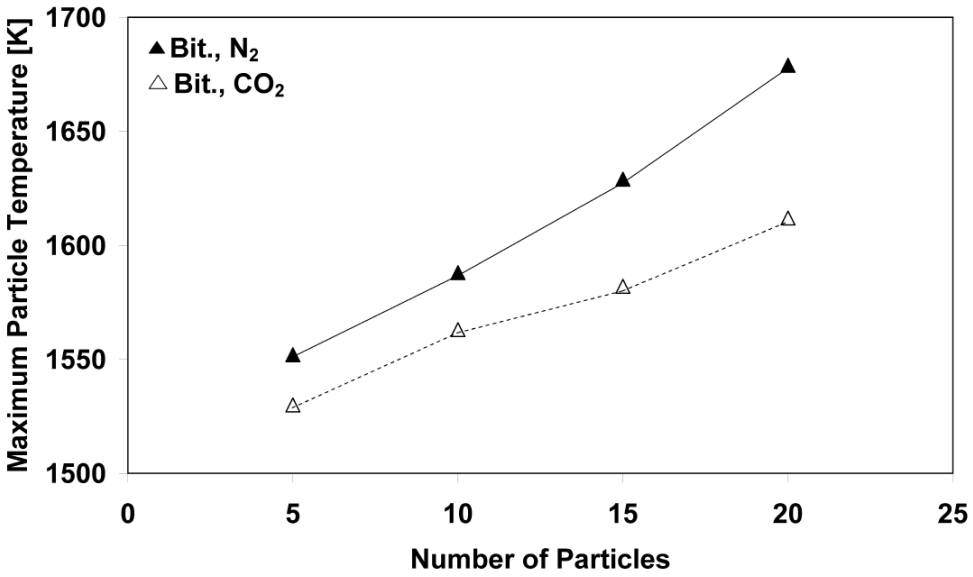

Figure 9 Maximum particle temperatures of the hottest particle achieved during combustion of multiple particles at 30 vol. %. d_p = 1.7 – 2.36 mm. $T_{reactor}$ = 1073 K.

That the NO emission decreases with particle concentration/mass has previously been reported [5,6,45] and is ascribed to a larger surface area available for heterogeneous NO reduction and a lower availability of O_2 during combustion similar to the effect of stoichiometry in continuous processes [3,4,46]. The effect of increasing particle concentration/mass is known to decrease as the concentration/mass increases [5,6,45] and the emission levels in figure 8, representing particle masses between 14.9 – 93.7 mg, could be interpreted as being close to an asymptotic value wherefore the effect of particle concentration on NO emission is minor.

In figure 9 the increase in particle temperature, caused by an increased heat of reaction mutually exchanged between the particles, sand bed and gas, is steepest for combustion in N_2. This is due to the higher specific heat capacity of CO_2, that is know also to influence ignition behavior and temperature profiles in pulverized combustion [4,47], limitations in burning rate caused by the lower O_2 diffusion coefficient in CO_2 [48] and possibly by increased absorption of particle radiation in CO_2.

3.4 The Effect of Particle Mass

Figure 10 and figure 11 shows the effect of particle mass on NO emission from combustion in 40 vol. % and 30 vol. % O_2, respectively. In figure 10 both the emissions for lignite- and bituminous char decreases initially with particle mass, which is also the case for the bituminous char in figure 11. However at some point, as the particle mass increases, the emissions start to increase for bituminous chars in both figures. In figure 11, where experiments have been carried out with very large particles (> 10 mm), a peak is seen in NO emission between 0.1 – 0.15 g of char after what point the emissions decrease again as the particle mass is further increased. In figure 10 there is no noticeable difference in NO emission between O_2/N_2 and O_2/CO_2 for lignite char whereas the emission for bituminous char seems to be slightly lower in O_2/CO_2 than in O_2/N_2 before it reaches its minima. In figure 11 the emission in O_2/CO_2 is significantly lower than in O_2/N_2.

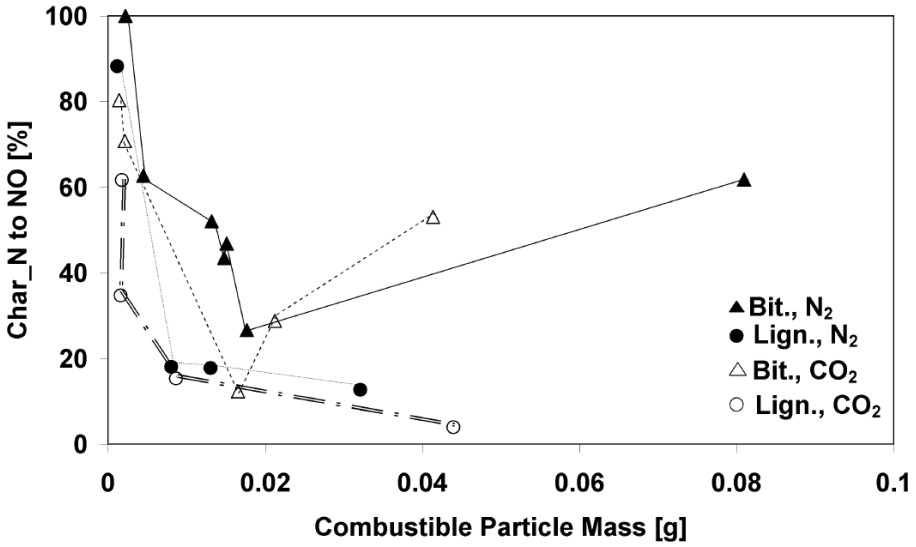

Figure 10 NO emissions from single particle combustion at 40 vol. % O_2 as a function of particle mass. d_p = 0.71 – 7 mm. $T_{reactor}$ = 1073 K.

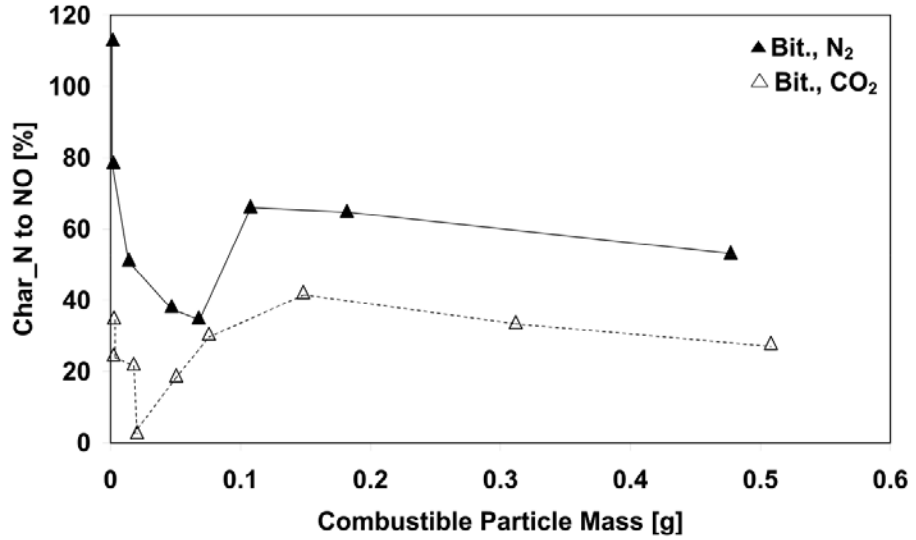

Figure 11 NO emissions from single particle combustion at 30 vol. % O_2 as a function of particle mass. d_p = 1.3 – 12.1 mm. $T_{reactor}$ = 1073 K.

Particle temperatures and burnout times belonging to the experiments in figure 10 are shown in figure 12 and figure 14, respectively. Values belonging to figure 11 are shown in figure 13 and figure 15. In figure 12 the particle temperatures increase initially with particle mass until approximately 0.01 g after which the profiles flatten (for bituminous char in O_2/N_2 there is an outlier that breaks this trend). There is no consistent difference to be found between temperatures of bituminous char whereas the temperature of lignite

char is consistently lower in O_2/CO_2. In figure 13 particle temperatures are fluctuating around a constant value irrespective of particle mass with a consistent trend of lower temperatures in O_2/CO_2.

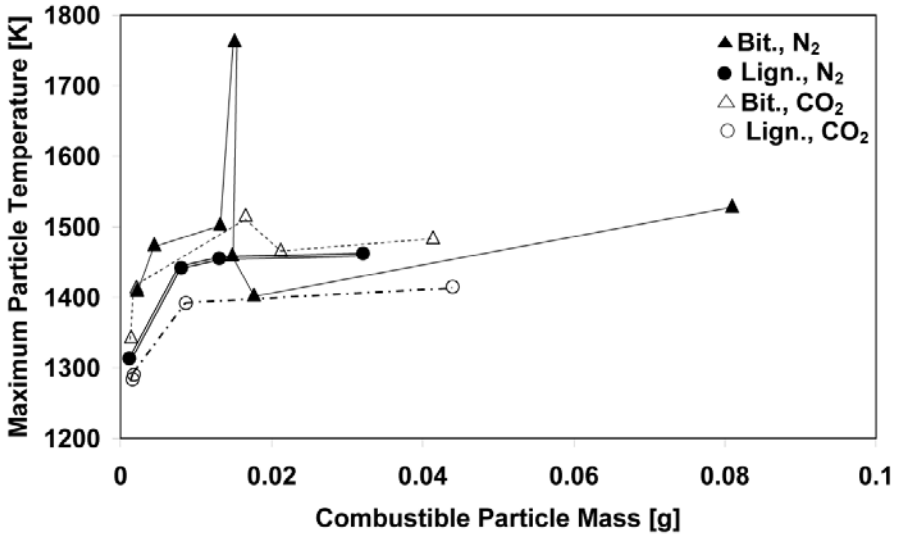

Figure 12 Maximum particle temperatures achieved during single particle combustion at 40 vol. % O_2 as a function of particle mass. d_p = 0.71 – 7 mm. $T_{reactor}$ = 1073 K.

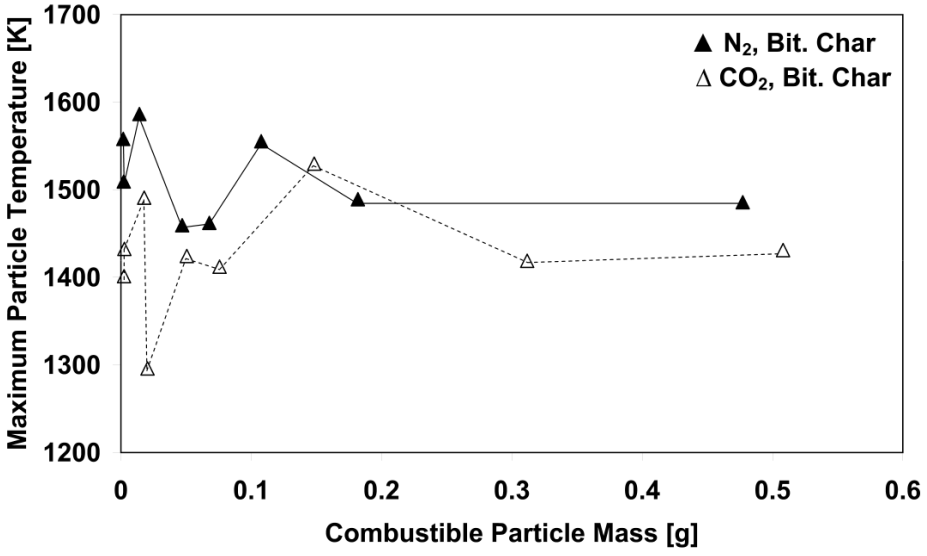

Figure 13 Maximum particle temperatures achieved during single particle combustion at 30 vol. % O_2 as a function of particle mass. d_p = 1.3 – 12.1 mm. $T_{reactor}$ = 1073 K.

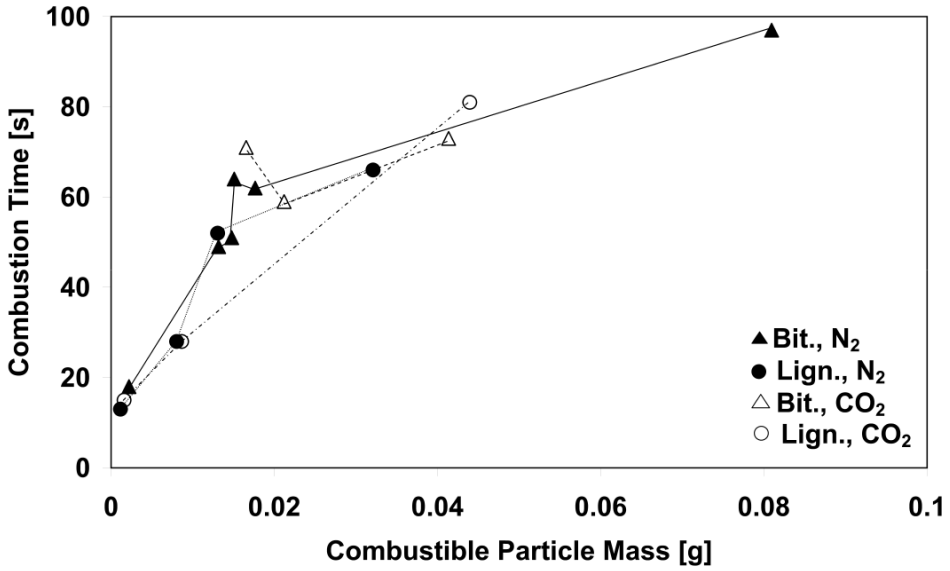

Figure 14 Burnout times for single particle combustion at 40 vol. % O_2 as a function of particle mass. d_p = 0.71 – 7 mm. $T_{reactor}$ = 1073 K.

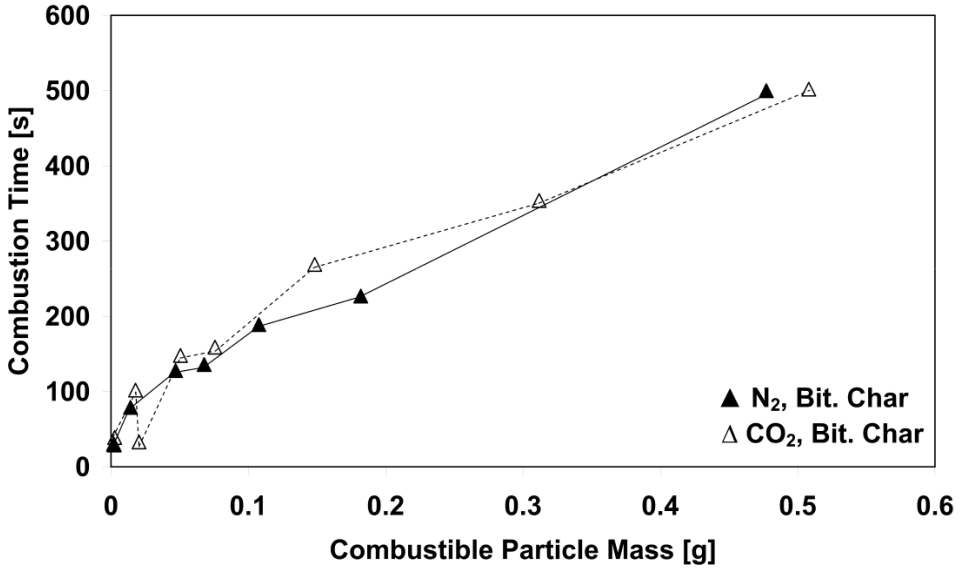

Figure 15 Burnout times for single particle combustion at 30 vol. % O_2 as a function of particle mass. d_p = 1.3 – 12.1 mm. $T_{reactor}$ = 1073 K.

That the char-N conversion in figure 10 and figure 11 initially decreases with increases in particle size is expected [5,15,43,49] and is caused by an increase in char surface area available for NO reduction. It is however surprising that the NO emissions from bituminous char increases after an initial decrease and that a peak seems to exist in figure 11. The reason for this is not obvious and the discussion to come is therefore an attempt to elucidate phenomena that could contribute to this behavior.

In figure 14 and figure 15 burnout times can be seen to increase rapidly for both lignite char and bituminous char as the particle size increase initially (most clearly in figure 14). Camera recordings and visual inspection show that the ash layer remains around the particles after each experiment, which could imply that combustion at lower particle masses is taking place under either kinetic- or external mass transfer control as the burnout time here and in the figures are roughly proportional to $R_0^{1/3}$ [50]. Considering the high particle temperatures in figure 12 and figure 13 and the trend of lower particle temperatures in O_2/CO_2 in figure 13 it is more likely that external mass transfer affects the combustion rate. This is not unambiguous though since it would then be expected that the burnout times in O_2/N_2 were significantly lower than in O_2/CO_2, which is not supported by figure 14 and figure 15. CO_2 gasification could however contribute to char consumption in O_2/CO_2 thereby lowering the observed burnout time. As the particle mass increases further the steepness of the profiles in figure 14 and figure 15 reduces and is roughly proportional to $R_0^{2/3}$, now indicating that the combustion regime is shifting to ash diffusion control. The proportionality between burnout time and particle size has been reported previously for similar sized particles [51]. It is also worth noticing that the shift in proportionality in figure 14 and figure 15 takes place at the sample masses where the minima's in NO emissions are found in figure 10 and figure 11. If these sample masses represents a shift from a combustion process being primarily dominated by external mass transfer control to a combustion process dominated primarily by ash layer diffusion it could significantly affect the NO emission from the particles.

When combustion is taking place under external mass transfer control for small to medium particle sizes (cf. figure 10 and figure 11) the diffusion of NO through the ash layer away from the core surface should not be inhibited since the diffusion coefficient of NO is similar to that of O_2 but the NO-char rate constant is an order of magnitude smaller

than for the O_2-char reaction [15]. The O_2 concentration in the ash layer will also be low meaning that gaseous species such as HCN (cf. the discussion in section 3.2) will be available for NO reduction and also have a higher possibility of escaping the particle before oxidation. At higher particle sizes where combustion is limited by O_2 diffusion in the ash layer it is not unlikely that the thicker ash layer will cause resistance towards NO diffusion as well and cause a higher concentration to develop at the core surface. This increase in concentration will cause more of the NO to diffuse into the porous char core and enhance the reduction here [15,43]. The higher average concentration of O_2 in the ash layer for the case with ash layer diffusion control will also cause a more efficient oxidation of species such as HCN and hence a lower availability for NO reduction. The transport phenomena discussed above would be expected to facilitate a generally lower NO emission in O_2/CO_2 and an earlier shift in rate limiting step, especially when the O_2 concentration decreases. This is in fact what is seen in figure 10 and figure 11. The peak in emission observed in figure 11 would then by the reasoning above represent the shift in rate limiting step. This explanation is not unambiguous, however, and has not been quantified and the effect of the ash layer is further complicated due to an ash content that decreases with increasing particle size (cf. section 2.2) wherefore further studies are needed. These studies should also include experiments at higher reactor temperatures using smaller particle sizes as the effect of internal mass transfer would be expected to decrease with decreasing particle size.

4. Conclusion

Isothermal laboratory scale fixed bed combustion of millimeter sized lignite- and bituminous char particles have been carried out in O_2/N_2 and O_2/CO_2 at a reactor temperature of 1073 K using a Charged Coupled Device (CCD) camera to record particle surface temperatures. Char-N to NO conversions has been investigated at inlet O_2 concentrations between 5 and 80 vol. % for both single and multiple particle combustion.

Single particle combustion at O_2 concentrations between 5 vol. % and 80 vol. % showed a decrease in char-N to NO conversion from 80 % to 15 % for bituminous char burning in O_2/N_2 and from 40 % to 15 % for bituminous char burning in O_2/CO_2. Lignite char burning in O_2/N_2 and O_2/CO_2 showed a decrease in char-N to NO conversion similar to

that of bituminous char in O_2/CO_2 in the same range of O_2 concentrations. For all these experiments increases in particle temperatures between 550 K and 700 K were measured as the O_2 concentration increased.

The effect of increasing the particle concentration from 5 to 20 at a constant O_2 concentration of 30 vol. % on char-N to NO conversion was minor even though the temperature of the particles increased up to approximately 150 K.

Increasing the particle size/mass at constant O_2 concentrations of 30 vol. % and 40 vol. % decreased char-N to NO conversion initially for both lignite- and bituminous char, from 40 - 100 % at approximately 2 mg down to 2 - 20 % at approximately 20 mg. However for bituminous char a minimum in char-N to NO conversion was observed after which the conversion increased to a peak value of 40 – 60 % at app. 100 - 150 mg. For very large particles (> 150 mg) the char-N to NO conversion decreased again. An effect on char-N to NO conversion, when replacing N_2 with CO_2, was only observed for bituminous char that showed consistently lower emissions in O_2/CO_2 than in O_2/N_2. NO emissions from lignite char combustion was generally lower than for bituminous char combustion.

The results of this study are difficult to explain using only transport phenomena, such as differences in O_2 diffusion rate between N_2 and CO_2 and changes in combustion regime, and they suggest that further research into the quantification of ash and char catalyzed NO reduction should be included with an analysis of the gaseous N-species that could be present in and around the char. Especially the presence of HCN, either as a primary oxidation product or a product of secondary pyrolysis, is important to elucidate, as its influence on NO chemistry is changed significantly when CO_2 replaces N_2.

The use of the CCD camera has proven a reliable tool to measure in situ particle temperatures and its ability to display the combustion process as film will be a valuable tool in future modeling efforts.

Acknowledgement

The research leading to these results has received funding from the Danish Agency for Science, Technology and Innovation, Energinet.dk under PSO-10069 “Advanced Diagnostics of Oxy-Fuel Combustion Processes”, Vattenfall Research and Development AB and ALSTOM Power Systems Gmbh. The support and funding from these entities are greatly valued.

References

[1] Buhre BJP, Elliot LK, Sheng CD, Gupta RP, Wall TF. Oxy-fuel combustion technology for coal-fired power generation. Prog Energy Combust Sci. 2005;31:283-7

[2] Toftegaard MB, Brix J, Jensen PA, Glarborg P, Jensen AD. Oxy-fuel combustion of solid fuels. Prog Energy Combust Sci 2010;36:581-625

[3] Hu Y, Naito S, Kobayashi N, Hasatani, M. CO_2, NO_x and SO_2 emissions from the combustion of coal with high oxygen concentration gases. Fuel 2000;79:1925-2

[4] Liu H, Zailani R, Gibbs BM. Comparisons of pulverized coal combustion in air and in mixtures of O_2/CO_2. Fuel 2005;84:833-0

[5] Ninomiya Y, Yokoi K, Arai N, Hasatani M. Characteristics of emission of char NO during the combustion of a single particle of coal char. Int Chem Eng 1989;29:512-6

[6] Glarborg P, Jensen AD, Johnson JE. Fuel nitrogen conversion in solid fuel fired systems. Prog Energy Combust Sci 2003;29:89-3

[7] Thomas KM. The release of nitrogen oxides during char combustion. Fuel 1997;76:457-3

[8] Miller JA, Bowman CT. Mechanism and modeling of nitrogen chemistry in combustion. Prog Energy Combust Sci 1989;15:287-8

[9] Molina A, Murphy JJ, Winter F, Haynes BS, Blevins LG, Shaddix CR. Pathways for conversion of char nitrogen to nitric oxide during pulverized coal combustion. Combust Flame 2009;156:574-7

[10] Aarna I, Suuberg EM. A review of the kinetics of the nitric oxide-carbon reaction. Fuel 1997;76:475-1

[11] Chambrion P, Kyotani T, Tomita A. C-NO reaction in the presence of O_2. 27'th Symposium (International) on Combustion 1998:3053-9

[12] Chambrion P, Kyotani T, Tomita A. Role of N-containing surface species on NO reduction by carbon. Energy Fuels 1998;12:416-1

[13] Chambrion P, Suzuki T, Zhang Z-G, Kyotani T, Tomita A. XPS of nitrogen-containing functional groups formed during the C-NO reaction. Energy Fuels 1997;11:681-5

[14] Chambrion P, Orikasa H, Suzuki T, Kyotani T, Tomita A. A study of the C-NO reaction by using isotopically labelled C and NO. Fuel 1997;76:493-8

[15] Gupta H, Fan L-S. Reduction of nitric oxide from combustion flue gas by bituminous coal char in the presence of oxygen. Ind Eng Chem Res 2003;42:2536-3

[16] Guo F, Hecker WC. Kinetics of NO reduction by char: Effects of coal rank. 27'th Symposium (International) on Combustion 1998:3085-3092

[17] Orikasa H, Tomita A. NO and N_2 formation behavior during the high-temperature O_2 gasification of coal char. Energy Fuels 2003;17:405-1

[18] Zhao Z, Li W, Qiu J, Wang X, Li B. Influence of Na and Ca on the emission of NO_x during coal combustion. Fuel 2006;85:601-606

[19] Zhao Z, Qiu J, Li W, Chen H, Li B. Influence of mineral matter in coal on decomposition of NO over coal chars and emission of NO during char combustion. Fuel 2003;82:949-7

[20] Bueno-López A, Soriano-Mora JM, García-García A. Study of the temperature window for selective reduction of NO_x in O_2-rich gas mixtures by metal-loaded carbon. Catal Commun 2006;7:678-684

[21] Wu SL, Iisa K. Kinetics of NO reduction by black liquor char. Energy Fuels 1998;12:457-463

[22] Aarna I, Suuberg EM. The role of carbon monoxide in the NO-carbon reaction. Energy Fuels 1999;13:1145-1153

[23] Mendiara T, Glarborg P. Ammonia chemistry in oxy-fuel combustion of methane. Combust Flame 2009;156:1937-9

[24] Normann F, Andersson K, Leckner B, Johnsson F. Emission control of nitrogen oxides in the oxy-fuel process. Prog Energy Combust Sci 2009;35:385-7

[25] Giménez-López J, Millera A, Bilbao R, Alzueta MU. HCN oxidation in an O_2/CO_2 atmosphere: An experimental and kinetic modeling study. Combust Flame 2010;157:267-6

[26] Normann F, Andersson K, Leckner B, Johnsson F. High-temperature reduction of nitrogen oxides in oxy-fuel combustion. Fuel 2008;87:3579-5

[27] Park J, Park JS, Kim HP, Kim JS, Kim SC, Choi JG, Cho HC, Cho KW, Park HS. NO emission behavior in oxy-fuel combustion recirculated with carbon dioxide. Energy Fuels 2007;21:121-129

[28] Mendiara T, Glarborg P. Reburn chemistry in oxy-fuel combustion of methane. Energy Fuels 2009;23:3365-2

[29] Molina A, Eddings EG, Pershing DW, Sarofim AF. Char nitrogen conversion: implications to emissions from coal-fired utility boilers. Prog Energy Combust Sci 2000;26:507-1

[30] Wang W, Brown SD, Hindmarsh CJ, Thomas KM. NO_x release and reactivity of chars from a wide range of coals during combustion. Fuel 1994;73:1381-1388

[31] Yu J, Lucas JA, Wall TF. Formation of the structure of chars during devolatilization of pulverized coal and its thermoproperties: A review. Prog Energy Combust Sci 2007;33:135-0

[32] Arenillas A, Rubiera F, Parra JB, Pis JJ. Influence of char structure on reactivity and nitric oxide emissions. Fuel Process Technol 2002;77-78:103-9

[33] Wang Z, Zhou J, Wen Z, Liu J, Cen K. Effect of mineral matter on NO reduction in coal reburning process. Energy Fuels 2007;21:2038-3

[34] López D, Calo J. The NO-carbon reaction: The influence of potassium and CO on reactivity and populations of oxygen surface complexes. Energy Fuels 2007;21:1872-7

[35] Johnsson JE. Formation and reduction of nitrogen oxides in fluidized-bed combustion. Fuel 1994;73:1398-5

[36] Levy JM, Chan LK, Sarofim AF, Beér JM. NO/char reactions at pulverized coal flame conditions. 18’th Symposium (International) on Combustion:111 – 0

[37] Chan LK, Sarofim AF, Beér JM. Kinetics of the NO-carbon reaction at fluidized bed combustor conditions. Combust Flame 1983;52:37-5

[38] Fan W, Lin Z, Li, Y, Kuang J. Experimental study of the effects of CO_2 on the noncatalytic reduction reaction of NO by carbonaceous materials. Energy Fuels 2009;23:2429-6

[39] Park D-C, Day SJ, Nelson PF. Nitrogen release during reaction of coal char with O_2, CO_2 and H_2O. Proc. Combust. Inst. 2005;30:2169-5

[40] Orikasa H, Tomita A. A study of the HCN formation mechanism during the coal char gasification by O_2. Energy Fuels 2003;17:1536-0

[41] Winter F, Wartha C, Löffler G, Hofbauer H. The NO and N_2O formation mechanism during devolatilization and char combustion under fluidized-bed conditions. 26'th Symposium (International) on Combustion 1996:3325-4

[42] Liu Y, Che D. Releases of NO and its precursors from coal combustion in a fixed bed. Fuel Process Technol 2006;87:355-2

[43] Visona SP, Stanmore BR. Modeling NO_x release from a single coal particle II. Formation of NO from char-nitrogen. Combust Flame 1996;106:207-8

[44] Goel S, Zhang B, Sarofim AF. NO and N_2O formation during char combustion: Is it HCN or surface attached nitrogen. Combust Flame 1996;104:213-7

[45] Molina A, Eddings EG, Pershing DW, Sarofim AF. Nitric oxide destruction during coal and char oxidation under pulverized-coal combustion conditions. Combust Flame 2004;136:303-2

[46] Hu YQ, Kobayashi N, Hasatani M. Effects of coal properties on recycled-NO_x reduction in coal combustion with O_2/recycled flue gas. Energy Convers. Manage. 2003;44:2331-0

[47] Molina A, Shaddix CR. Ignition and devolatilization of pulverized bituminous coal particles during oxygen/carbon dioxide coal combustion. Proc. Combust. Inst. 2007;31:1905-2

[48] Brix J, Jensen PA, Jensen AD. Coal devolatilization and char conversion under suspension fired conditions in O_2/N_2 and O_2/CO_2 atmospheres. Fuel 2010;89:3373-0

[49] Hayhurst AN, Lawrence AD. The amounts of NO_x and N_2O formed in a fluidized bed combustor during the burning of coal volatiles and also of char. Combust Flame 1996;105:341-7

[50] Levenspiel O. Chemical Reaction Engineering. 3rd ed. John Wiley & Sons, Inc;1999

[51] Blackham AU, Smoot LD, Yousefi P. Rates of oxidation of millimetre-sized char particles: simple experiments. Fuel 1994;73:602-2

6 Conclusions

This work is divided into four parts each treated consecutive in the articles enclosed in the thesis. The first article describes and presents experimental work carried out on suspension fired coal combustion in O_2/N_2 and O_2/CO_2 atmospheres. Experiments in this part of the work have been carried out in an isothermal Entrained Flow Reactor (EFR) to determine coal conversion during devolatilization and char combustion. The second article deals with determination of intrinsic reaction kinetics of combustion and CO_2 gasification of char collected in the EFR. This part of the work is carried out in a non-isothermal ThermoGravimetric Analyzer (TGA). Using the kinetic expressions obtained in the second part, the data from the first part is modelled using a detailed char conversion model in the third article. The fourth article investigates NO emission and particle temperatures from char combustion in O_2/N_2 and O_2/CO_2 atmospheres in a laboratory scale Fixed Bed Reactor (FBR). In the following the findings in each article will be outlined along with their implications on the future of Oxy-Fuel Combustion (OFC). The results will first be summarized on an article basis and their implications then discussed at the end of the section.

Article I presents devolatilization and combustion experiments carried out in N_2 or CO_2 based atmospheres with bituminous El Cerrejón coal in an isothermal electrically heated EFR at temperatures between 1173 K – 1673 K and inlet O_2 concentrations between 5 – 28 vol. %. Char was sampled from just after complete devolatilization and to complete burnout, covering residence times up to 1 s. Devolatilization experiments did not show a noticeable change in volatile yield when N_2 was replaced with CO_2 under otherwise similar conditions. Scanning Electron Microscopy (SEM) on, and Brunauer-Emmett-Teller (BET) surface measurements of, sampled char from devolatilization experiments in N_2 and CO_2 did not show differences between the two atmospheres either. These findings suggest that the presence of high concentrations of CO_2 does not influence char properties of the investigated coal under suspension fired conditions. The char conversion profiles, obtained from sampling during combustion, did not show differences between N_2 and CO_2 based atmospheres at temperatures between 1173 K and 1373 K across the range of investigated O_2 concentrations. At the reactor temperatures 1573 K and 1673 K and an inlet O_2 concentration of 5 vol. % the experimental char conversion profiles show

a faster char conversion in O_2/N_2 than in O_2/CO_2. This is believed to be due to the lower diffusion coefficient of O_2 in CO_2 (~ 22 %) at these conditions. At the high reactor temperatures and low concentration of O_2 char conversion takes place under significant influence of external mass transfer control, which means that the faster O_2 diffusion in N_2 will enable a faster conversion rate than during combustion in CO_2. None of the experimental conversion profiles have suggested an effect of CO_2 gasification on char conversion.

Article II presents TGA reactivity profiles of EFR-char formed in both O_2/N_2 and O_2/CO_2 atmospheres. In the experiments a heating rate of 5 K/min was used to reach peak temperatures of 1273 K and 1373 K. The O_2 and CO_2 concentrations were 5 vol. % and 80 vol. % in the conducted combustion and gasification experiments, respectively. From the TGA experiments it was found that CO_2 gasification did not affect char conversion in the temperature window where the char was consumed by O_2 in the TGA. Reactivity measurements on char sampled during EFR devolatilization in O_2/N_2 and O_2/CO_2 at 1573 K and 1673 K and on partly converted EFR-char sampled at 1173 K and 1673 K at inlet O_2 concentrations of 28 vol. % and 5 vol. %, respectively, did not show any differences. These findings are in line with, and support, the conclusions on the work of the first article, namely that the presence of high concentrations of CO_2 does not change char conversion rate for the examined coal. The reactivity curves of char formed and partly consumed in the EFR at 1173 K with an inlet O_2 concentration of 28 vol. % in N_2 or CO_2 showed that two char phases of distinctively different reactivity are present. The phases showed up as two peaks in the reactivity profiles and will be discussed further in the context of article III. From reactivity measurements on EFR-char devolatilized at 1173 K – 1673 K intrinsic kinetic parameters were found for combustion in O_2. The kinetic expression includes both an activation term, as is common for Arrhenius kinetics, and a deactivation term to account for the thermal effect of devolatilization temperature on resulting char reactivity. Intrinsic kinetics for CO_2 gasification has also been found, though using only EFR-char devolatilized at 1273 K, 1473 K and 1573 K due to a lack of samples. It was found that the devolatilization temperature in the EFR did not affect the char reactivity towards CO_2 gasification wherefore only an Arrhenius activation term is present in the rate constant for this reaction.

Article III first presents a detailed COal COmbustion MOdel (COCOMO) encompassing the three char morphologies; cenospheres, network- and dense chars, each distributed between six discrete particle sizes. Input to model simulations are taken from relevant literature studies and found from measurements of Particle Size Distribution (PSD) and BET analysis. The intrinsic kinetic expressions for combustion and gasification, found in article II, are used to describe char conversion rate. All physical parameters relating to mass and energy balances are calculated as temperature dependent properties of either the particles or surrounding gas mixture.

When COCOMO was used to model the char conversion profiles from article I, a reasonable consistency was in general found between simulations and experiments. At a reactor temperature of 1173 K and inlet O_2 concentrations of 5 vol. % and 28 vol. % the model was found to over predict char conversion. At a reactor temperature of 1273 K and an inlet O_2 concentration of 5 vol. % the model also over predicted char conversion. The reason for the over predictions at the low O_2 concentrations at these temperatures is found in an experimental delay in heterogeneous ignition after completed devolatilization. This delay is not captured by COCOMO, which cause absolute deviations between calculated and experimental degrees of char conversion. The conversion rate is however predicted accurately by the model. At a reactor temperature of 1173 K and an inlet O_2 concentration of 28 vol. % TGA experiments in article II revealed the existence of two char phases of distinctively different reactivity. SEM images of char sampled at these conditions showed unreacted fractions of char even at very high overall degrees of conversion. The formation of the un-reactive fraction of the char is believed to be caused by a fierce second devolatilization brought upon by a rapid heat release after particle ignition at the high O_2 concentration. Simulations indicate that excess particle temperatures of 500 – 600 K are reached at heating rates as high as 20000 K/s shortly after heterogeneous ignition. As has previously been suggested in the literature, it is possible that the deactivation takes place due to interactions between products of secondary devolatilization and mineral matter; though the mineral matter itself may also promote deactivation at these conditions. Because COCOMO assumes a homogeneous char deactivation, only depending on char particle temperature, the phenomena above is not captured and hence the degree of char conversion is over estimated by the model.

Application of the intrinsic kinetic parameters from article II to predict char conversion at suspension fired conditions has proven to work satisfactorily in the case of combustion. At the highest reactor temperatures the effect of CO_2 gasification on char conversion was however slightly over predicted. Despite this slight over prediction simulations with COCOMO does show that a potential contribution from gasification on char conversion can take place in the case of high reactor temperatures and low concentrations of O_2 where combustion is limited by external mass transfer resistance.

In article IV data on NO emission and particle temperature are presented for isothermal combustion of millimeter sized bituminous and lignite char particles in O_2/N_2 and O_2/CO_2 atmospheres in a FBR. O_2 concentrations were between 5 and 80 vol. % and the reactor temperature was kept constant at 1073 K. Particle temperatures were measured and recorded using a Charged Coupled Device (CCD) camera, operated by software developed specifically for the setup. Within the range of O_2 concentrations used during the experiments, the char-N to NO conversion was found for both single- and multiple particle combustion. Single particle combustion, covering the entire range of O_2 concentrations, showed a decrease in the char-N to NO conversion from 80 – 15 % and 40 – 15 % for bituminous char burning in O_2/N_2 and O_2/CO_2, respectively, when the O_2 concentration increased across the interval. Char-N to NO conversion for lignite char in both O_2/N_2 and O_2/CO_2 showed a behavior nearly identical to that of bituminous char burning in O_2/CO_2. Particle temperature measurements, recorded during these experiments, showed an increasing particle excess temperature as the O_2 concentration increased with peak particle excess temperatures reaching 550 – 700 K at 80 vol. % O_2.

The effect on char-N to NO conversion of increasing the particle concentration from 5 to 20 particles at 30 vol. % O_2 in N_2 and CO_2 was only minor for O_2/CO_2. A drop of app. 15 % was seen in O_2/N_2 as the particle concentration increased. During the experiments peak particle excess temperatures up to 150 K in O_2/N_2 were recorded as the particle concentration increased. When it was the particle size/mass of single particles that was increased at constant O_2 concentrations of 30 vol. % and 40 vol. % in N_2 or CO_2 the effect on char-N to NO conversion was however marked. Initially the char-N to NO conversion decreased in both O_2/N_2 and O_2/CO_2 as the particle mass increased from app. 2 – 20 mg. The decrease in char-N to NO conversion was significant from 40 – 100 %

down to 2 – 20 % in the interval of applied particle masses. After this point the char-N to NO conversion for the bituminous coal began to increase as the particle mass was increased form app. 20 mg to app. 100 – 150 mg, where it had a second peak at values between 40 – 60 %. After this point the char-N to NO conversion decreased again with further increases in particle size/mass.

In all of the experiments carried out in this article it has been a general observation that the change of atmosphere, from N_2 based to CO_2 based, facilitates a significant drop in char-N to NO conversion for the bituminous coal char. In the case of lignite char combustion the gaseous atmosphere was however not found to influence the char-N to NO conversion, which was in general lower than that of bituminous char. This could be due to a lower influence of CO on NO reduction over the more reactive lignite char.

When the results of this study are sought explained transport phenomena such as differences in O_2 diffusion rate and combustion regimes can not stand alone. The behavior observed during the experiments suggests that ash and char catalysis along with the influence of primary products such as HCN and NH_3 should be subjects of further investigation. No further attempts to quantify the influence of these parameters have been made in this article.

During the experiments the use of the CCD camera has proven a valuable and reliable tool for in situ measurements of particle temperature.

The four articles, the results of which are described above, allows for the following general conclusions.

- From the experimental char conversion profiles in article I and from the reactivity profiles in article II there is not found any influence of CO_2 gasification during devolatilization and char conversion in the range of reactor temperatures and O_2 concentrations used in the EFR and TGA. The only effect of the change in gaseous atmosphere seems to be a lower char conversion rate in O_2/CO_2 during combustion under external mass transfer control due to a lower diffusion coefficient of O_2 in CO_2.
- From the TGA experiments in article II it has been shown that the intrinsic kinetics of combustion is not affected by the presence of high concentrations of

CO_2 for the bituminous coal used here. When heterogeneous ignition is fierce, under high concentrations of O_2, the char may deactivate significantly thereby forming phases of different reactivity.

- Using the char conversion model COCOMO good predictions of char burnout was obtained using kinetic parameters for combustion and gasification obtained from TGA experiments on EFR-char in article II. At high reactor temperatures gasification kinetics did however cause a slight over prediction of gasification rate.
- In article IV it was found that the effect of gaseous atmosphere on NO emission is marked for bituminous coal char with significantly lower emissions in O_2/CO_2 than in O_2/N_2. For lignite coal char there does not seem to be an effect of gaseous atmosphere on the NO emission.

The general conclusions on the content of this thesis give rise to the following reflections on the future of OFC with respect to fuel conversion and NO emission.

- Concerns on fuel conversion in retrofitted and Greenfield OFC-plants, fuelled with bituminous coal of reactivity similar to El Cerrejón coal, should not be directed to reaction kinetics or devolatilization behavior but rather to the temperature profiles of particles and gas in the boiler as it will be these temperatures that determine the value of the rate constant for char combustion.
- The contribution from gasification to char conversion and CO levels should not be a major focus, when operation is conducted using bituminous coal of reactivity similar to El Cerrejón coal.
- Reasonably accurate model predictions of char conversion are achievable for boiler design purposes using established kinetic expressions and physical gas phase data already available.
- If a Greenfield plant is operated at O_2 concentrations that are too high there is a risk of poor burnout efficiency due to significant thermal deactivation of the char. However, as the EFR experiments of article I were conducted at very high stoichiometric ratios of O_2 (~ 15) the inlet O_2 concentration of 28 vol. %, where

the present deactivation was observed, is not directly transferable to a practical boiler where volatile combustion will lower the inlet O_2 concentration significantly at the much lower stoichiometric ratios used here.

- The possibility to influence OFC plant economy positively through reductions in NO emission is most promising for bituminous coal rather than lignite coal.

7 Future Work

This work has dealt extensively with the nature of coal conversion in O_2/CO_2 environments compared to O_2/N_2 environments. The work has been carried out using bituminous El Cerrejón coal and conclusions on intrinsic kinetics, devolatilization behavior and char morphology are therefore based entirely on the chemical and physical properties of this coal. For an easy applicable evaluation of a coals combustion behavior under industrial OFC conditions it is recommended that further experiments are conducted using relevant coals of other properties, such as lignite- and subbituminous coal. For this to be fruitful for industrial applications the behavior of the coals with respect to intrinsic kinetics (for both combustion and gasification), devolatilization and char morphology must be related to easy measurable properties such as proximate- and ultimate analysis and/or TGA reactivity measurements under standardized conditions. With respect to the influence of gasification this thesis only treats gasification by CO_2 as this is the most abundant reactive gaseous species in an OFC boiler. That gasification by H_2O is neglected in this work entails, however, that the results and conclusions of the work applies to an OFC plant operating with dry recycle of flue gas. In the case of a plant operating with wet recycle the water content in the boiler may be as high as 30 vol. % and it will therefore not be possible to ignore a possible contribution from H_2O gasification to fuel conversion. It is therefore recommended that future investigations include H_2O in the reactive gas mixture.

The emission of NO has only been dealt with experimentally in this work and under conditions different from those of suspension fired boilers. Even though the results on NO emission, presented in the thesis, allow for a general discussion several future contributions could help utilize the promise of lower NO emissions in OFC. As a direct

continuation of this work further FBR experiments should be carried out under well defined, easily controllable conditions in order to quantify the effect of increased CO levels and catalysis on NO reduction. These parameters must be encompassed in a model used to isolate the effects of transport phenomena, ash and char catalysis and CO enhancement in NO emission from char combustion. The possible presence of HCN and NH_3 as primary reaction products complicates the investigation as these species are difficult to measure in experiments. Attempts could be made using advanced IR diagnostics but the design of such experiments lies outside the expertise of this author. If a successful model could be developed for well defined conditions, experiments carried out at suspension fired conditions are a necessary next step. The use of a validated model to treat the data obtained in these experiments will be essential for practical conclusions that can be used by plant entrepreneurs.